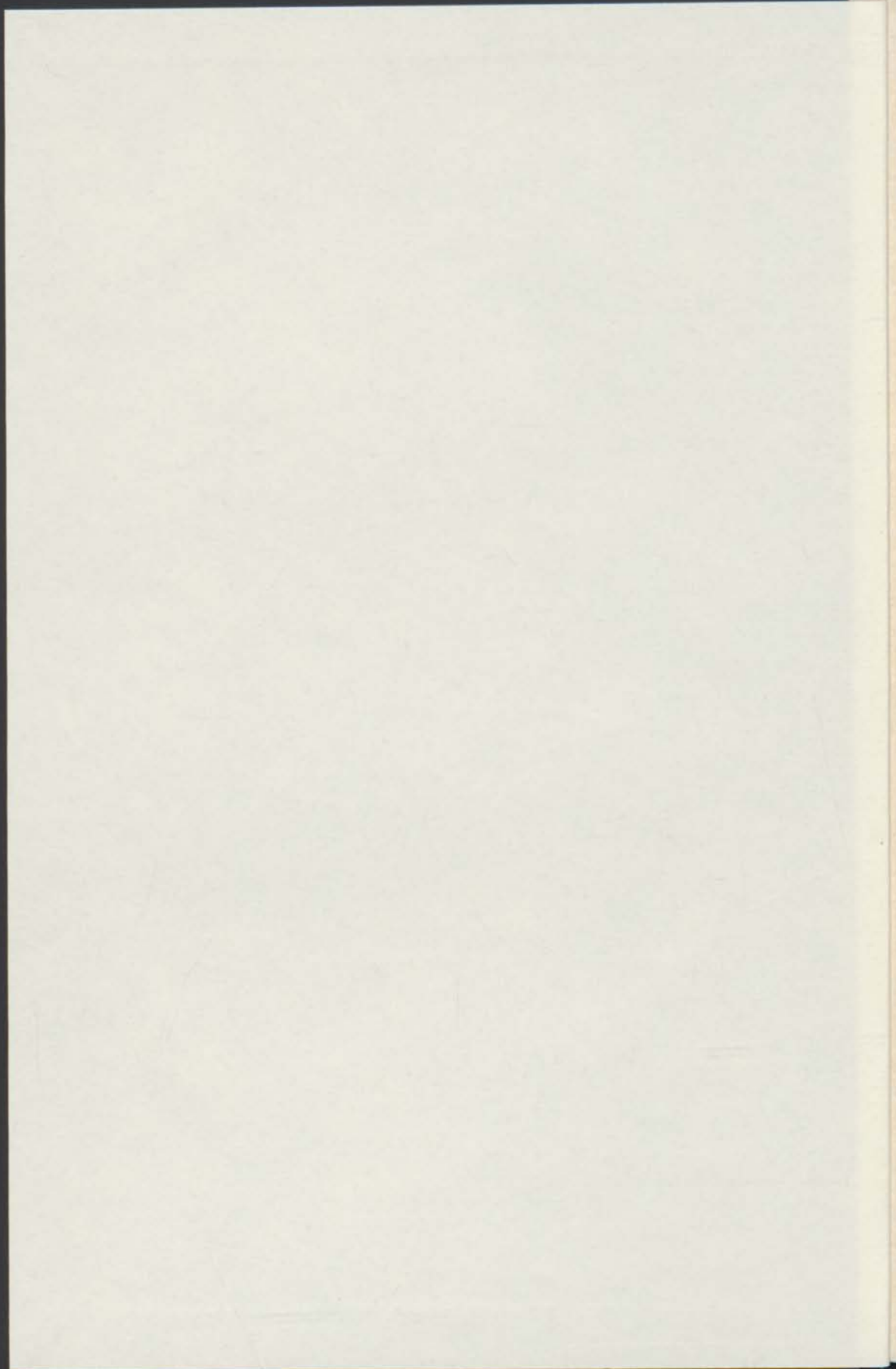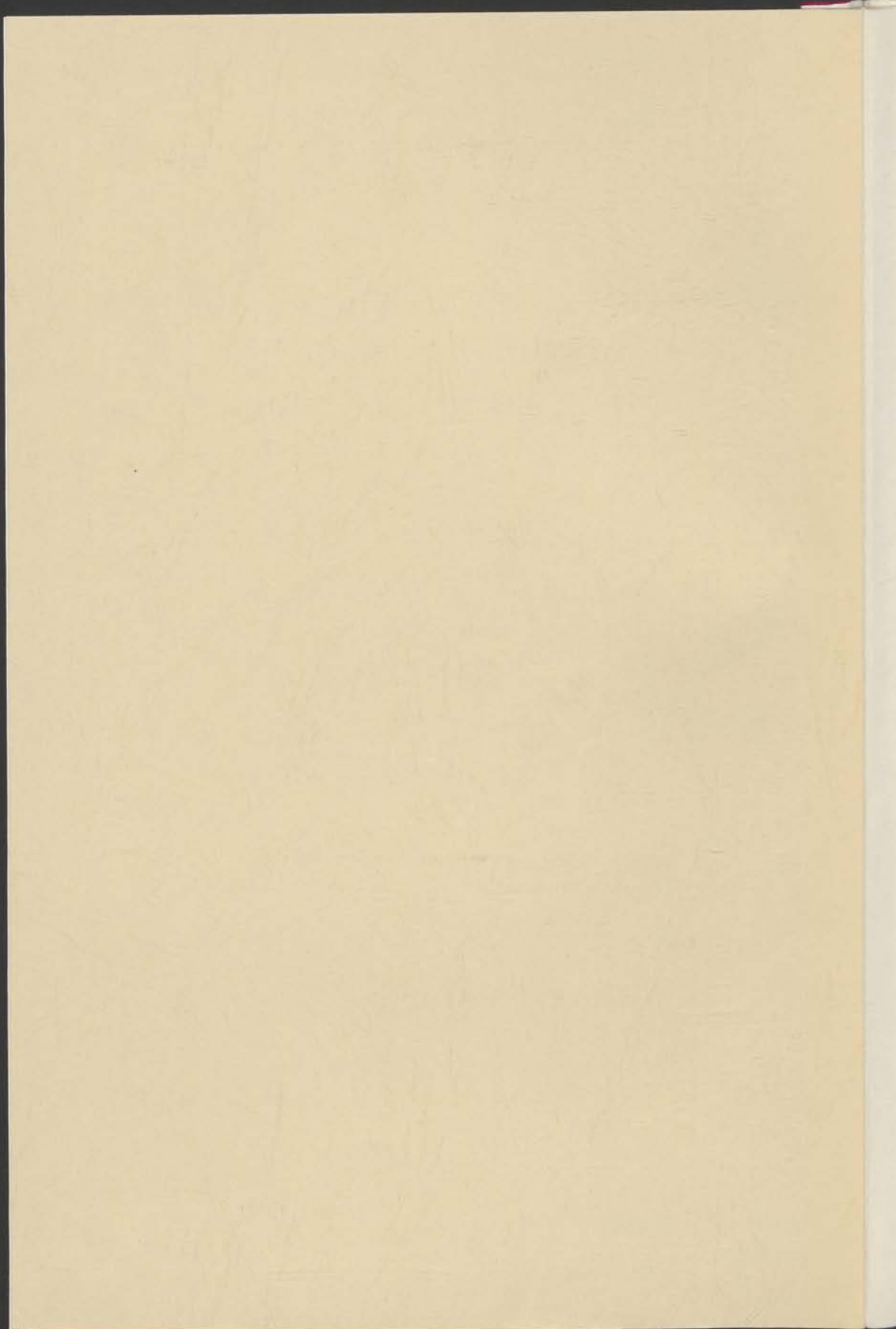PARAMAGNETIC RELAXATIONS STUDIED
BY A BRIDGE OPERATING
FROM 200 Hz TO 1 MHz

PARAMAGNETIC RELAXATIONS STUDIED BY A BRIDGE OPERATING FROM 200 Hz TO 1 MHz

A.J. de VRIES

PARAMAGNETIC RELAXATIONS STUDIED BY A BRIDGE OPERATING FROM 200 Hz TO 1 MHz

PARAMAGNETIC RELAXATIONS STUDIED BY A BRIDGE OPERATING FROM 200 Hz TO 1 MHz

DOOR

ADRIANUS JOHANNES DE VRIES

GEBOREN TE RHEDEN IN 1927

Voor Mieke
en de kinderen

CONTENTS

INTRODUCTION

Paramagnetic relaxation is not a new subject and this thesis can be seen as an extension of the work done by many research workers. Some initial trials in the early twenties did not give clear results, but a theoretical paper by WALLER [1] and experimental results published by GORTER [2], DE HAAS and DU PRÉ [3] formed the first solid base for the following researches. It was soon clear that at least two relaxation mechanisms could be observed:

    1. spin-spin relaxation,

    2. spin-lattice relaxation.

The main part of this thesis is directed toward a further study of the spin-lattice relaxation phenomena. Spin-lattice relaxation has been and is studied in Leiden by several methods. Without being complete, the following methods can be cited:

a) GORTER [4] measured x''/x_0 by means of a calorimetric method in the frequency range from 100 kHz to 100 MHz. An R. F. beat method was also used quite early to measure x'/x_0 for a sample. The detuning of an oscillator can be used to determine this quantity. The same method has been used by VERSTELLE [5] and others.

b) The susceptibility of a paramagnetic salt can be measured by means of bridge methods. DE HAAS and DU PRÉ [3] used a Hartshorn bridge in the frequency range between 10 Hz and 100 Hz. This method was also used by BIJL [6] and refined by VAN DER MAREL [7] and VAN DEN BROEK [8]. These last two workers were able to measure in the frequency range 3 Hz - 1200 Hz and by means of a switching technique in the range 0 - 1 Hz.

c) VERSTELLE [5] developed the use of a twin-T bridge for measuring both x'/x_0 and x''/x_0 in the frequency range from 200 kHz to 20 MHz.

d) BÖLGER [9] studied spin-lattice relaxation by means of saturation techniques.

By means of these methods a large amount of data has been collected. A very short summary will be attempted here. Most of the measurements with bridges of the Hartshorn type have been done at helium temperatures ($1^\circ K - 4^\circ K$); it was

found that in the hydrogen range (14°K - 20°K) the relaxation times were often too short to be measured. Different measurements on the same salts did not reproduce very well, or even showed large differences, and theoretical predictions of the relaxation time versus temperature and magnetic field have seldom been confirmed. Measurements of relaxation parameters by means of the (relatively) high frequency methods have given more consistent results. Most of these measurements have been done at hydrogen, nitrogen or room temperatures. For some specimens relaxation parameters have been measured by different bridges in different temperature intervals (see GORTER [10]).

Up to the present it had been impossible to combine some of these data in a meaningfull way, i.e. in the case of manganese tutton salt. It was therefore judged desirable to construct a bridge capable of measuring in the frequency range of 1 kHz - 1 MHz. This project has been completed and in the following thesis we describe the design and the construction of a bridge, which measures magnetic susceptibilities and can determine relaxation times ρ in the ranges from 1 μ sec - 5 m sec and from 100 m sec - several minutes. Measuring results on a series of paramagnetic salts are given.

CHAPTER 1

SURVEY OF THE THEORY OF PARAMAGNETIC RELAXATION

1.1 DEFINITION

Paramagnetic relaxation is the name given to the phenomena which occur
when the magnetization of paramagnetic substances does not follow instantane-
ously changes in the magnetic field. The definition comprises a number of dif-
ferent processes. In the following we will discuss two groups of these proces-
ses: spin-lattice relaxation and spin-spin relaxation.

1.2 NORMAL PARAMAGNETISM

In this section we will give a very short summary of normal paramagnet-
ism. For a more complete introduction we refer to any standard textbook
(DEKKER [11]).

One can define normal paramagnetic substances as those materials in
which the ratio χ between the magnetization M and the applied magnetic field
H which induces the magnetization varies approximately inversely with the
temperature expressed in degree's Kelvin. In general M and H are vectors
and are not necessarily in the same direction and χ is a tensor. In this thesis
we will suppose M to be in the same direction as H, making χ a scalar. If
this condition is not fulfilled, M should be interpreted as the component of the
magnetization in the direction of H. The same holds for χ.

Normal paramagnetism occurs if certain conditions are satisfied. The
substance under consideration should contain magnetic ions, i.e. ions with a
permanent magnetic dipole moment, capable of being aligned with an external
magnetic field, and each permanent magnetic dipole should be substantially in-
dependent of its neighbor, otherwise ferromagnetism (or antiferromagnetism)
can occur. A substance can be paramagnetic in one temperature range and
ferromagnetic or antiferromagnetic at lower temperatures. The permanent
magnetic dipoles are explained by the summation of the magnetic moments
associated with the orbital momentum and spin momentum of the electrons.
Following quantum theoretical arguments, a partly filled electron shell is

11

required to produce an effective magnetic moment. The valence electrons should be excluded, however, because in ionic crystals these electrons are thought to be transferred to neighboring ions, such that both ions have a complete outer shell. Paramagnetism therefore occurs in the elements of the so-called transition groups. Of the transition groups two groups have been mainly studied,

  a) The iron group with an incomplete 3d shell,

  b) the lanthanides or rare earths group with an incomplete 4f shell.

  If a large number n of magnetic dipoles, each with a magnetic moment μ, is placed in a magnetic field H and the system is in thermal equilibrium at a temperature T one finds, using classical statistical mechanics, that

$$M = n\mu \left[\operatorname{ctg}\left(\frac{\mu H}{kT}\right) - \frac{kT}{\mu H} \right] \tag{1-1}$$

where k is Boltzmann's constant, $k = 1.38 \times 10^{-16}$ erg deg^{-1}.

For $\frac{\mu H}{kT} \ll 1$ this gives Curie's law

$$M = n\mu^2 H / 3kT$$

By means of quantum theory one can derive the following expression for n free magnetic ions in a magnetic field H:

$$M = n g J \mu_B \, B_j(x) \tag{1-2}$$

where $B_j(x) = \frac{2J+1}{2J} \operatorname{ctgh} \left[\frac{(2J+1)x}{2J} \right] - \frac{1}{2J} \operatorname{ctgh} \frac{x}{2J}$

and $x = g J \mu_B H / kT$.

The meaning of the symbols is as follows:

  g is the Landé factor

  μ_B is the Bohr magneton (0.927 x 10^{-20} erg Oe^{-1})

  J is the total angular momentum quantum number.

For $x \ll 1$ we can simplify expression (1-2) and obtain

$$\chi = \frac{M}{H} = n p^2 \mu_B^2 / 3kT \tag{1-3}$$

with $p = g \left[J(J+1) \right]^{\frac{1}{2}}$ (1-4)

defined as the effective number of Bohr magnetons.

Formula (1-3) can be written as $\chi = \frac{C}{T}$ (1-5)

in which the Curie constant is given by $C = n p^2 \mu_B^2 / 3k$ (1-6)

  If we consider paramagnetic ions in a crystal, the situation is more complicated. The crystal field leads to a rearrangement of energy levels. In the ions of the iron group the electrons determining the paramagnetic properties are in the outer shell, the influence of the crystal field is large and the susceptibility can approximately be described by (1-3) with $p = g \lceil S(S+1) \rceil^{\frac{1}{2}}$ (1-7)

in which S is the total spin quantum number, while g is usually not very different from the spin value $g = 2$. The common expression is that the orbital moment has been "quenched" by the crystal field.

For rare earth crystals (1-3) and (1-4) often give a reasonably good approximation, except for Sm^{3+} and Eu^{3+}. The electrons determining the paramagnetic properties are in an inner shell and are less effected by the crystal field than in the case of the iron group. If we substitute for n in formula (1-3) aN in which a is the number of magnetic atoms per molecule and N is Avogadro's number (6.02×10^{23}) X is the susceptibility per mole. The Curie constant per mole will be given by

$$C = a N p^2 \mu_B^2 / 3k \qquad (1-8)$$

By means of (1-8), (1-4) or (1-7) and using the specific weight of the substance we can compute the susceptibility X_v per unit volume.

In table I-1 we have computed the Curie constants per unit volume for some of the substances we have measured (which equals the volume susceptibility at $1^\circ K$, if the specimen still obeys Curie's law at that temperature).

Substance	Curie constant (cm^{-3} deg.)
$Mn(NH_4)_2(SO_4)_2 \cdot 6H_2O$	$20. 10^{-3}$
$Mn(NH_4)_2(SO_4)_2 \cdot 6H_2O$ diluted with Zn 60:1	$0.34. 10^{-3}$
$Cu(NH_4)_2(SO_4)_2 \cdot 6H_2O$	$1.7. 10^{-3}$
$Co(NH_4)_2(SO_4)_2 \cdot 6H_2O$	$9. 10^{-3}$
$Cu SO_4 \cdot 5H_2O$	$3.4. 10^{-3}$
$Gd_2(SO_4)_3 \cdot 8H_2O$	$108. 10^{-3}$

TABLE I-1. Theoretical Curie constants for some paramagnetic salts

Few salts follow Curie's law exactly. A better approximation is given by the Curie-Weiss law

$$X = \frac{C}{T - \theta} \qquad (1-9)$$

The term θ is often composed of several contributions, three important ones are:

1. Deviations from Curie's law which are due to exchange forces
2. Deviations from Curie's law due to splittings of the ground state levels, which can be described to a first approximation by a Curie-Weiss law, as long as the quantity kT is large compared to the splittings concerned.
3. Deviations from Curie's law due to the difference between the local field H_1 and the externally applied magnetic field H_c. This last contribution (θ_3) to θ in (1-9) is in the first approximation given by

$$\theta_3 = (\tfrac{4}{3}\pi - \alpha) C \qquad (1-10)$$

13

assuming a demagnetization factor α can be defined. Formula (1-10) gives the first order correction as worked out by LORENTZ [12], ONSAGER [13], and VAN VLECK [14]. The higher order corrections as calculated by the three authors, are different and for a survey we refer to DE KLERK [15]. For an isotropic sample, the demagnetization factor can only be calculated easily in a few cases. KITTEL [16] lists the following examples.

Shape	Axis	α
Sphere	any	$4\pi/3$
Thin slab	normal	4π
Thin slab	in plane	0
Long circular cylinder	longitudinal	0
Long circular cylinder	transverse	2π

TABLE I-2

1.3 PARAMAGNETIC SPIN-LATTICE RELAXATION

In 1.1 we defined paramagnetic relaxation. If the magnetic field is suddenly increased from H to $H + \Delta H$ the increase of magnetization is sketched in fig. I.1. The long delay needed before the equilibrium value for M is reached is normally due to slow energy transport between the magnetic moments and the lattice vibrations of the crystal.
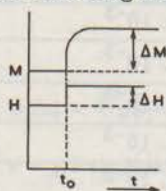
magnetization as a function of time due to a step in H_c

Fig. I-1.

Another way to observe spin-lattice relaxation is by measuring the susceptibility by means of an ac signal, producing a small magnetic field variation, which in general is superimposed on a constant field H_c. If one measures the differential susceptibility, defined as $\frac{dM}{dH}$, one finds that if the measuring frequency is increased, the susceptibility changes. In this thesis we will only consider cases in which the magnetic field H_c, and the variation dH are in the same direction. We measure only the component dM in the direction of H_c. Furthermore we will always mean the differential susceptibility $\chi = \frac{dM}{dH}$ when using the symbol χ.

The two different methods of observing paramagnetic relaxation are linked together by the Fourier-transform, as shown by VERSTELLE [5].

Existing theory about spin-lattice relaxation can be divided into two categories.

1) The thermodynamical theory of CASIMIR and DU PRÉ [17] gives an excellent explanation of several features of spin-lattice relaxation. It describes the relaxation phenomena in the transition range where the magnetization changes in general from an isothermal process to an adiabatic process. Thermodynamically it can be shown that the decrease in the susceptibility (with a constant

14

field H_c present) for a high measuring frequency is due to cyclic heating and cooling of the spin system.

If the magnetic field increases by ΔH, the temperature of the spin system increases, counteracting part of the associated increase in magnetization.

2) The thermodynamic formalism, however, cannot predict the magnitude of the relaxation times and the relation between the relaxation time and the temperature T. WALLER[1] wrote in 1932 the first important theoretical paper on this subject using quantum mechanics. Since then KRONIG, VAN VLECK, ORBACH and others have written several papers and explained or predicted the results of experiments. In section 1.5 we will list some of these theoretical results.

1.4 THE THERMODYNAMICAL THEORY

1.4.1 General theory

In the thermodynamical theory of the spin-lattice relaxation, the main postulate is the internal equilibrium of the spin system at all times considered. This condition will be fulfilled in many cases, but not always, as can also be seen from some of our experimental results.

To describe the phenomena, a system is selected containing only degrees of freedom connected with the magnetic properties of the substance. It is supposed to be separable from the other properties and can have a temperature T_s different from that of the lattice. Thus the heat motion of the lattice is not included in this hypothetical system.

The thermodynamic theory starts with the first law of thermodynamics, written for a magnetic system as:

$$dQ = dE + MdH \tag{1-11}$$

in which E is the enthalpy, called by GORTER the spectroscopic energy, and dQ the heat flow to the spin system. In the simplest model described by the thermodynamical theory the lattice temperature T_L is supposed to be kept constant by the bath and a simple energy contact is supposed to exist between the spin system and the bath (fig. I-2). It is supposed that the heat transfer per second between the spin system and the lattice can be described by

magnetic system $C_H \cdot C_M \cdot T_S$
α
lattice T_L

$$-\frac{dQ}{dt} = \alpha (T_S - T_L) \tag{1-12}$$

BÖLGER[10] introduced:

$$-\frac{dQ}{dt} = \frac{\eta}{T_S} (T_S - T_L) \tag{1-13}$$
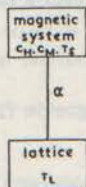
thermodymamic model for description of relaxation

Fig. I-2.

for small fluctuations of T_S around T_L, (1-12) is equivalent to (1-13) with

$$\alpha = \frac{\eta}{T_S} \tag{1-14}$$

The fluctuations are in the actual bridge in the worst case less than $\pm 6\%$ of T during a normal measurement. We will use (1-12) because it simplifies our formulas somewhat. M and H in formula (1-11) take the place of p and V respectively in the standard formulas of thermodynamics if the "spectroscopic energy" is identified with the energy of the system.

We can then write (1-12) as:

$$-\frac{dQ}{dt} = \alpha (T_S - T_L) = -C_H \left(\frac{\partial T_S}{\partial M}\right)_H \frac{dM}{dt} - C_M \left(\frac{\partial T_S}{\partial H}\right)_M \frac{dH}{dt} \quad (1-15)$$

T_S can be eliminated by:

$$\frac{dT_S}{dt} = \left(\frac{\partial T_S}{\partial M}\right)_H \frac{dM}{dt} + \left(\frac{\partial T_S}{\partial H}\right)_M \frac{dH}{dt} \quad (1-16)$$

with C_H and C_M as specific heats of the spin system at constant magnetic field and constant magnetization respectively.

In the measuring procedure we will in general vary H by superimposing on a constant field H_c a field which varies sinusoidally at frequency f. Supposing a linear system, M and T_S can be expected to fluctuate periodically around an equilibrium value M_c and T_L respectively. Substitution of

$$T_S - T_L = \text{Re}\left[\overline{T} e^{j\omega t}\right], \quad M - M_c = \text{Re}\left[\overline{M} e^{j\omega t}\right], \quad H - H_c = \text{Re}\left[\overline{H} e^{j\omega t}\right]$$

with $\omega = 2\pi f$ in (1-15) and (1-16) gives:

$$\alpha \overline{T} = -j\omega \overline{M} C_H \left(\frac{\partial T_S}{\partial M}\right)_H - j\omega \overline{H} C_M \left(\frac{\partial T_S}{\partial H}\right)_M \quad (1-17)$$

and

$$\overline{T} = \left(\frac{\partial T_S}{\partial M}\right)_H \overline{M} + \left(\frac{\partial T_S}{\partial H}\right)_M \overline{H} \quad (1-18)$$

Elimination of $\overline{T}$ gives $\quad \overline{x} = \frac{\overline{M}}{\overline{H}} = \left(\frac{\partial M}{\partial H}\right)_{T_S} \left[\frac{C_M}{C_H} + \frac{C_H - C_M}{C_H} \frac{1}{1 + j\rho f}\right]$

with $\rho = 2\pi C_H \alpha^{-1}$ $\hfill (1-19)$

Defining $F = \dfrac{C_H - C_M}{C_H}$ and with $\overline{x} = x' - jx''$ and $x_0 = \left(\dfrac{\partial M}{\partial H}\right)_{T_S}$

(x_0 can be interpreted as the susceptibility measured in zero magnetic field and with zero frequency) gives

$$\frac{x'}{x_0} = 1 - F + \frac{F}{1 + \rho^2 f^2} \quad (1-20) \quad \text{and} \quad \frac{x''}{x_0} = \frac{F \rho f}{1 + \rho^2 f^2} \quad (1-21)$$

(1-21) can be written in slightly different form

16

$$\log \chi''/\chi_0 = \log F + \log \frac{\rho f}{1 + \rho^2 f^2} \tag{1-22}$$

From expression (1-22) we see that if χ''/χ_0 is plotted on a logarithmic scale against f all absorption curves described by (1-22) have a similar shape. If the frequency f is also plotted on a logarithmic scale the curve is symmetrical around $\rho f = 1$. In fig. I-3 we give the calculated curves of χ'/χ_0 on linear scale and χ''/χ_0 on logarithmic scale for $F = 1$ and $F = 0.4$.

This formalism was developed by CASIMIR and DU PRÉ[17] and if the dispersion χ' and the absorption χ'' can be represented by (1-20) and (1-21) we will say that the curves are good Casimir Du Pré curves (abbreviated by C.d.P. curves). By adding $(\chi'/\chi_0)^2$ and $(\chi''/\chi_0)^2$ as given by (1-21) and (1-22) one can easily prove that χ' and χ'' lie on a semi-circle if plotted in an Argand diagram as shown in fig. I-3 as an insert. We have used this method occasionally to determine ρ if χ'/χ_0 and χ''/χ_0 are known at a single frequency. We will call $\rho = 2\pi C_H/\alpha$ the relaxation time, which is defined as the inverse of the frequency in which the absorption is a maximum and the dispersion is halfway between its initial and final value. Occasionally we call $f = \frac{1}{\rho}$ the relaxation frequency. The dispersion χ'/χ_0 will reach a constant value $1 - F = \frac{C_M}{C_H}$ when the measuring frequency fulfils the condition $\rho f \gg 1$. χ' is then called the adiabatic susceptibility χ_{ad}. By means of the relaxation measurements we are thus able to determine the ratio of two specific heats C_M and C_H.

Casimir_Du Pré relaxation curves for F=0.4 and F=1.0 $\frac{\chi'}{\chi_0}$ (f) on a linear scale, $\frac{\chi''}{\chi_0}$ (f) on a logarithmic scale. Also inserted is an example of an Argand diagram for a C.d.P. relaxation with F=0.7

Fig. I-3.

In the following we will derive a relation between the F-value and between the constant magnetic field H_c. At a temperature where Curie's law still applies (down to 1°K for many salts, depending on the splittings of the energy levels) it can be shown that the magnetic specific heat can be represented by $C_M = b/T^2$. Making use of Curie's law (in the temperature range considered) and by using

$$C_H = C_M - T_S \left(\frac{\partial M}{\partial T_S}\right)_H \left(\frac{\partial H}{\partial T_S}\right)_M$$

17

(similar to the relation between C_p and C_v) we can derive:

$$F = \frac{C H_c^2}{b + C H_c^2} \quad \text{and thus} \quad 1 - F = \frac{b}{b + C H_c^2} \tag{1-23}$$

The value of b/C can easily be computed from the adiabatic susceptibility χ_{ad} by

$$\frac{b}{C} = \frac{H_c^2}{\dfrac{\chi_o}{\chi_{ad}} - 1} \tag{1-24}$$

To determine b/C we computed the value of b/C at a large number (≈ 30) of different fields following formula (1-21), including a diamagnetic correction if necessary and averaged the result to obtain a higher accuracy.

1.4.2 The determination of long relaxation times

   In the preceding section we described the first method to measure relaxation times. For long relaxation times we have used a method similar to the one used by VAN DEN BROEK[8]. The constant magnetic field H_c is changed abruptly by ΔH and the change of the differential susceptibility $\frac{dM}{dH}$ is observed as a function of time with a measuring frequency f such that $f\rho \gg 1$. If the experiment is done we observe the variation of $\frac{dM}{dH}$ on an oscilloscoop and obtain the pattern shown in fig. I-4. We will explain the pattern and compute the value of h and g assuming equation (1-23) to be valid. At a time $t < t_o$ the differential susceptibility is given by:
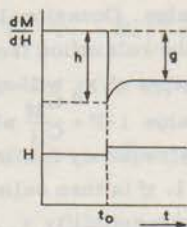
adiabatic susceptibility
as a function of time due to a step in H_c

Fig. I-4.

$$\chi'(t < t_o) = \chi_o(1 - F) = \frac{b}{b + C H_c^2} \chi_o$$

For $t = \sim$ we find $\chi'(t = \sim) \simeq \dfrac{b}{b + C[H_c^2 + 2\Delta H\, H_c]} \chi_o$

and $g = \chi'(t < t_o) - \chi'(t = \sim) = \dfrac{2\Delta H\, b C\, H_c}{[b + C H_c^2]^2} \chi_o$ (1-25)

18

At a time $t_o + \Delta t$ in which $\rho_{ss} \ll \Delta t \ll \rho_{sl}$, ρ_{ss} representing the spin-spin relaxation time required to bring the spin system into internal equilibrium and ρ_{sl} representing the spin-lattice time, the value of the differential susceptibility can be computed from (1-15) and (1-16) and by equating $dQ = 0$ (the spin system can be considered adiabatic if $\Delta t \ll \rho_{sl}$).

$$T_S \,(t = t_o + \Delta t) - T_L = \frac{C_H - C_M}{C_H} \, \Delta H \left(\frac{\partial T_S}{\partial H}\right)_M \qquad (1-26)$$

From the differential equation:

$$-\alpha \,(T_S - T_L) = C_H \left(\frac{\partial T_S}{\partial M}\right)_H \frac{dM}{dt} + C_M \left(\frac{\partial T_S}{\partial H}\right)_M \frac{dH}{dt}$$

and:

$$T_S - T_L = \left(\frac{\partial T_S}{\partial M}\right)_H dM + \left(\frac{\partial T_S}{\partial H}\right)_M dH$$

follows:

$$T_S - T_L = \left(T_S - T_L\right)_{t = t_o + \Delta t} \cdot e^{-\frac{t}{\tau_{sl}}} \qquad (1-27)$$

where

$$\tau_{sl} = \frac{C_H}{\alpha} = \frac{\rho_{sl}}{2\pi}$$

We see that the spin temperature relaxes to its final value T_L with a time constant $\tau_{sl} = \frac{\rho_{sl}}{2\pi}$. The adiabatic susceptibility relaxes with the same time constant and can be observed, giving the value for τ from which the ρ can be computed.

The value to be determined is:

$$\chi'_{ad} = \frac{dM}{dH} \quad \text{at} \quad t = t_o + \Delta t$$

$$(\chi_{ad})_{t_o + \Delta t} - (\chi_{ad})_{t < t_o} = \frac{T_L}{T_S (t = t_o + \Delta t)} \cdot \frac{b}{b + C\,(H_c + \Delta H)^2} \, \chi_o \qquad (1-28)$$

Substitution of (1-26) in (1-28) gives:

$$h = (\chi_{ad})_{t_o + \Delta t} - (\chi_{ad})_{t < t_o} = \frac{3\,\Delta H\, b\, C\, H_c}{[\,b + C\, H_c^2\,]^2} \, \chi_o \qquad (1-29)$$

Comparing (1-29) with (1-25) gives the result that $g = 1.5\,h$, a relation which can be observed in fig. II-30 showing a photograph of an actual relaxation curve. From (1-29) follows that h is proportional to H_c^{-3} for fields large compared to $(b/C)^{\frac{1}{2}}$ and for constant ΔH. From (1-26) we can easily deduce that if

$$H_c > (b/C)^{\frac{1}{2}}$$

$$\frac{T_S - T_L}{T_L} = \frac{\Delta H}{H} \quad \text{for} \quad t = t_o + \Delta t \tag{1-30}$$

Technically it is not easy to keep the ratio $\Delta H/H$ constant for large fields, a fast field change costs a relatively large effort. Even if (1-30) were fulfilled, the sensitivity of this method is inversely proportional to H_c^{-2}.

1.4.3 Extension of the thermodynamic theory

In some cases the Casimir-Du Pré formalism gives a good description of the experimentally observed relaxation curves. Often mainly at low temperatures, however, the curves obtained are more complicated. Several models have been proposed to describe these cases. In one model the lattice has not always the same temperature as the bath, an extra heat resistance between the lattice and the bath is postulated and it can be shown that more complicated relaxation curves can be expected. EISENSTEIN [18] refined this model by dropping the assumption that the temperature in the sample is uniform and by introducing a finite heat conductivity.

In $Cu K_2 Cl_4 . 2H_2O$ VAN DEN BROEK [8, 19] found experimentally extremely broadened relaxation curves, the broadening being due to a non-uniform temperature in the sample, not equal to the bath temperature. The regions of the sample in good heat contact with the bath will have the shortest relaxation time; the relaxation time ρ_{hf} defined by

$$\rho_{hf} = \lim \frac{\chi''(f)}{f[\chi'(f) - \chi_{ad}]} \tag{1-31}$$

will be close to the spin-lattice relaxation time of these regions and will approach the true relaxation time at the bath temperature.

FUOSS and KIRKWOOD [20] postulate a distribution of relaxation times. For a given distribution, it is always possible to compute the associated relaxation curves, the inverse procedure is difficult and no general method seems to be available.

We will not discuss in detail the models introduced to describe complicated relaxations. Both VAN DER MAREL [7] and VAN DEN BROEK [8] have described them in some detail.

In all the systems considered one finds, that for a given F-value the top of the absorption curve and the slope S of the dispersion curve are less than the associated values given by Casimir-Du Pré.

To describe the deviation of a set of relaxation curves from true C.d.P. curves VAN DEN BROEK [8] introduced a deviation parameter

$$d^* = \frac{(1 - 2h/F) + (1 - S/1.15F) \times 0.69}{2} \tag{1-32}$$

in which h is the value of the maximum absorption χ''/χ_o as a function of the frequency and S is the slope of the dispersion curve at a value of χ'/χ_o halfway between χ'_o and χ'_{ad}.

1.5 SURVEY OF THE THEORETICAL PREDICTIONS FOR SPIN-LATTICE RELAXATION TIMES

The interaction between the spin system and the crystal has been discussed in many papers by several authors. WALLER [1], in the first important paper on this subject (1932), studied the interaction between the phonons and the magnetic moments. In this study he identifies two different processes for energy transfer between the spin system and the lattice:

1. The direct processes in which an energy quantum $\hbar\omega$ is exchanged with the lattice, associated with a change of occupation of two Zeeman levels, governed by $\hbar\omega = \pm \Delta E$ (1-33)
   This gives rise to a change of the magnetization M.
2. The indirect processes or quasi Raman processes in which the magnetic ion relaxes by emission of an (virtual) energy quantum $\hbar\omega_1$ with simultaneously an absorption of a quantum $\hbar\omega_2$ governed by the energy balance $\hbar(\omega_2 - \omega_1) = \Delta E$ (1-34)

The spin-lattice relaxation times calculated by WALLER were extremely long and the mechanism he proposed (modulation of the magnetic interaction between different magnetic ions) is presently considered not to be the most effective one. HEITLER and TELLER [21] and also FIERZ [22] considered the effect of the phonons on the electrical splittings of the basic energy levels but also failed to obtain values for the spin-lattice relaxation time in agreement with experimental results. KRONIG [23] and VAN VLECK [24], taking into account excited levels, studied and made detailed calculations on processes in which the main mechanism in the spin-lattice relaxation is the interaction between the orbital momentum and the phonons, which modulate the electric field; this influences the spins through the spin-orbit coupling.

More recently ORBACH [25, 26, 27, 28] made calculations using a somewhat different mathematical approach and obtained predictions similar to those of VAN VLECK, but stated them in a more general form. In his calculations ORBACH computed also the effectiveness of a two phonon process, referred to as an Orbach process, not taken into consideration by VAN VLECK. The general condition for this process is the presence of excited levels with an energy spacing Δ to the lowest set of levels, while $\Delta < k\theta_D$ (θ_D representing the Debye temperature). Calculations for $kT \ll \Delta$ give a relaxation time depending exponentially on the temperature. In the predictions for the relaxation time a distinction is made between Kramers and non-Kramers salts. A Kramers salt is generally defined as a salt with an odd number of electrons in the electron shell,

responsible for the paramagnetism. KRAMERS[29] showed that in this case the internal field can split the $2J + 1$ levels of a ground state at most in half that number of Kramers doublets which can only be split by a magnetic field. The main theoretical predictions are summarized in table I-3.

	Direct process	Indirect process $(T \ll \theta_D, \ T \ll \frac{\Delta}{k})$	$T \gg \theta_D$
Kramers salts	dH^4T	$a \exp(-\Delta/kT) + bT^9$	eT^2
Non-Kramers salts	dH^2T	$a \exp(-\Delta/kT) + bT^7$	eT^2

TABLE I-3 General theoretical predictions for ρ^{-1}, the inverse of the spin-lattice relaxation time following VAN VLECK and ORBACH; a, b, d and e are constants having a weak field dependency.

For the quasi Raman processes the expected field dependencies can, in practice, be described by the BRONS-VAN VLECK[30] relation:

$$\rho = \rho_0 \frac{b + C H_c^2}{b + pC H_c^2} \tag{1-35}$$

The coefficient p is usually in the range from 0.2 - 0.7. In some cases 0.5 is predicted. Direct and indirect processes operate in parallel. At very low temperatures the direct process dominates. Above a certain transition temperature the indirect process is more efficient, this transition point between the direct and the indirect process can be expected to be at or above helium temperatures and below hydrogen temperature.

Table I-3 contains the generalized predictions and several exceptions can be found. ORBACH assumes, in his calculations for Kramers salts, a single doublet to be populated. In salts with a spin multiplet or with more than one populated doublet the situation is more complicated. In that case ORBACH and BLUME[31] expect, besides a T^{-7}, also a T^{-5} relationship in the Raman process if certain conditions about the size of the splittings are fulfilled. For S-state ions, calculations using higher order perturbations are needed. BLUME and ORBACH[32] expect for the direct process for Mn^{2+} in a cubic environment $\rho^{-1} \propto H^2T$. The same general result is expected by LEUSHIN[33,34] who calculates $\rho^{-1} \propto H^2T$ for a direct process and $\rho^{-1} \propto T^7$ at $T \ll \theta_D$ for a two phonon process. For a Raman process ORBACH[26] also indicates the possibility of a H^2T^7 instead of the T^9 relationship for ρ in a Kramers salt, depending on the energy spacings between a populated doublet and higher excited doublets. It should be pointed out that the formulas for the relaxation time are nearly always simplifications of more complicated formulas. The transition between the T^9 or T^7 and the T^2 relationship for ρ^{-1} in the Raman region goes gradually and is described by the term

22

$$\rho^{-1} \propto \int_0^{k\theta} \frac{\delta_1^n \cdot e^{\delta_1/kT}}{(e^{\delta_1/kT} - 1)^2} \, d\delta_1 \tag{1-36}$$

(see VAN VLECK[24]) with n = 8 and n = 6 respectively. A tabulation of this function is given by ZIMAN[35]. We have plotted the tabulated values on a double logarithmic scale (not in this thesis) and determined graphically the slope $\alpha_n = \rho T \frac{d\rho^{-1}}{dT}$ of the log ρ - log T curve at several values of T/θ_D.

T/θ_D	0.1	0.2	0.3	0.4	0.5	0.8	1.0
α_8	7.3	4.8	3.5	2.8	2.6	2.2	2.0
α_6	6.2	4.4	3.3	2.7	2.5	2.2	2.0

TABLE I-4. α_n as a function of T/θ_D.

Although no claim is made for the accuracy of these numbers, the table I-4 shows clearly that e. g. a T^9 relationship only can be expected for very small ratio's of T/θ_D. If a Debye temperature of 200°K is assumed we see that the T^9 relationship degenerates into a $T^{7.3}$ dependency near 20°K. Detailed calculations, giving a prediction for the magnitude of spin-lattice relaxation time in specific salts, are lengthy and difficult and have only been made in a few cases.

In all the theoretical calculations mentioned so far, it has been assumed that the phonons are and stay in perfect thermal contact with the bath. VAN VLECK[36] remarked in 1941 that, at low temperatures where a direct process prevails, only a narrow band of phonons is in contact with the spin system. If the heat transfer between the phonons and the bath is slow, the energy of the spin system can heat up the phonon system. The subject was brought up again in 1955 by GORTER, VAN DEN BROEK and BÖLGER[37] and more recently by SCOTT and JEFFRIES[38], who discussed it in more detail. Effectively a second relaxation process acts in series with the spin-lattice relaxation process, increasing the apparent relaxation times. If the phonon-bath relaxation time is long compared with the spin-lattice relaxation time, the term phonon-bottleneck applies. Bottleneck effects can be expected in the very low temperature regions where direct processes prevail, and $\rho^{-1} \propto T^2$ is expected.

At temperatures above and at the hydrogen range a satisfactory agreement between predictions and experimental results has been observed. At low temperatures the agreement has been poor in general (VAN DER MAREL[7] and VAN DEN BROEK[8]). The occurrence of Orbach processes has been demonstrated in rare earth ions by several investigators amongst others ORBACH et al[28], SCOTT and JEFFRIES[38], VAN DEN BROEK and VAN DER MAREL[39], direct processes are occasionally identified but in the majority of the measurements at low temperatures on ions of the iron group the results could not be explained in a satisfactory manner and the field and temperature dependence of a direct process have rarely been observed. By taking bottleneck processes into account the

experimental results could in some cases be described somewhat better, but relaxation times were often observed to increase upon diluting paramagnetic salts which was in complete contradiction with the expectations. VAN VLECK[36, 40] mentioned the possibility of "relaxation centers" formed by fast relaxing impurity ions or due to irregularities in the crystal. In the latter case the ion could have an unusually effective Stark-splitting such that large quanta could be transported to and from the lattice or the irregularity could produce relatively low lying electronic levels, increasing the effectiveness of a Raman process.

The magnetic ions close to this irregularity of the crystal could also have large exchange interactions, depending strongly on the distance and thus sensitive to lattice modulation. Such "exchange pockets" could form effective "relaxation centers". These "relaxation centers" would in certain cases bypass the bottleneck condition if spin-diffusion and cross-relaxation processes are able to transport the energy from the other magnetic ions to the relaxation centers. Several experiments showing the effect of impurities have been carried out, for a survey we refer to BÖLGER[9], who discussed the effect of impurities in detail.

1.6 SPIN-SPIN RELAXATION PROCESSES

The main part of this thesis deals with spin-lattice relaxation. In a few cases we detected spin-spin relaxation phenomena and in the explanation of some of our experimental results we have to introduce cross-relaxation processes to understand some experimental results. A detailed introduction of spin-spin phenomena is beyond the scope of this thesis and we will only mention a few sources of information.

WALLER[1] in his article made an estimate of the time needed to obtain equilibrium in a paramagnetic salt in the absence of an external magnetic field through the dipole-dipole interaction and calculated a characteristic time of the order of $\hbar/g\mu_B H_i$ where $g\mu_B H_i$ gives the order of the dipole-dipole interaction. For $H_i = 500$ Oe a value of 10^{-10} sec can be computed for the spin-spin relaxation time which later was shown to be the correct order of magnitude.

KRONIG and BOUWKAMP[41] predicted in 1938 the dependency of the relaxation time in a magnetic field H_c and obtained by simple reasoning:

$$\rho_{ss} = \rho_o \exp \frac{H_c^2}{H_o^2} \tag{1-37}$$

For ρ_o they used the same value as used by Waller ($\rho_o = \hbar/g\mu_B H_i$) while for H_o they found a value of the order of the internal field due to the dipole-dipole interaction. The symbol ρ_{ss} represents the spin-spin relaxation time. VERSTELLE[5] and LOCHER[42] found experimentally that spin-spin relaxation

phenomena in high magnetic fields can be described quite well by a formula of this type. Deviations occur at low values of the magnetic field.

CASPERS [43] in a much more elaborate manner, taking exchange influences into account also, obtained the same general result and was able to express the quantities ρ_0 and H_0^2 in terms of parameters of the crystal, obtaining a fair agreement between experiments and theory in the case of ammonium copper tutton salt. TJON [44] has also made quantum mechanical calculations of spin-spin relaxation phenomena. The formula he calculates for the relaxation time of copper ammonium tutton salt is somewhat different to that of CASPERS.

In the thermodynamic theory of Casimir-Du Pré for spin-lattice relaxation the internal equilibrium of the spin system is postulated. As will be shown in chapter 3, this condition is not always experimentally fulfilled. If the spin-spin interaction fails to produce equilibrium within the spin-lattice relaxation time, one can consider the system as a system of more or less independent spins as treated by GORTER and KRONIG [96] in 1936.

In some experimental work to be described we show the results of measurements on paramagnetic crystals with impurities added. The interaction processes which try to establish equilibrium in the spin system and the transport of energy therein, to and from different ions in the paramagnetic substance will fall under the general term of cross-relaxation processes, a term fairly recently introduced by BLOEMBERGEN [48]. After the appearance of another paper by BLOEMBERGEN, SHAPIRO, PERSHAN and ARTMAN [45], a large number of contributions have been made by several authors. We refer for a more complete listing to a review article by BLOEMBERGEN and PERSHAN [46] in 1961 and to a recent article by GRANT [47] (1964).

Transport of Zeeman energy over a certain distance in the lattice is possible by means of spin diffusion. BLOEMBERGEN [97] has (originally for nuclear spin diffusion) derived an expression for the diffusion coefficient for a simple cubic lattice with $S = \frac{1}{2}$ and finds for an order of magnitude for the diffusion coefficient

$$D \approx \frac{a^2}{8\,\rho_{ss}} \tag{1-38}$$

a representing the lattice constant and ρ_{ss} the spin-spin relaxation time.

1.7 SALTS USED FOR PARAMAGNETIC EXPERIMENTS

To fulfil the requirement that the magnetic dipoles should be substantially independent of their neighbors in a normal paramagnetic substance, salts are often selected with a relatively large spacing between the paramagnetic ions. Either salts containing several diamagnetic atoms or molecular groups can be used or a large percentage of the paramagnetic ions can be replaced by ions of a not too different ionic radius, but with completely occupied electronic shells

(i.e. Zn^{2+} can replace Mn^{2+}).

Most of our experiments have been done on tutton salts and we will give a short description of their structure. The general formula of the tutton salts is $M'' M'_2 (S^O O_4)_2 \cdot 6H_2O$ in which M'' is a divalent cation (Cu^{2+}, Mn^{2+}, Co^{2+} or any divalent ion of the 3d group), M' is a monovalent cation (K^+, Rb^+, $(NH_4)^+$, Cs^+) and in which the S^O in the $(S^O O_4)$ group can be either S or Se. Not all combinations exist at room temperatures. With Cu^{2+}, the tutton salts with Cs^+, K^+, $(NH_4)^+$ and Rb^+ are known, with Mn^{2+} the NH_4 tutton salt is well known while the K tutton salt is not reported to exist at room temperature. The crystal structure is monoclinic; $Mg(NH_4)_2(SO_4)_2 \cdot 6H_2O$ has been described in detail by HOFFMAN[49].

Each unit cell contains two molecules, the divalent cations (to which may belong the paramagnetic ions in the salts studied by us) are surrounded by a distorted octahedron of 6 water molecules. The ions are equivalent but not equal and are indicated by the indices I and II. The surroundings of the magnetic ions are often described as having approximately a tetragonal symmetry with a symmetric axis Z, making an angle α with the ac plane (a, b, and c are the crystallographic axes). The magnetic axes X_I, Y_I, Z_I of one complex are the mirror image in the ac plane of the X_{II}, Y_{II}, Z_{II} axes. The susceptibility of one complex along the Z axis is $\chi_{/\!/}$, the susceptibility perpendicular to the Z axis is assumed to be isotropic and is represented by $\chi_\perp$. The magnetic properties of the complete unit cell can be described by three mutually perpendicular magnetic symmetry axes K_1, K_2, K_3. The projection of Z on the ac plane forms the K_1 or the K_2 axis (the K_1 axis is defined as having a larger susceptibility than K_2). The K_3 axis is equal to the crystallographic b-axis, ψ is the angle between K_1 and c measured in the sense which makes the angle between a and c obtuse. The following formulas can be derived, in which χ_1, χ_2 and χ_3 are the susceptibilities along the K_1, K_2, and K_3 axes:

$$\chi_1 = \chi_{/\!/} \cos^2\alpha + \chi_\perp \sin^2\alpha$$
$$\chi_2 = \chi_\perp \qquad\qquad\qquad\qquad (1-38)$$
$$\chi_3 = \chi_{/\!/} \sin^2\alpha + \chi_\perp \cos^2\alpha$$

1.8 SURVEY OF THE PROPERTIES OF SOME MAGNETIC IONS

In this section we will give a short survey of the magnetic ions used in our experiments and some data (if available) about these ions in specific crystals. Most of the data have been obtained from the survey articles of BLEANEY and STEVENS[50] and BOWEN and OWEN[51].

1.8.1 Elements of the iron group

a) Mn^{2+}; $3d^5$; $^6S_{5/2}$

The manganese ion is a fairly special ion. The symbol $3d^5$ indicates that it has 5 electrons in the 3d shell, this makes the free ion an S-state ion (shell half filled), with no resultant orbital angular momentum. The g-factor is close to the free-spin value. The lowest level in the free ion is an orbital single state with a six-fold spin degeneracy.

In the hydrated salts, the electric field splits the sextet into three Kramers doublets with a small separation. In the manganese tutton salt the separation is of the order of 0.1 cm^{-1} (BLEANEY and INGRAM[52]), the salt follows Curie's law to below 1°K. The contributions of the dipole-dipole, exchange and nucleus-electron interactions and zero field splittings to the specific heat are not exactly known. For a discussion on this subject we refer to LOCHER[42]. The spin-lattice relaxation time is expected to be long, because of the small interaction of the spin system with the crystalline electric field (S-state ion). This is also experimentally found.

b) Co^{2+}; $3d^7$; $^4F_{9/2}$

A cubic field leaves a triple state as a lowest level. This triple state with a fourfold spin degeneracy is split into 6 Kramers doublets by the combined effect of the spin-orbit coupling and a tetragonal or trigonal field. The g-value of the lowest Kramers doublet is highly anisotropic with $g_{//}$ between 5.5 and 7 and $g_\perp$ between 2.5 and 3.5. In the tutton salt only this doublet is populated at low temperatures, giving the salt an effective spin $S' = \frac{1}{2}$. ABRAGAM and PRYCE[53] indicated (with reserve) a second doublet above this one at about 245 cm^{-1}. This relatively low energy makes the occurrence of an Orbach process, with a relaxation time depending exponentially on the temperature possible. VERSTELLE[5] found relatively short spin-lattice relaxation times at hydrogen temperatures ($\rho = 0.4\,\mu sec$ at 20°K). For more details we refer to chapter 3 and 4 of this thesis.

c) Fe^{2+}; $3d^6$; $^5D_4$

Fe^{2+} has an even number of electrons and the level degeneracy can be completely removed by spin-orbit coupling and a crystalline field of low symmetry. A cubic field makes an orbital triple state lowest with fivefold spin degeneracy. A rhombic field can split this into five single levels.

Not much is known about salts containing Fe^{2+}. TINKHAM[54, 55] studied resonance of Fe^{2+} in ZnF_2. No spin-lattice relaxation measurements done on Fe^{2+} salts are known to us; on the basis of the calculated scheme of energy levels short relaxation times may be expected.

d) Ni^{2+}; $3d^8$; $^3F_4$.

A cubic field leaves an orbital single state lowest, the triple spin degeneracy being split into a single and a double level in a trigonal or tetragonal field, but into three single levels in a rhombic field. Ni^{2+} has, as has Fe^{2+}, an even number of electrons in the paramagnetic shell and the degeneracy can be completely removed by an electric field. Nickel tutton salts, including ammonium nickel tutton salt have been studied by GRIFFITHS and OWEN[56] who find $g = 2.25$ and the spin triplet splits into three single levels with an overall separation of the order of only 3 cm^{-1}. Some initial relaxation measurements on $Ni(NH_4)_2(SO_4)_2 \cdot 6H_2O$ have been reported by BROER, DIJKSTRA and GORTER[57]. They find at $T = 77^\circ K$ $\rho \approx 10^{-7}$ sec with an estimated b/C of 90 $(kOe)^2$. It is expected that the relaxation times stay relatively short at lower temperatures due to the zero field splittings.

e) Cu^{2+}; $3d^9$; $^2D_{5/2}$.

The orbital levels split by a cubic field into an upper triple state and a lower double state. In a tetragonal or rhombic field this double state is further split into two Kramers doublets. In the tutton salts the g-value of the lowest doublet is anisotropic with $g_{//} = 2.4$ and $g_{\perp} = 2.1$. For more details on copper tutton salts we refer to chapter 3 and 4 of this thesis.

1.8.2 Rare earth elements

The diagrams of the energy levels of the rare earth salts are basically different from the iron group salts. The effect of the crystal field is relatively reduced, the Russell-Saunders coupling holds, $J = L + S$ (or $J = L - S$) is a good quantum number. The splittings produced by the crystal field are of the order of 10 cm^{-1} - 100 cm^{-1} and crystal fields of low symmetry will split the levels into singlets for an even number of electrons in the 4f shell and doublets for an odd number of electrons. The occupation of the levels will vary with temperature and the susceptibility will often not obey Curie's law.

a) Gd^{3+}; $4f^7$; $^8S_{7/2}$.

Gadolinium is an S-state ion and similarly to the manganese ion, long spin-lattice relaxation times have been found. The energy level splittings of $Gd_2(SO_4)_3 \cdot 8H_2O$ have been studied lately with a resonance technique by BOGLE and SYMMONS[58]. Their conclusion is that the ground state level is split by the crystal field into four doublets with a spacing of respectively 0.222, 0.271 and 0.380 cm^{-1}, giving a total splitting of 0.873 cm^{-1}.

b) Dy^{3+}; $4f^9$; $^6H_{15/2}$.

Several paramagnetic salts containing dysprosium have been examined. Dysprosium salts are Kramers salts and an electric field of low symmetry will

split the ground state into 8 Kramers doublets. No data are available on dysprosium sulphate, but dysprosium ethyl sulphate has been extensively studied (VAN DEN HANDEL[59], COOKE[60] et al, GRAMBERG[61] and other workers. The susceptibility is reported to be highly anisotropic, for the lowest Kramers doublet $g_\perp \approx 0$ and $g_{//} = 10.76$ as reported by GRAMBERG[61]. The same author indicates 5 doublets at about 0, 16, 20, 59, and 68 cm^{-1} at $58^\circ K$. Relaxation measurements on this salt have been reported by VAN DEN BROEK and VAN DER MAREL[39] and by ORBACH[26]. An Orbach process has been calculated and measured with $\rho^{-1} \approx 0.2 \times 10^7 \exp(-23/T)$.

CHAPTER 2

DESIGN OF A MEASURING SYSTEM FOR THE MEASUREMENT OF PARAMAGNETIC RELAXATION IN THE FREQUENCY RANGE BETWEEN 200 Hz AND 1 MHz

2.1 PURPOSE

The purpose of the measurements is the determination of the magnetic susceptibility of crystals, powders or other samples. The magnetic susceptibility is often measured by either inserting a sample in a coil and measuring the increase of inductance and of losses for this coil, or by inserting this sample in a system of coils and measuring some quantity associated with the magnetic properties of the sample e.g. magnetic coupling.

In paramagnetic measurements the increase of inductance of a coil is small and in the following design our goal was to be able to detect variations of inductance of the order of 10^{-7}, while the maximum variation that could be expected was of the order of 10^{-2}.

2.2 MEASURING METHOD

Inductances are nearly universally measured by means of bridge-circuits.

The requirements we have for the sensitivity and accuracy of the measurements are different from those usually obtainable by means of standard bridges.

In a standard bridge it is usually desirable to measure a certain quantity with an absolute accuracy in the order of $10^{-2} - 10^{-3}$ in a certain frequency range. It is often necessary to be able to express the unknown easily into the elements of the bridge, this requires bridge elements of high purity.

For the measurements of paramagnetic relaxation the requirements are different. The value of the magnetic susceptibility is small and if we insert the sample in a coil, the coil inductance will vary only slightly ($< 10^{-2}$).

30

Therefore the bridge has to be extremely stable, such that variations of the bridge itself are not larger than the effects to be obtained.

An accuracy of 1% is sufficient in many cases. This means in this case that a variation of the magnetic effects of a sample of 1% should be detected if an outside parameter (for instance magnetic field) is varied.

These and other considerations prompted us to follow a different approach from the usual one for standard bridges. This approach is mainly applicable if one of the elements in a bridge changes by only a small amount e.g. < 1%.

For the initial description of the apparatus it will be sufficient to assume that if a paramagnetic sample is inserted in a coil with an original inductance L_o, the inductance will change to

$$L_1 = L_o (1 + 4\pi q \chi), \text{ where } \chi = \chi' - j\chi'' \qquad (2-1)$$

and q denotes the filling factor. The complex χ has a definite meaning in all expressions for the impedance of L_1 in the complex notation. If the coil has an ohmic series resistance R_s, the impedance of the coil with the sample inserted will be

$$R_s + j\omega L_1 = R_s + \omega L_o . 4\pi q \chi'' + j\omega L_o (1 + 4\pi q \chi') \qquad (2-2)$$

We see that in this expression a positive χ' (paramagnetic sample) will increase the inductance and the losses of the coil will increase due to χ''.

If one employs a bridge in the usual way, it would be balanced with a coil in one of the branches and the parameters noted down. A sample is inserted in a coil and the bridge balanced again and the new parameters combined with the old set give sufficient information to determine the magnetic properties of the sample.

In the approach described here, we have means for balancing the bridge approximately and also means to measure accurately the bridge output.

The bridge is balanced without a sample and the residual bridge output is noted down. After insertion of the sample the bridge output voltage is again measured and the difference of the output voltages is related to the magnetic properties of the specimen.

In measuring paramagnetic relaxation the absolute value of the magnetization is not of direct importance. The important quanties are $\frac{\chi'}{\chi_o}$ and $\frac{\chi''}{\chi_o}$.

These quantities can be determined by computing the ratios of two magnetic effects.

One direct advantage of this method is that it is not necessary to calibrate the variable elements of the bridge or to have elements with a high purity. The only requirement is to be able to balance the bridge so that the residual output is of the same order as the observed effect, otherwise overloading of the amplifiers may result.

In paragraph 2.3 it is shown that the bridge output voltage depends linearly on the variation of one of its elements as long as the variation is smaller

than 1%.

As is indicated, purity of elements is of no concern, which is a large advantage for a bridge operating over a wide frequency range. The emphasis can therefore be placed on stability of the elements of the bridge.

Besides variations of elements, one has in practice a certain amount of variations of the measuring frequency.

The effect of frequency variations on the equilibrium varies in different bridges. In a frequency independent bridge, the detector output is in first approximation independent of the measuring frequency, three examples are indicated in fig. II-1.
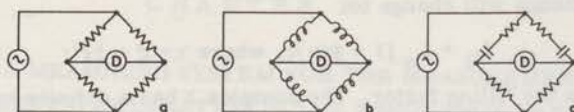
Three examples of frequency independent bridge.

Fig. II-1.

In a frequency dependent bridge the output depends strongly on the measuring frequency. A resonant bridge is an example of this and is indicated in fig. II-2.

It can be remarked that a completely frequency independent bridge is very difficult to construct e.g. if one of the condensors in the bridge indicated in fig. II-1 contains a parallel resistor the bridge ceases to be frequency independent.

$$R_1 R_4 = R_2 R_3$$
$$\omega L = \frac{1}{\omega C}$$
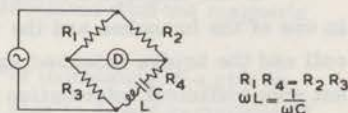
Example of a frequency dependent bridge

Fig. II-2.

It is logical that a frequency independent bridge is desired if high stability is necessary. In the resonant bridge one would have to stabilize the frequency to 5.10^{-8} to obtain a detector stability of 10^{-7}.

This reason prompted us to select a frequency independent bridge, or better said, we tried to approximate one.

Another advantage of a frequency independent bridge is that second and third harmonics are not enhanced in the bridge. For the detector circuits it is easier, if the ratio between second and higher harmonics compared with the basic signal is as low as possible. A bridge which is in equilibrium for all frequencies will have this property.

Before we give a general description of the detector circuit it is necessary to give a more detailed description of the adopted measuring technique and a general description of the bridge.

32

2.3 INITIAL DESCRIPTION OF THE MEASURING BRIDGE

The bridge used, is basically a Wheatstone bridge, each arm with a coil as its major element, shown in fig. II-3. The coils L_3 and L_4 are would on a common glass cylinder and are located inside a cryostat. In the introduction, the measurement of the magnetic properties was supposed to be accomplished by inserting the sample into one of the coils of the bridge. In the actual bridge the sample is moved from coil L_3 to coil L_4 and from the difference of unbalance of the bridge one can compute χ' and χ''.
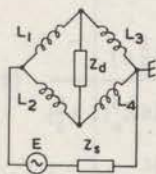
simplified diagram of bridge

Fig. II-3.

The output due to the sample will be doubled by this procedure. The coils L_3 and L_4 are wound such that a magnetic field common to both coils will produce no output signal in the detector (see fig. II-22).

The sample is cooled to low temperatures by means of liquid hydrogen or helium.

The coils L_1 and L_2 are at room temperature and are contained in a box which houses the other elements used to balance the bridge more accurately. L_1 and L_2 and also L_3 and L_4 are made equal as closely as possible, but it is technically difficult to make the elements such that a balance better than 1% is obtained. Variable elements to obtain a better balance will be described in paragraph 2.7.

We will first analyze a principle limitation of the bridge. As was indicated in the introduction, the output signal of a bridge is in the first approximation a linear function of the variation of one of the elements, as long as the variation is not too large.

This statement is correct in general, but not in all cases. In the following analysis we will study the properties of a simplified form of the particular bridge, calculate its linear range and indicate under which conditions the linearity does not hold.

For this analysis we will suppose that the bridge consists of 4 arms, three of them identical with an impedance Z, the fourth arm deviating by a small amount δ from this value (fig. II-4). The detector and source impedances are $\bar{Z}_d$ and $\bar{Z}_s$ respectively.

Thevenin's theorem states that the current through the detector branch $\bar{Z}_d$ can be found by means of the equivalent circuit of fig. II-4. E' is the voltage between A and B if the impedance $\bar{Z}_d$ is disconnected and $\bar{Z}_i$ is the impedance between the points A and B if the voltage source E is shorted and the impedance $\bar{Z}_d$ is disconnected.
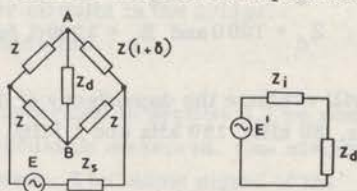
Bridge and associated equivalent circuit

Fig. II-4.

33

Calculations give:

$$\bar{E}^1 = -\frac{\delta\,\bar{Z}\,\bar{E}}{4\bar{Z}(1+\frac{\delta}{2}) + 4\bar{Z}_s(1+\frac{\delta}{4})} \tag{2-3}$$

$$\bar{Z}_i = (\bar{Z}+2\bar{Z}_s)\,\frac{4\bar{Z}^3(1+\frac{3}{4}\delta) + 12\bar{Z}^2\bar{Z}_s(1+\frac{5}{6}\delta) + 8\bar{Z}\,\bar{Z}_s^2(1+\frac{1}{2}\delta)}{4\bar{Z}^3(1+\frac{1}{2}\delta)+20\bar{Z}^2\bar{Z}_s(1+\frac{9}{20}\delta)+32\bar{Z}\,\bar{Z}_s^2(1+\frac{7}{16}\delta)+16\bar{Z}_s^3(1+\frac{\delta}{4})} \tag{2-4}$$

These expressions for $\bar{E}^1$ and $\bar{Z}_i$ can be substituted in:

$$\bar{I}_d = \frac{\bar{E}^1}{\bar{Z}_i + \bar{Z}_d} \tag{2-5}$$

to give the full expression for the detector current $\bar{I}_d$.

From (2-3) we see that the variation in the expression for E' yields an output proportional to δ, but that terms such as $(1+\frac{\delta}{2})$ disturb the linearity.

One has to substitute actual values of circuit elements to be able to calculate the non-linearity. By doing this one sees that only a few terms in the expression (2-4) have significant values.

Under certain conditions equation (2-3) shows that the linearity is strongly affected.

If in (2-3) $\bar{Z} = -\bar{Z}_s$, (2-3) becomes $\bar{E}^1 = -\frac{\delta\,\bar{Z}\,\bar{E}}{\bar{Z}\frac{\delta}{4}} = -4\bar{E}$ \hfill (2-6)

This could happen if for instance the $\bar{Z}$'s consisted of coils L_1 and $\bar{Z}_s$ was a condensor C_1 such that $\omega L_1 = \frac{1}{\omega C_1}$ \hfill (2-7)

We see that resonance between the bridge elements and the source impedance of the generator affects the linearity and should be avoided.

To calculate the accuracy we will assume the following conditions which approximate the actual bridge values:

$\bar{Z} = (0.05 + j\omega\,0.04)\,\Omega$

$Z_d = 1\,\Omega$ and $Z_s = 30\,\Omega$ \quad for \quad $1\,kHz < f < 30\,kHz$

$Z_d = 100\,\Omega$ and $Z_s = 2000\,\Omega$ for $30\,kHz < f < 1\,MHz$

We will evaluate the dependency of I_d on δ for the following frequencies: 1 kHz, 5 kHz, 30 kHz, 150 kHz and 1 MHz. The results are indicated in table II-1.

34

Frequency	I_d proportional to	Conditions
1 kHz	$\delta \left(1 - \frac{\delta}{4}\right) E$	$Z_d = 1\,\Omega$
5 kHz	$\delta \left(1 - \frac{\delta}{2}\right) E$	$Z_s = 30\,\Omega$
30 kHz	$\delta \left(1 - \frac{\delta}{2}\right) E$	
30 kHz	$\delta \left(1 - \frac{\delta}{4}\right) E$	$Z_d = 100\,\Omega$
150 kHz	$\delta \left(1 - \frac{\delta}{4}\right) E$	$Z_s = 2000\,\Omega$
1 MHz	$\delta \left(1 - \frac{\delta}{2}\right) E$	

TABLE II-1. Evaluation of linearity of bridge circuit.

From these evaluations we can conclude that in the worst case calculated I_d is proportional to $\delta (1 - \delta/2)$ instead of being proportional to δ.

This result is expressed in the table II-2.

δ	$\delta \left(1 - \frac{\delta}{2}\right)$
0.001	$0.9995 . \delta$
0.01	$0.995 \ . \delta$
0.1	$0.95 \ . \delta$

TABLE II-2. Linearity of the bridge.

This shows that the deviation from linearity is $\frac{1}{2}\%$ if a sample with a δ of 0.01 is used. Only a sample with a strong magnetic effect would have a value of $\delta = 0.01$. If a higher accuracy is desired a smaller sample should be taken.

2.4 DETECTOR CIRCUIT

If one wants to measure very small variations, a good signal to noise ratio is desirable to produce a usable signal for the detector. Three means can be employed to obtain this result.

a) Application of a large signal to the bridge.
b) The use of low-noise components or circuits in the bridge.
c) A detector circuit with a narrow bandwidth.

By adopting the measuring technique described in section 2.2 we added the requirement that the output of the bridge could be measured. One simple amplitude measurement is not sufficient however. The output signal of the bridge contains two components, one component due to a variation of the inductance of the coil, another due to the variation of the losses of the coil, indicating an absorption by the sample.

These components will have a phase difference of $\frac{\pi}{2}$ as is illustrated in the following example. Assume for simplicity in fig. II-3: $Z_s = 0$, $Z_D = \infty$, $L_1 = L_2 = L_4 = L_0$ and $L_3 = L_0(1 + 4\pi q \chi)$. If $\overline{V}_D$ represents the voltage across the detector one can compute

$$\overline{V}_D = \frac{2\pi q \chi}{2 + 4\pi q \chi} \overline{E}$$

If $|4\pi q \chi| \ll 1$

$$\overline{V}_D \approx \pi q \chi \overline{E}$$

$$\overline{V}_D \approx \pi q (\chi' - j\chi'') \overline{E} \tag{2-8}$$

From this expression one sees that $\overline{V}_d$ consists of two components in quadrature, one containing χ' and the other containing χ''. It can be shown that inclusion of $\overline{Z}_s$ and $\overline{Z}_d$ does not affect this property.

The separate measurements of these components can be done with a synchronous detector.

As the exact treatment of some types of synchronous detectors is very complicated [62], a short simplified description of one type will be given to illustrate the principle.

Assume a voltage generator with an emf $E = A \cos \omega_s t$. This voltage generator with its source resistor R is connected to a double pole double throw switch, which in its turn is connected to a load resistor R (fig. II-5).

We assume that the switching action happens instanteneously at a constant rate ω_c. The position of the switch can be illustrated in the following diagram (fig. II-5).

Fig. II-5.
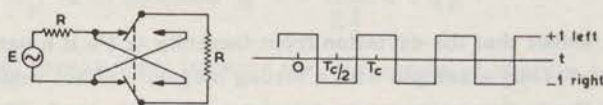
simplified modulator and associated timing diagram

The output current I_R in the load resistor R can be found by multiplying the current supplied by the generator E with the Fourier development of the switching function.

$$I_R = \frac{E}{2R} \left[\frac{4}{\pi} (\cos \omega_c t - \frac{1}{3} \cos 3 \omega_c t + \frac{1}{5} \cos 5 \omega_c t \dots) \right] \tag{2-9}$$

Substitution of $E = A \cos(\omega_s t - \varphi)$ yields

$$I_R = \frac{A}{2R} \left[\frac{2}{\pi} \cos(\omega_c t + \omega_s t - \varphi) + \frac{2}{\pi} \cos(\omega_c t - \omega_s t + \varphi) - \frac{2}{3\pi} \cos(3\omega_c t + \omega_s t - \varphi) \dots \right] \tag{2-10}$$

From this we can see that the original signal with the frequency ω_s is translated into a large number of signals with different frequencies.

Often it is possible by good choise of ω_s and ω_c to eliminate all but one of these components by means of filters.

36

If $\omega_s < \omega_c$, a low-pass filter with a cut-off frequency of ω_c will pass only the component $\omega_c - \omega_s$. In that particular case a signal with a frequency ω_s is converted into a signal with a frequency of $\omega_c - \omega_s$. The device is often called a modulator or demodulator, depending on the function.

If one chooses $\omega_c = \omega_s$ one obtains the following expression for the output current.

$$I_R = \frac{A}{2R}\left[\frac{2}{\pi}\cos\varphi + \frac{2}{\pi}\cos(2\omega_s t - \varphi) - \frac{2}{3\pi}\cos(4\omega_s t - \varphi)\ldots\right] \qquad (2-11)$$

The formula (2-11) shows that all terms represent ac components, except the first one, which represents a dc component.

One obtains the important conclusion that the output of the device in this particular case contains a dc component which depends linearly on the amplitude A of the input signal $E = A\cos\omega_s t$ and also on the phase angle between the input signal E and the switching signal applied to the device. For this purpose one can define the phase of the switching signal as the phase of the first harmonic of the square wave.

If the device is used as indicated here, it is often called a synchronous detector.

The operation of the device can be further explained with the help of a vector diagram (fig. II-6).

Suppose we feed a signal E into a synchronous detector to which we also apply a switching signal of the same frequency with the phase relationship as indicated in fig. II-6. The switching signal is represented by the dotted line.

The input signal can be resolved into two components $E_{//}, E_{\perp}$. The component $E_{//}$ will produce a dc component as indicated by formula (2-11), the component $E_{\perp}$ will not produce any dc components because the phase angle between it and the reference switching signal is $\frac{\pi}{2}$.

Vector diagram showing analysis of E

Fig. II-6.

It is thus shown here that a synchronous detector is capable of measuring the component of a signal E in phase with a reference switching signal.

In our application, we apply the output of the bridge, after amplification, to two synchronous detectors in parallel. Both synchronous detectors have a switching signal with the same frequency as the signal applied to the bridge. The phase of the applied switching signals can be varied with the restriction that the phase difference of the switching signals applied to the two detectors is always $\frac{\pi}{2}$.

As has been shown in 2.4, the bridge output signal contains two components in quadrature, one associated with χ' and the other with χ''. One detector is aligned in phase with the χ' component and the other is then automatically in phase with the χ'' component.

From the dc voltages produced at the output of the synchronous detectors the ratios $\frac{X'}{X_o}$ and $\frac{X''}{X_o}$ can be computed.

This detection procedure will at the same time fulfil requirement c of section 2.4. By filtering the output with a low-pass filter with a cut-off frequency f_1 one produces a virtual detector bandwidth of $2f_1$. This result is very difficult to obtain in any other way. This is illustrated in fig. II-7 in which we assume that we have the desired signal together with a large number of disturbing components. Fig. II-7^a shows the desired signal f_o surrounded by a large number of spurious signals or noise. A filter with the characteristic sketched in fig. II-7^b can only eliminate some components and the residu is shown by fig. II-7^c.

If this composite signal is fed into an amplitude detector the resulting dc will have little correlation with the desired signal.

If this signal is fed into a synchronous detector with a frequency f_h and the output passed through a low-pass filter the resulting signal is indicated in fig. II-7^e. It can be appreciated that the separation of $f_h - f_o$ is easier in e) than in a) due to the larger relative spacing of the components.

In fig. II-7^f, the switching signal is made identical in frequency with the desired signal. The output of the synchronous detector is shown in fig. II-7, by converting the (mathematical) negative frequencies to positive ones we obtain fig. II-7^h. A simple low-pass filter can be designed with a characteristic shown in fig. II-7^i, resulting in a noise free desired signal as indicated in fig. II-7^j.

illustration of the use of coherent detection to improve signal to noise performance

Fig. II-7.

With this procedure one can easily obtain a detector bandwidth of 2 Hz at 500 kHz. This would be very difficult to achieve with normal filters. A very narrow filter would also make the tuning of the measuring equipment difficult.

In the system described the signal applied to the bridge is also applied as a switching signal to the synchronous detectors.

2.5 DESCRIPTION OF THE BLOCKDIAGRAM OF THE MEASURING SYSTEM

The reasoning given in the preceding paragraphs enables us to sketch in fig. II. 8 the blockdiagrams of the measuring system as proposed.

The measuring bridge 2 is fed by a variable oscillator 1, tunable from 200 Hz - 1 MHz. The output of the bridge is amplified in an amplifier 3, the output of the amplifier being connected to a pair of synchronous detectors
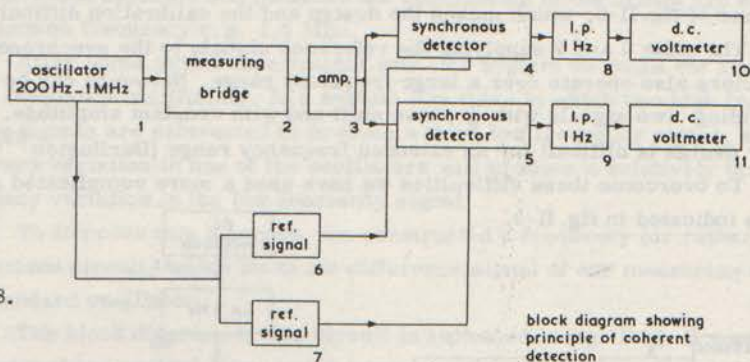
Fig. II-8.

block diagram showing principle of coherent detection

4 and 5. Two switching signals are derived from the oscillator signal in 6 and 7. These switching signals are $\frac{\pi}{2}$ out of phase and applied to the synchronous detectors. The output of the synchronous detectors will be a measure of the amplitude of the two quadrature components of the output signal from the bridge. The output signal of the synchronous detectors is filtered by means of low-pass filters and applied to the dc voltmeters 10 and 11.

A system as described above would work, but is not really practical for several reasons.

a) It has been indicated that a synchronous detector acts as a very narrow band pass filter if followed by a low-pass filter. The amplitude of the input signal should, however, be below a certain limit, to keep the synchronous detector in its linear operating range.

If no additional selectivity is used between the bridge and the synchronous detector and if wide band circuits are used, the peak value of thermal noise and undesirable harmonics of the signal may be many times larger than the signal to be measured and this noise could overload and disturb the operation of the synchronous detector.

It can be remarked that additional selectivity to discriminate against harmonics of the bridge signal is highly desirable from another point of view. Even in a frequency independent bridge the output amplitude of the harmonics will be many times larger than the balanced residual basic harmonic. The synchronous detector will produce not only a dc component from an input signal with the same input frequency and phase as the reference signal, but

will also to a smaller extent produce a dc signal if a signal is applied to its input having a frequency which is a multiple of the reference signal.

Removing these harmonics is a necessity because relaxation effects at the second or third harmonic of the measuring frequency would be interpreted as relaxation effects at the basic frequency.

b) The synchronous detectors operate over a large frequency range, in the scheme of fig. II-8, which makes the design and the calibration difficult.

The units 6 and 7 supplying the reference signals to the synchronous detectors also operate over a large frequency range. Networks can be designed providing two signals with $\frac{\pi}{2}$ phase shift and with constant amplitude, but their design is difficult for an extended frequency range (Darlington [63]).

To overcome these difficulties we have used a more complicated system as is indicated in fig. II-9.
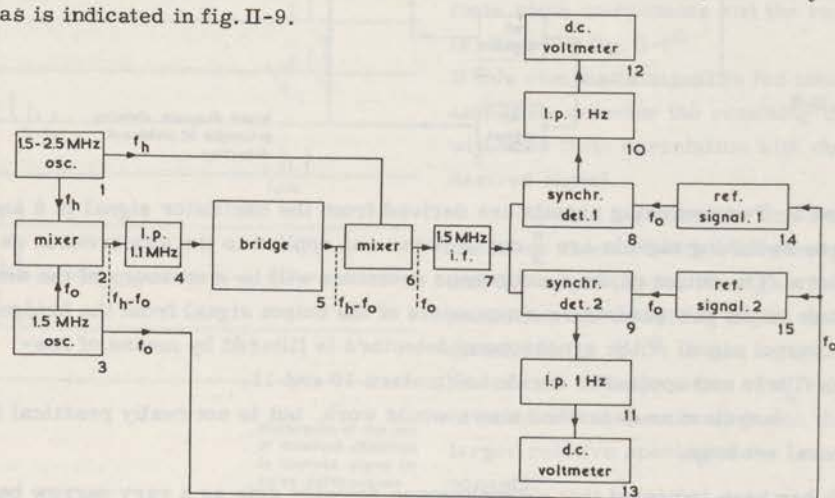
Fig. II-9.   simplified blockdiagram with fixed frequency synchronous detectors

In this system we start with two oscillators 1 and 3. The oscillator 3 is a fixed frequency, crystal controlled oscillator at 1.5 MHz. Oscillator 1 is variable from 1.500 - 2.500 MHz. The output signals of these two oscillators are mixed in 2 and their difference is supplied via a low-pass filter to the bridge 5. The output signal of the bridge is applied to a convertor which uses as a carrier the same variable oscillator. As a result the output signal of the bridge will be converted into a signal of 1.5 MHz, identical in frequency to the oscillator 3.

The output signal of the mixer 6 is applied to 1.5 MHz intermediate frequency amplifier in which the signal is amplified and filtered by means of coil filters and a crystal filter. The output of this amplifier 7 is supplied to two synchronous detectors. The switching signal to the synchronous detectors is

derived from the same 1.5 MHz oscillator 3, feeding the mixer 2. This switching signal is phased in the reference generators 14 and 15 such that the outputs of the reference generators have a phase difference of $\frac{\pi}{2}$.

It can be appreciated from this description that our two objectives have been met by means of a more complicated system. By means of heterodyning, we have been able to introduce selectivity at a fixed frequency and our critical circuits which separate and measure the components of the bridge are also at one common frequency e.g. 1.5 MHz.

After some initial experiments with this system we found the stability of the frequency insufficient. In a system like this, in which two high frequency signals are subtracted to produce a third low frequency signal, a small frequency variation in one of the oscillators will produce a relatively large frequency variation in the low frequency signal.

To improve this situation, we constructed a frequency (or rather phase) comparison circuit, which locks the difference signal of our measuring system to a standard oscillator.

The block diagram of this circuit is indicated in fig. II-10. It contains an automatic phase control loop, which compares the signal from the mixer 8 with

Fig. II-10.

system for frequency stabilization
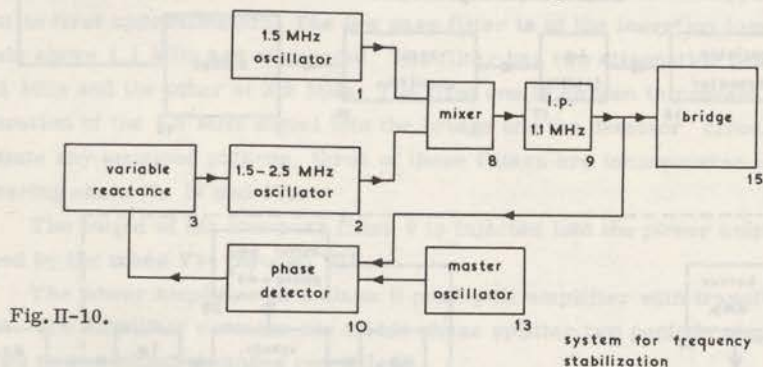
that of the master oscillator 13. It derives a dc potential in the phase detector 10 which depends on the phase difference of the two signals. This dc potential is applied to a variable reactance element 3 which controls the variable oscillator 2. In this manner the frequency stability of the signal applied to the bridge can be made as good as that of the reference oscillator used (Approximately 10^{-5} after initial warming-up).

As a reference oscillator we used a generator made by Siemens, Mess sender 10 Hz - 1 MHz type 3W38 b, c. The locking in of the oscillators was observed on the oscilloscope 35 (fig. II-11).

2.6 DESCRIPTION OF THE DIAGRAMS OF THE MEASURING SYSTEM

For the circuit description we refer to the diagrams in fig. II-12, II-13 and II-14, while the numbers in parenthesis refer to the complete block diagram

41

(fig. II-11). Starting in the transmitter we find V22[b] as a crystalcontrolled os-
cillator (1), at a frequency of 1.5 MHz. The large inherent stability provides a
reliable signal against which most tuned circuits in the receiver can be aligned.
The variable frequency oscillator V20[b] is of the Clapp type, chosen for stability

complete blockdiagram of
measuring system

Fig. II-11.

42
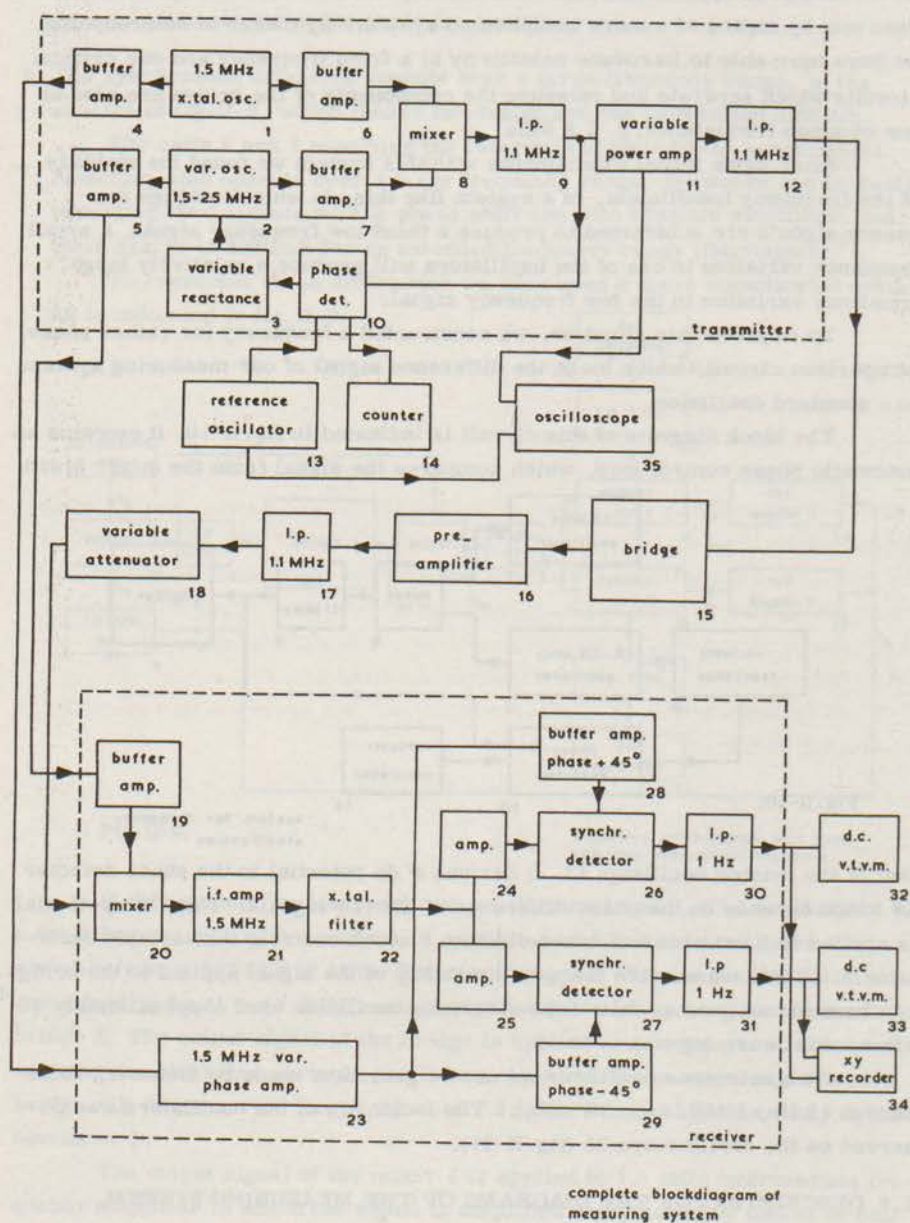
reasons. $V22^a$ (4) and $V20^a$ (5) form buffer amplifiers to feed the high frequency signals to the receiver. The four diode ring modulator (mixer 8) is fed through two buffer amplifiers V21 (7) and V23 (6).

For a brief description of the operation of the mixer we refer to paragraph 2.4, the essence being that the diodes are periodically closed and opened by a carrier (switching voltage).

The variable oscillator voltage is selected as the carrier and a relatively large voltage is applied to the diodes. The injection of the 1.5 MHz signal into the circuit is relatively small.

A mixer of this type produces in general signal components with a frequency of $np \pm mq$ in which p (the signal with the large amplitude) is often called the carrier and q (the relatively small signal) is called the input signal; $n = 1, 3, 5 \ldots$ and m is an integer.

In the case that the signal is small compared to the carrier the only significant terms are $np \pm q$ with $n = 1, 3, 5$ etc.

In our case the signal p-q forms the desired signal (200 Hz - 1 MHz), the other components are eliminated by the low-pass filter (9). The mixer is of a double balanced type, i.e. the carrier and the input signal do not appear in the output in first approximation. The low pass filter is of the insertion loss type. Signals above 1.1 MHz are attenuated. The filter has two attenuation peaks, one at 1.5 MHz and the other at 2.2 MHz. The first one is chosen to prevent any penetration of the 1.5 MHz signal into the bridge and the detector circuits. To attenuate any spurious pick-up, three of these filters are incorporated in the measuring chain (9, 12 and 17).

The output of the low-pass filter 9 is injected into the power amplifier (11) formed by the tubes V24 through V28.

The power amplifier is a class B push-pull amplifier with transformer output. The amplifier contains one triode phase splitter, two pentode amplifiers and two power output pentodes type EL 83.

A four position switch selects one of four different taps on two different output transformers. One is an iron core transformer for the frequency range of 200 Hz - 30 kHz, the other is a ferrite transformer for the range of 30 kHz - 1 MHz.

A simple 4-position attenuator with a continuous potentiometer enables us to reduce the signal to the bridge to any level desired.

For optimum signal to noise performance, the bridge is directly connected to the pre-amplifier but a large signal will paralyze this amplifier, if the bridge is not close to balance. Reducing the signal applied to the bridge solves this problem.

The output signal from the low-pass filter (9) is also connected to the phase detector (10). The tube $V29^a$ is a triode pre-amplifier. $V29^b$ is a phase splitter connected to a two diode phase detector.

transmitter

Fig. II-12.

If the output signal of (10) has the same frequency as the reference oscillator (13), a dc voltage results, the magnitude of which is a measure of the phase difference of the two signals.

This dc voltage is applied as a regulating voltage to a variable reactance element (3), for which a semi-conductor diode D_1 is used.

The capacity of a diode in its non-conducting mode, varies with the dc voltage applied to its terminals and the diode is used as a variable condensor across the oscillator circuit.

In practice the system, if locked in, will at low frequencies follow the reference oscillator over a range of approximately 2 kHz. The frequency range over which it will lock in is approximately 200 Hz.

The output of the power amplifier (11) is connected through a low-pass filter (12) (fig. II-11) to the measuring bridge (15) which will be discussed in the following chapter.

The output of the bridge (15) is connected to a pre-amplifier (16). This amplifier is a wide band amplifier designed to pass frequencies from 200 Hz to 1 MHz and its circuit is shown in fig. II-13. The first stage has a gain of approximately 50 db while the second stage provides mainly power gain and
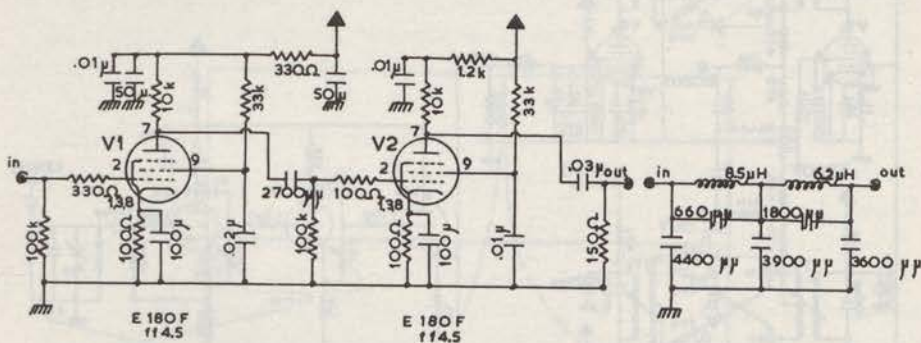
Fig. II-13.   Pre-amplifier and l.p. filter.

matches the output of the first tube to the variable attenuator (18). A low-pass filter (17) is inserted between the amplifier and the attenuator in order to eliminate further any spurious high frequencies. The cut-off frequency of this filter is 1.1 MHz.

The variable attenuator is a standard 50 ohm attenuator produced by Rohde and Schwartz (type DPR BN 18042/50), which enables us to regulate the input signal to the synchronous detector. We can change the measuring sensitivity over a range of 90 db.

The output of the variable attenuator is applied to the mixer (20) contained in the receiver, shown in fig. II-14.
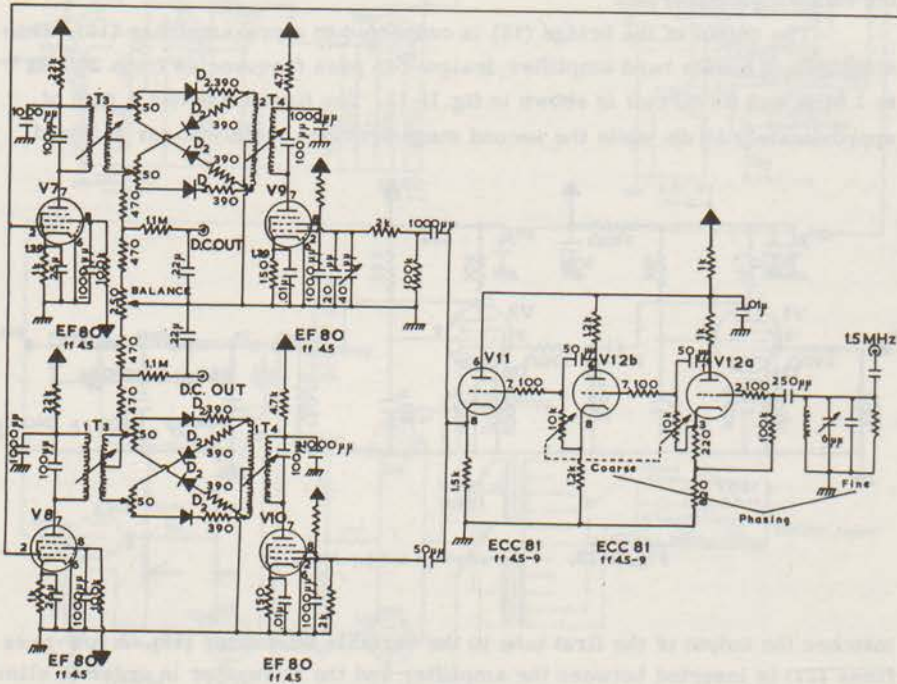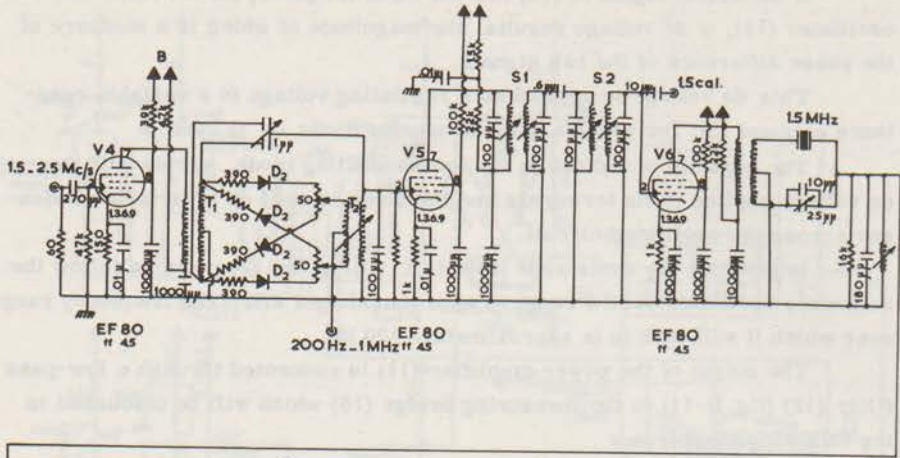
receiver

Fig. II-14.

The mixer (20) is again a four diode mixer providing good linearity and a good balance for carrier and signal.

A good carrier balance is essential in the case the bridge is used at low frequencies. The carrier frequency is close to 1.5 MHz in that case and a large carrier leak may disturb any following amplifier.

The output of the mixer (20) is connected to the I. F. amplifier (21), which contains two amplifier pentodes E. F. 80 and five tuned circuits, tuned at 1.5 MHz, and one crystal filter at the same frequency. The tuned circuits provide an I. F. amplifier with a 3 db bandwidth at 10 kHz and a 20 db bandwidth in the order of 30 kHz.

To reduce the amount of noise entering the synchronous detector, better selectivity was desired. A simple crystal filter was constructed using an ordinary oscillator crystal. The selectivity curve for this filter is shown in fig. II-15.

The crystal filter is essentially a bridge circuit. At all frequencies except the resonant frequency of the crystal, the impedance of the crystal is equal to the impedance of a condensor. By adjusting the value of the condensor in the other arm to this same capacity, the output of the filter will be zero, except at the resonant frequency of the crystal, provided the tap on the second-

selectivity curve of crystal filter
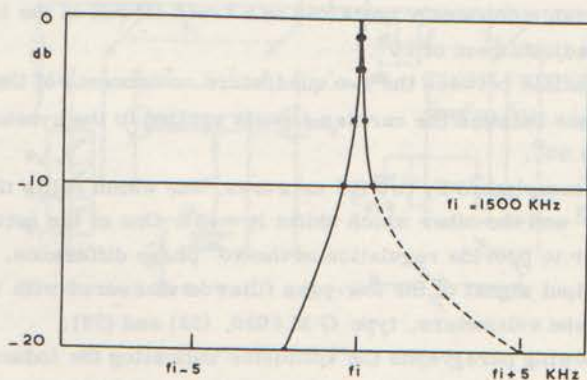
Fig. II-15.

ary of the transformer feeding the filter, is a mid-tap. By adjusting the frequency of the tuned circuit at the output of the filter one can influence the frequency of the pass-band slightly.

Due to the fact that an oscillator crystal was used, the filter showed some spurious side responses. These were, however, completely eliminated by the coil filters.

The output of the crystal filter (22) is connected to the driving amplifiers (24) and (25), consisting of V7 and V8.

These amplifiers provide the signal to the synchronous detectors (26) and (27), which are again of the 4-diode type.

The reference 1.5 MHz signals are supplied through two carrier amplifiers (28) and (29) to the detectors and the output of the synchronous detectors are dc coupled to the RC low-pass filters (30) and (31).

Balancing potentiometers provide a means for obtaining a zero dc output signal from the detectors if the output of the bridge is shorted.

The 1.5 MHz signal generated in the transmitter is supplied to the receiver through a buffer amplifier.

If the output of one synchronous detector has to indicate the variation of the inductance only, a certain fixed phase relationship should exist between the input signal and the carrier signal at the synchronous detector.

To adjust this phase relationship a calibrated variable phase amplifier (23) is inserted between the buffer amplifier (4) and the carrier amplifiers (29) and (28) driving the synchronous detectors. This variable phase amplifier (V11 and V12a,b) is common to the two synchronous detectors, such that both detectors are corrected simultaneously. By means of the potentiometers in the triode circuits of V12 the phase can be adjusted continuously over a range of nearly 270° while a small variable condensor contained in a tuned circuit at the input provides a calibrated fine adjustement of 20°.

To differentiate between the two quadrature components of the bridge, the phase difference between the carrier signals applied to the synchronous detectors must be 90°.

This is accomplished by two RC networks, one which shifts the phase of the signal $+45^{\circ}$ and the other which shifts it -45°. One of the networks is adjustable in order to provide regulation of the 90° phase difference.

The dc output signal of the low-pass filter is measured with two Philips Vacuum tube voltmeters, type G M 6020, (32) and (33).

In the following paragraphs the voltmeter indicating the inductive variations will be often called the L voltmeter, the one indicating the losses will be called the R voltmeter.

2.7 DETAILED DESCRIPTION OF THE MEASURING BRIDGE

In this paragraph we will describe in more detail the bridge circuit used for measuring the magnetic proporties of the samples.

We refer to paragraph 2.2 and 2.3 for the principle of the system. In these paragraphs it has been explained that means have to be provided to obtain an approximate balance. The elements used for balancing are not calibrated, and this relaxes the requirements on the bridge very much, and all emphasis can be placed upon stability of the elements, and ease of construction. As a by-
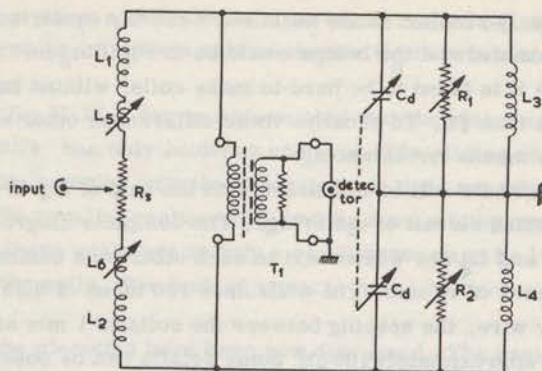
Fig. II-16.

simplified diagram
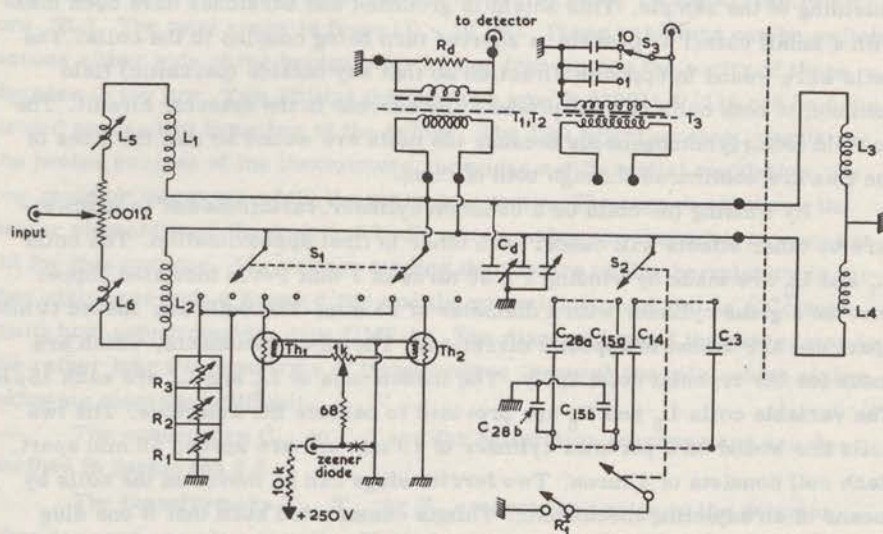
Fig. II-17.   complete diagram

measuring bridge

product, the frequency range in which this bridge can operate is large. Actual measurements have been made from 200 Hz - 1 MHz, which is a ratio of 5000. The useful range of the Hartshorn bridge, used for measuring paramagnetic relaxation in Leiden, is from 3 Hz - 1200 Hz giving a ratio of 400. The large ratio is mainly due to the fact that no requirements are necessary for the purity of the elements.

As is indicated in paragraph 2.3, the basic bridge in simplified form is a Wheatstone bridge, given in fig. II-3. The coils L_3 and L_4 are closely similar and located in the cryostat, the coils L_1 and L_2 are in the bridge housing

49

and are also closely similar. If the coils were exactly equal, no further elements would be needed and the bridge would be in equilibrium for all frequencies. In practice it is found to be hard to make coils, without tuning elements, which differ less than $\frac{1}{2}$%. To equalize these differences other elements are added to provide means for balancing.

These elements will be discussed with the help of fig. II-16 which is a somewhat simplified circuit of the bridge. The complete diagram is indicated in fig. II-17. L_3 and L_4 are wound next to each other on a common glass cylinder with a diameter of 16 mm. The coils have 150 turns of 0.25 mm Povin insulated copper wire, the spacing between the coils is 1 mm and the inductances are each approximately $100 \mu H$. Some details can be observed in fig. II-20, in which the cryostat has been sketched. On the inside of the glass cylinder, a small layer of silver has been deposited to provide electrical shielding of the sample. This shield is grounded and scratches have been made with a small chisel to prevent a shorted turn being coupled to the coils. The coils were wound in opposite direction so that any outside (parasitic) field common to both coils can not produce any current in the detector circuit. The ac field is fairly homogeneous because the coils are wound so that the lines of the flux are continuous through both of them.

By winding the coils on a common cylinder, variations due to temperature or other effects will cancel each other in first approximation. The coils L_1 and L_2 are made by winding 2 x 50 turns of 1 mm Povin insulated copper wire on a glass cylinder with a diameter of 35 mm. The coils are spaced 10 mm apart and are wound in opposite directions. The same comments, which are made for the cryostat coils apply. The inductances of L_1 and L_2 are each $35 \mu H$. The variable coils L_5 and L_6 are provided to balance the inductors. The two coils are wound on a pertinax cylinder of 10 mm and are spaced 50 mm apart. Each coil consists of 4 turns. Two ferrite slugs can be moved in the coils by means of an adjusting mechanism. This is constructed such that if one slug moves into one coil, the other moves out of the second coil, providing a differential adjustement.

The losses of the coils will in general not be exactly equal. At low frequencies (below 10 kHz), the series resistance of the coils is the most important quantity. This can be compensated for by means of a potentiometer of 0.001Ω. The resistance of the coils in the bridge housing is 0.160Ω and the resistance of the coils in the cryostat at nitrogen temperatures is of the same order.

At high frequencies (above 10 kHz) other types of losses are predominant. Dielectric losses increase and losses due to the proximity of metal parts to the coils are important. A large parallel resistor, indicated by R_1 and R_2 is very effective to overcome these losses.

At very high frequencies (100 kHz - 1 MHz), unequal parallel capacities

of the coils will produce a severe unbalance which cannot be adjusted by means of the coils L_5 and L_6. A differential condensor C_d is provided to balance this unequal capacity.

Studying fig. II-17 it can be appreciated that the main bridge circuit, formed by the coils, has only soldered contacts. The sliding contact of the potentiometer R_s is in series with the generator and does not affect the balance of the bridge. The parallel resistors R_1 and R_2 have sliding contacts, but the current through these resistors is only a small percentage (< 1%) of the current flowing through the coils. The lack of contacts in the main circuits improve the overall stability.

Most of the elements have been now discussed. The resistors R_1 and R_2 consist actually of several elements shown in fig. II-17. For frequencies up to approximately 100 kHz two Peekel cascade resistor decade boxes (R_1 and R_2) are used. Two decades have been added to this by using 1% metal film resistors (R_3). The total range is from $1\,\Omega$ - $10\,M\Omega$. These resistors can be switched across either side of the bridge. For higher frequencies the purity of these decades is too low. Two Philips thermistors type B 832015 P/330 can be connected across two branches of the bridge. The $1\,k\Omega$ potentiometer, regulating the heater current of the thermistors, provides a differential regulation, i.e. one resistor increases while the other decreases. The capacity between the heater element is of the order of 3 pF, which makes the thermistors very useful for this purpose. The voltage feeding the heaters of the thermistors is further stabilized with a Zener diode and the potentiometer of $1 k\Omega$ is a Colvern multi turn potentiometer, type CMT 11. The disadvantage of the thermistor is the rather long timeconstants of these devices (several seconds) which makes adjusting somewhat difficult.

The condensors C_{28} to C_{-3} are for calibration purposes and are described in paragraph 2.8.

The transformers T_1, T_2, or T_3 connect the bridge to the detector. They are made as plug-in units. T_1 and T_2 have Philips ferrite cores. The transformer T_1 is used from 2 kHz to 30 kHz, with a primary impedance of $1\,k\Omega$ and a secondary impedance of $30\,k\Omega$, T_2 is used from 30 kHz to 1 MHz and is designed for a primary impedance of $100\,\Omega$ and a secondary impedance of $1000\,\Omega$. These values were selected to provide a good matching of the bridge to the detector circuits, with a good signal to noise performance as a result.

The transformers are wide-band networks, which eliminate tuning.

For the frequency range of 200 Hz - 2 kHz a tuned transformer T_3 is used. At these low frequencies, the harmonics of the measuring frequency are strongly enhanced in comparison with the basic signal and they tend to overload the synchronous detectors. A tuned transformer is inserted for these frequencies and by means of a 10-position switch S_3, 10 different condensors can be connected across the coil.

If one tries to compute the sensitivity of the bridge, and includes all the elements, the equations would be too cumbersome to handle. This is fortunately not necessary because the result obtained in paragraph 2.3 formula (2-3), in which the detector current variation is computed if one of the branches is varied, will not alter much if the branches of the bridge are not equal. In the derivation nothing is specified about the impedance $\bar{Z}$ and a formula similar to (2-3) would be obtained for a large range of values for the impedance $\bar{Z}$.

The coils L_1 and L_2 and also L_3 and L_4 are so close to each other that they have an appreciable magnetic coupling. Analyzing the effect of this coupling in a circuit similar to that of fig. II-17 would be very complicated, but we will show that this magnetic coupling does not affect the system in any undesirable way, in a simplified bridge circuit. We shall assume that the bridge can be represented by the circuit of fig. II-18. The bridge is fed from a current source I. We shall further assume that $L_1 = L_2 = L_A$ with a mutual inductance M_A and $L_3 = L_4 = L_B$ with a mutual inductance M_B associated with this pair of coils. If a magnetic sample is inserted into L_3 the inductance will increase to $L_3 = L_B(1 + \delta)$ but we will assume that M_B is not altered by insertion of the sample.

Due to the symmetry of the circuit, the bridge will be in equilibrium without a sample. With the insertion of a sample, the unbalance current can be computed, by first computing the voltage E between the terminals P and Q, if the detector impedance $\bar{Z}_d$ has been removed, then computing the impedance $\bar{Z}_i$ between P and Q with the current source removed and finally compute the current with the relation:

diagram to evaluate
mutual coupling of coils

Fig. II-18.

$$\bar{I}_d = \frac{\bar{E}}{\bar{Z}_i + \bar{Z}_d} \tag{2-12}$$

Calculation shows:

$$\bar{E} = j\omega\bar{I} \frac{\delta}{2} \frac{L_B (L_A - M_A)}{L_A + L_B - M_A - M_B} \tag{2-13}$$

$$\bar{Z}_i = 2j\omega \frac{(L_B - M_B)(L_A - M_A)}{L_A + L_B - M_A - M_B} \tag{2-14}$$

In the actual circuit the coupling coëfficients have been calculated for the coils in the cryostat and for the set of coils in the bridge housing. We find $M_A = 0.08\ L_A$ and $M_B = 0.1\ L_B$. If one compares the calculated case with a fictitious one in which the coils do not have any mutual coupling, one obtains the result that in actual case the voltage $\bar{E}$ is approximately the same as in the fictitious case, while the impedance $\bar{Z}_i$ is approximately 10% smaller. One sees from the equations (2-13) and (2-14) that the principle of operation is not at all affected, and that only the power available to the detector has been changed

52

slightly, if one assumes a real load impedance representing the detector.

In this section we tried to show that in a non-absolute bridge, one has considerably more freedom in design, resulting in possible improvements in frequency range, sensitivity, etc.

2.8 CALIBRATION OF THE MEASURING SYSTEM

From paragraph 1.4 it is clear that for most paramagnetic relaxation measurements it is sufficient to measure the relative variation of the magnetization of a sample. The important quantities in paramagnetic relaxation are $\frac{\chi'}{\chi_o}$ and $\frac{\chi''}{\chi_o}$. The ratios $\frac{\chi'}{\chi_o}$ and $\frac{\chi''}{\chi_o}$ are determined by observing the detector current variation if the sample is moved from one coil to the other. In measuring spin-lattice relaxation phenomena at frequencies below 1 MHz one can assume that $\chi(\omega = 0, \ H = 0) \approx \chi(\omega, H = 0)$ because the effect of the spin-spin relaxation can be neglected. By dividing the variations at a given magnetic field H_o by the corresponding variation in zero magnetic field we obtain the desired quantities.

For this reason we call this bridge a relative bridge. In most other bridges which could be called absolute bridges, the absolute value of the three quantities χ', χ'' and χ_o can be determined knowing the weight of the sample.

In several cases we would like to know also the absolute magnitude of a magnetic effect. If a magnetic sample obeys the Curie law, or an approximation of it, the magnetization can be used to determine the temperature of the sample. The absolute measurement of a magnetic effect has been made possible in this bridge by means of an indirect calibration method. To do this we produce in the bridge a known disturbance which we compare with the disturbance of the balance due to a magnetic effect. We obtained a given disturbance in the bridge by switching an impedance in parallel with one of the branches of the bridge, being careful that the unwanted extra capacitive disturbance was eliminated. For these calibration elements we used capacitors because they can easily be obtained for a large range of values and have in general a very high purity. The disturbance of our bridge by a condensor depends however, on the frequency. The impedance of the coil is proportional to the frequency, the impedance of a condensor is inversely proportional to the frequency. Therefore we need a different condensor for each measuring frequency. This has the advantage that a large range of calibrated disturbances is available for one frequency.

In the following we will express numerically the effect of adding a condensor in parallel to one of the coils in the cryostat. To calculate this effect we will represent the bridge by the simplified diagram of fig. II-19. The detector current will be given by:

$$\bar{I}_d = \frac{\bar{E}}{D} [\bar{Z}_1 \bar{Z}_4 - \bar{Z}_2 \bar{Z}_3] \tag{2.15}$$

The denominator D is polynomial in $\bar{Z}_1, \bar{Z}_2, \bar{Z}_3, \bar{Z}_4$, and $\bar{Z}_d$. The bridge is always operated close to equilibrium i.e. $\bar{Z}_1 \bar{Z}_4 - \bar{Z}_2 \bar{Z}_3$ will vary strongly, the de-

53

nominator $\bar{D}$ will vary only to a smaller degree. To a good approximation one can state:

$$\Delta \bar{I}_d = \frac{\bar{E}}{\bar{D}} \Delta (\bar{Z}_1 \bar{Z}_4 - \bar{Z}_2 \bar{Z}_3) \qquad (2\text{-}16)$$
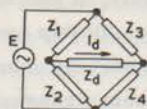
Fig. II-19. Diagram to compute calibration elements

Next we shall assume that the impedance $\bar{Z}_4$ consists of a coil L in series with a resistor R_s. One can object that in the actual bridge $\bar{Z}_4$ will be more complicated due to parallel losses and a parallel capacitance. A more complete calculation shows that these will not materially effect the final results of this calculation. If the inductance L_4 varies by ΔL the difference in the detector output can be expressed by:

$$\Delta_1 \bar{I}_d = \frac{\bar{E}}{\bar{D}} \cdot j\omega \Delta L \cdot \bar{Z}_1 \qquad (2\text{-}17)$$

If one connects an impedance $\bar{Z}_g$ parallel to $\bar{Z}_4$ such that $\bar{Z}_g \gg \bar{Z}_4$ one obtains

$$\Delta_2 \bar{I}_d = - \frac{\bar{E}}{\bar{D}} \frac{\bar{Z}_1 \bar{Z}_4^2}{\bar{Z}_g} \qquad (2\text{-}18)$$

For each frequency the value of the condensor is chosen in such a way that it produces a disturbance equivalent to a relative variation of the measuring coil of approximately 3.10^{-5} (The bridge was used with an earlier cryostat with different coils for which the ratio was 10^{-5}).

This disturbance of 3.10^{-5} we shall call in the following a STANDARD DISTURBANCE. N is the number of standard disturbances.

The value of the condensor can be computed by means of equations (2-17) and (2-18). For relative high frequencies ($\omega L \gg R_s$):

$\bar{Z}_4 = j\omega L$ and $\bar{Z}_g = \frac{1}{j\omega C}$ which on substitution in (2-17) and (2-18) gives:

$$j\omega\Delta L = - \frac{(j\omega L)^2}{\frac{1}{j\omega C}} \text{ and } C = \frac{\Delta L}{L} \cdot \frac{1}{\omega^2 L} \qquad (2\text{-}19)$$

For standardization purposes we chose a series of measuring frequencies F_M separated from one another by half an octave and designated by the index M. The index M goes in the bridge from 1 through 27 and the associated frequencies are given by $f_M = 82.8 \times 2^{M/2}$ Hz (2-20). The frequencies form a logarithmic series, convenient for calculation and plotting. Measurements can be done, however, at any frequency. The calibration condensors are designated by C_P and the values are given in this bridge by $C_P = 1.15 \times 2^{-P}$ µF (2-21) in which P goes from -3 through 28. The calibration condensor C_P will produce at the frequency F_M a calibration equal to the standard disturbance if $P = M$. Otherwise the calibration will be equal to 2^{M-P} standard disturbances.

The range of condensor values is very large as can be judged from (2-21). The values for frequencies above 30 kHz are too small to be practical. The following arrangement is used to solve this difficulty. The appropriate condensor

is selected by means of a switch S_2 and the calibration is performed by closing a relay. For frequencies up to 10.6 kHz a single condensor is used (e.g. C_{14} in fig. II-17). For the higher frequencies a small condensor e.g. C_{28a} is connected to the bridge in series with a large condensor C_{28b}. By shorting this condensor one obtains a small variation of the effective capacity. At 960 kHz (F_{27}), C_{27a} is 3 pF and C_{27b} is 1100 pF providing an effective capacitive variation of 0.008 pF by shorting C_3.

The exact values of the condensors are still difficult to obtain, so we calibrated them by means of a given inductance variation. A given magnetic disturbance was produced by means of a paramagnetic crystal of $Mn(NH_4)_2(SO_4)_2 \cdot 6H_2O$. The χ_o can be assumed to be independent of frequency in this frequency range at zero magnetic field. With this crystal as a reference we determined the correction factor C_{cc} of the calibration condensors, with $C'_p = C_{cc} \times C_p$ in which C'_p is the value of the calibration condensor used in the bridge.

Another difficulty is added in the case of low frequencies, because R_s is not small anymore in comparison with ωL. A variation in inductance or a disturbance of the bridge by means of a parallel condensor will produce detector currents which at low measuring frequencies do not have the same phase relationship in reference to a certain fixed phase, i.e. the phase of the signal applied to the bridge. In practice the phase of the detection system is aligned such that a pure inductance variation produces a variation on the L voltmeter only.

Equation (2-17) can be written as:

$$\frac{\Delta_1 \bar{I}_d}{\frac{E}{D} \bar{Z}_1} = j\omega \Delta L$$

If the calibration is done for a condensor with high purity, equation (2-18), with $\bar{Z}_4 = R_s + j\omega L$, can be written as:

$$\frac{\Delta_2 \bar{I}_d}{\frac{E}{D} \bar{Z}_1} = -\frac{(R_s + j\omega L)(R_s + j\omega L)}{\frac{1}{j\omega C}} = j\omega C(-R_s^2 + \omega^2 L^2) + 2\omega C R_s \omega L$$
$$= ja + b$$

If the series resistors R_s were zero, we would obtain:

$$\frac{\Delta_2 \bar{I}_d}{\frac{E}{D} \bar{Z}_1} = j\omega^3 CL^2 = ja'$$

A short calculation shows that $a' = \dfrac{a + \sqrt{a^2 + b^2}}{2}$ \hfill (2-22)

Formula (2-22) shows us how to compute the effective calibration value a' if as well as the L, the R voltmeters show a deflection, (a and b respectively) if a standard disturbance of the bridge is made.

The system of a logarithmic frequency scale and the use of other logarithmic units make it possible to compute quickly magnetic effects and temperatures of samples obeying Curie's law.

If a sample follows a Curie-Weiss law $\chi = \frac{C}{T - \theta}$ we can define a fictitious temperature $T' = T - \theta$ and the equations (2-23) through (2-25) can be used by substitution of T' instead of T.

The answers to computations which are only simple additions and subtractions give $\log T$ and $\log \rho$ which are often used directly in graphs.

The formulas interconnecting the different variables are given below and can be derived from (2-17) and (2-18).

$$N_T = \frac{V_m}{V_c} \left(\frac{f_m}{f_c}\right)^2 C_{cc} \qquad (2-23-a)$$

$$20 \log N_T = 20 \log \frac{V_m}{V_c} + 40 \log \frac{f_m}{f_c} + 20 \log C_{cc} \qquad (2-23-b)$$

$$20 \log N_T = 20 \log \frac{V_m}{V_c} + 6 (M - P) + 20 \log C_{cc} \qquad (2-23-c)$$

N_T = Magnetic effect at temperature T expressed in calibration units.

V_m = Voltmeter reading due to a magnetic sample at zero magnetic field.

V_c = Voltmeter reading due to calibration.

f_m = Measuring frequency.

f_c = Calibration frequency, i.e. frequency at which one standard disturbance is produced by the calibration condensor.

C_{cc} = Correction factor for the calibration condensor.

M = Number of measuring frequency.

P = Number of calibrating element.

If a sample obeys Curie's law, the unknown temperature T_x can be calculated if the magnetic effect is known at that, and at a known temperature T_o.

For T_x is found:

$$20 \log T_x = 20 \log T_o + 20 \log N_{T_o} - 20 \log N_{T_x} \qquad (2-24)$$

If one defines N_1 as the number of calibration units of a sample at $1^\circ K$, the formula simplifies to:

$$20 \log T_x = 20 \log N_1 - 20 \log N_{T_x} \qquad (2-25)$$

2.9 THE GENERATION OF THE CONSTANT MAGNETIC FIELD

All the measurements have been done with a quasi-constant magnetic field parallel to the ac field used for measuring susceptibility. The magnet used,

is about 30 years old and was constructed by Prof. dr. W.H. KEESOM. It is an ironfree solenoid with an inner diameter of 13 cm and a height of 90 cm. It has an inner core of brass, thus reducing the effects of ac fluctuations on the dc current, feeding the solenoid. The dc current is now supplied by a stabilized rectifier constructed by Standard Electric and Transforma which can supply 100 V at 200 A with a stability of 0.005% after 3 hours, and a ripple current of less than 20 mA. This rectifier can be remotely controlled. The current can be varied continuously at a rate of approximately 4A/sec or in steps. The steps range from 5A to 20A, depending on the average current.

The field strength in the center of the magnet is reported to be 22.46 Oe/A and to be homogeneous to less than 1% over an axial distance of 25 cm. We recalibrated the magnet by means of proton resonance. Our measurement was done at a dc current of 25A and gave 22.52 Oe/A, in good agreement with the given value. For this, one of the fixed current positions of the rectifier was used which is reported to be accurate within 0.1%.

Long relaxation times $\tau (> 20\,\text{msec.})$ are measured by varying the dc field abruptly. For this purpose a second coil is inserted into the main magnet. This second coil is wound on a Celleron cylinder of 10 cm inner diameter, 1800 turns on a coil of 40 cm give a field of 53 Oe/A which is homogeneous to within 1% over a length of 15 cm. This coil was constructed by Dr. VAN DEN BROEK[20] who used this method of measurement. He inverted the current by a manually controlled switch and used the method for measuring relaxation times τ greater than 200 msec. We made several improvements, which will be discussed in paragraph 2.14.

2.10 THE DESIGN OF THE CRYOSTAT

The design of the measuring system in the cryostat was found to be critical. The requirements can be summarized as follows:

1. It must be possible to insert a specimen in a set of coils and move it from one coil to the other.
2. The specimen must be cooled with helium or hydrogen or any normal cooling liquid.
3. The wire of the measuring coils should not make direct contact with the cooling liquid. Bubbles of vapour make sizable dielectric disturbances at higher frequencies (Some later experiment proved this to be true).
4. The measuring coils should be stable. Moving the specimen should not produce any undesirable effects.
5. Electrical shielding should be provided to insure that only magnetic effects due to the specimen are measured and no dielectric properties.

We will only describe some major problems encountered.

57

Our initial experiments were done in a cryostat containing a measuring system sketched in fig. II-20a. A metal can C, soldered to a plate R contained a set of measuring coils L_3 and L_4. The can was filled with helium gas, providing a thermal contact with the bath while preventing disturbance of the coils by bubbles. Three German silver tubes connected the compartment to the top of
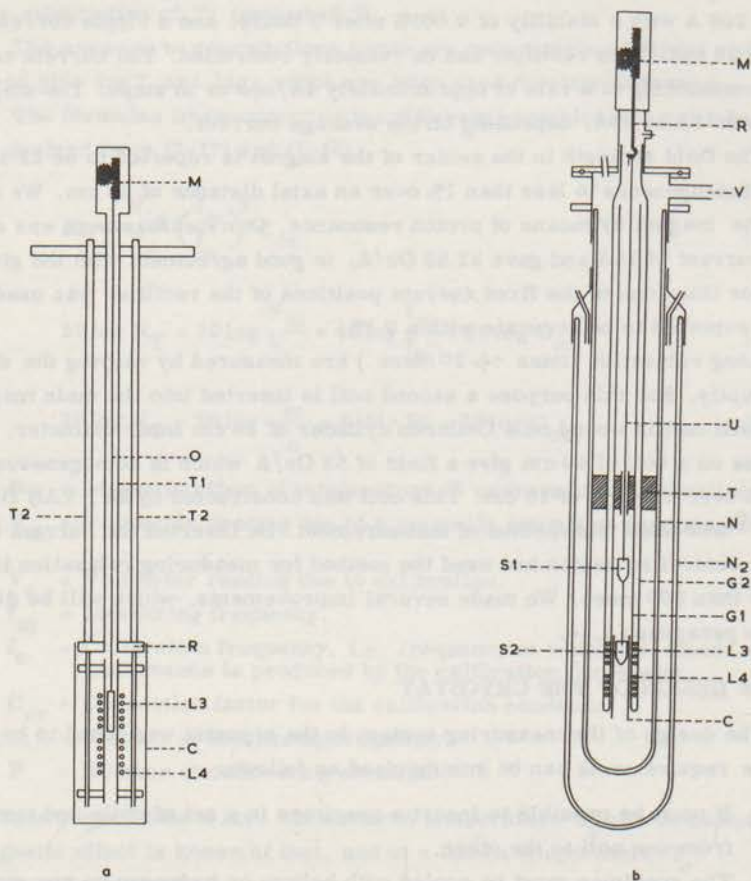
Fig. II-20. Construction of equipment in cryostats.

the cryostat. The two outside tubes T_2 were used as coaxial conducters. A single copper wire, in the middle of the tube carried the bridge current, the metal of the tubes acting as a return lead. The two coils L_3 and L_4 were wound on a glass tube, which was fastened by means of metal rods and pertinax rings to the plate R. The specimen was moved from one coil to the other by means of a rod, which ran through T_1 and which was activated by a mechanism M, containing a small electrical motor.

We had hoped that the effect of the metal can on the two coils would balance. This was not the case and the changing dc magnetic field affected the balance severely.

In the following we will call the influence on the balance by a magnetic field a FIELD effect. In principle a field effect is not serious in our system, because in general it will be the same for the two positions of the specimen. The desired effect is a difference of the two readings and any field effect will be cancelled. In this case the field effect was large compared to the effect to be investigated, requiring rebalancing for most values of the magnetic field. We replaced the metal can by a glass tube, but had a lot of trouble finding a fluid-proof seal between glass and metal, which could be easily removed and also could withstand the low temperature.

We still found severe field effects at certain frequencies. These were finally traced down to electro-magnetical coupling of mechanical oscillators to the measuring coils. The metal tubes T_1 and T_2, amongst others, formed mechanical oscillators with a high quality factor and a very small coupling was sufficient to influence the system. We once measured all the resonances and the results can be seen in fig. II-21. We found that the field effect, produced by these oscillators, was linear with H_c^2 (fig. II-21). We have analyzed this in appendix A and can explain it. The analysis may be important, if experiments are contemplated with a high dc magnetic field. Due to the dependency, this problem could pose a limiting factor in a future design.

In the cryostat of fig. II-20a we were able to reduce the mechanical coupling by use of cotton wool in C and by damping the tubes T_1 and T_2 with rubber.

At helium temperatures we found another serious field effect. The system contained several soldered joints, the solder became superconductive at helium temperatures. The superconductivity was removed by the dc magnetic field and manifested itself as a varying ohmic resistance in series with the coils. These effects were serious at low measuring frequencies.

In the following we will call the influence on the balance produced by moving the sample from one coil to the other the COMMUTATION-EFFECT. In the cryostat of fig. II-20a we had a severe commutation-effect. We were never able to determine the cause but presume that movement of the rod changed the temperature gradient temporarily. The two tubes T_1 and T_2 acted similarly to a bimetal switch, resulting in change of inductance or capacitance of the connecting wires. This effect had a time-constant of the order of a minute. These difficulties prompted us to use a different system, which is much simpler and is shown in fig. II-20b. The coils L_3 and L_4 are wound on a glass tube of 15 mm inside diameter. The two coils and the connecting leads form one continuous copper wire without soldered joints (see fig. II-22). There is one soldered joint at P, but it is in series with the generator and does not affect the balance in

59

$$L = \frac{VQ}{1+V^2Q^2}$$

5.3

5.1   5.2 kHz   .7 .6 .5 .4 .3 .2 .1   1 2 3 4 5 6 7 8

2
3
4
5

A   B

$$R = \frac{1}{1+V^2Q^2}$$

$$\omega_0 = \frac{1}{\sqrt{L_1 C_1}}$$

1 H.O   Oe
2 H.1000 Oe
3 H.2000 Oe
4 H.3000 Oe
5 H.4000 Oe

$$V = \frac{\omega}{\omega_0} - \frac{\omega_0}{\omega}$$

$$Q = \frac{1}{R_1}\sqrt{\frac{L_1}{C_1}}$$

Fig. II-21.

5.0   5.1   5.2   .7 .6 .5 .4 .3 .2 .1   1 2 3 4 5 6 7 8
         measured   calculated   VQ

$$-2, -3, -4, -5, -6 \quad \log \frac{(R)_{peak}}{\omega L_{bridge}}$$

1   2   3   4 5 6 7 8 9 1   2   3   4 5 6 7 8 9 1
1 kHz   10 kHz   100 kHz
mechanical resonances in measuring system

D
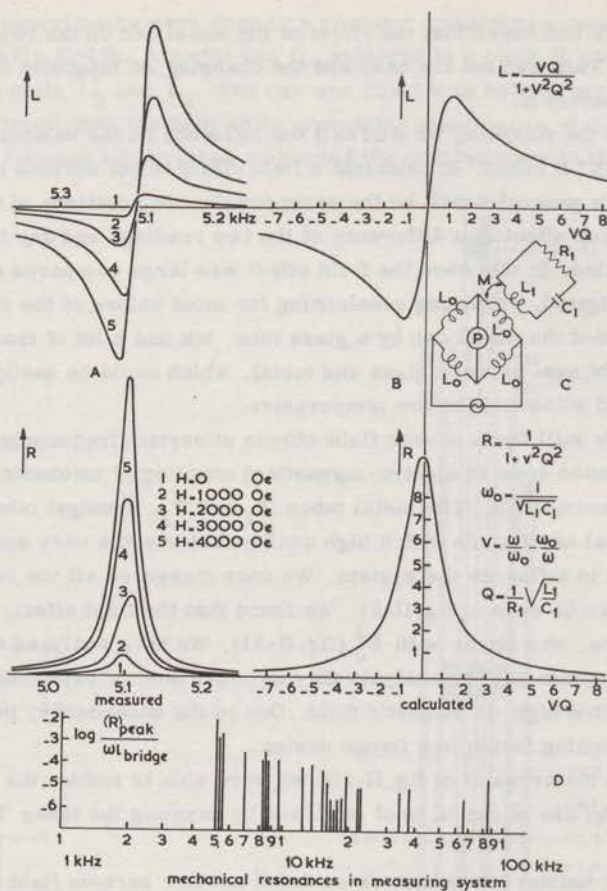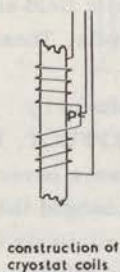
first approximation. The three wires from the coil system lie along the glass tube with a layer of cellophane adhesive tape wound around the tube to fasten the wires. The whole system is inserted into a second glass tube, which is joined to the first at the bottom. These tubes extend to the top of the cryostat and the outer one is connected with lacquer to the top. To equalize the pressure inside and outside the glass tubes we made a hole through the top of the tubes. There is no cooling fluid in direct contact with the coils, but the specimens are immersed in the cooling fluid inside the inner glass tubes.

construction of
cryostat coils

Fig. II-22.

A Faraday screen is provided to prevent capacity changes across the coil, caused by movement of the specimen, because these would be indistinguishable from magnetic effects. The screen is a silver layer deposited chemically

on the inside of the glass tube G_1. By means of a miniature chisel 12 axial cuts were made in the silver so that it does not form a shorted turn. Movement of the sample would soon damage the silver layer so a thin cylinder C made of cellophane tape, inserted into the inner glass tube, is used to provide mechanical protection.

It can be pointed out that the paramagnetic effects of all these materials are not important as long as they are not too strong. The effects on the two coils L_3 and L_4 balance in first approximation and any residual effect will be seen as a field effect only and does not influence the final result. Any paramagnetic effect of the specimen holder is, however, important and cannot be separated from the effects of the sample. Mostly we have used specimen holders made of lorival and casein. Neither materials showed paramagnetic effects.

Initially we worked with one specimen holder and a hoisting mechanism with two stops. Recently we designed a new mechanism with four stops, so now two specimen holders can be used. The specimen holders S_1 and S_2 are tied together and connected by a thin nylon wire U (fishing line) to a rod R which can be moved vertically by means of a motor M. The rod is pushed through an O-ring, which seals the motor mechanism from the interior of the cryostat. Micro switches control the movement of the vertical rod. If the specimen holder S_2 is in one of the measuring coils, the holder S_1 is effectively above the field of the coils. If the specimen in holder S_1 is being measured, S_2 is below the set of coils. Two switches control the motor. One selects the specimen, the other positions the specimen in either the upper or the lower coil. The mechanism M can easily be removed from the top of the cryostat and the specimens can be inserted through the top without taking the cryostat apart. The cryostat is a double glass cryostat. The outer glass N_2 is normally filled with fluid nitrogen, the inner one N_1 can be charged with any cooling liquid. The standard temperature regions can be attained by reducing the pressure of the bath through the outlet tube V.

Most of the disturbing effects found in the first cryostat were corrected. The only undesirable effect, which could not be cured is a resonance condition close to 90 kHz. The mechanism of this resonance is described in appendix A. The glass tube on which the coil has been wound, acts as a mechanical resonator coupled to the electrical system. This resonance practically prohibited the use of a measuring frequency of 85 kHz in our standard series. If small magnetic samples are measured, the results above 3000 Oe measured at the neighboring frequencies (60 kHz and 120 kHz) will show deviations. These limitations are, however, not serious, as we seldom use all frequencies.

In some experiments we initially cool the cryostat by filling it with helium or hydrogen, evaporating the liquid afterwards by means of an electric element in the bottom of the cryostat, which can dissipate a maximum of 30 W in a cooling fluid. We then observe the specimen while the temperature of the cryostat slowly

increases, due to the heat influx in the cryostat. To slow down the heating process we installed a 200 gram brass buffer (T) in the middle of the cryostat. The buffer is made of screening which is rolled around the glass tube and fills the space over a height of 10 cm. A similar heat buffer can be inserted inside the glass tube G_1. Two copper wires of 1.5 mm extend down from the outer heat stop T to the bottom in the cryostat. The intention is to provide a uniform temperature in the lower part of the cryostat. No measurements have been made of the temperature gradient in the cryostat. The temperature of the specimen is determined from the susceptibility using (2-25). The temperature increase around 10°K is of the order of 0.5°K in 5 minutes. At higher temperatures this increase slows down. In the same time interval we are able to make good estimates of the relaxation time.

2.11 DESCRIPTION OF THE MEASUREMENT PROCEDURE

After having described the bridge and associated electronic equipment, the measuring procedure will be given in detail.

Suppose we want to measure a set of relaxation curves as depicted in fig. II-23. Such a set is measured at a constant temperature with measuring frequency f and field strength H_c as independent parameters. The normal procedure is to vary H_c while keeping f constant.

1. First the reference oscillator is set at the desired frequency and the transmitter is tuned to equal the frequency of the reference oscillator, which can be observed on an oscilloscope showing a Lissajous figure. The automatic phase lock will keep the frequencies locked together.

2. The bridge variables are adjusted such that an approximate equilibrium is reached, which can be observed on the R and L vacuum tube voltmeters (32 and 33 fig. II-11) fed from the synchronous detectors. A small table provides the approximate settings of the variables for each frequency.

3. The attenuator is adjusted such that commutation of the sample results in a variation of the voltmeter reading of approximately 500 mV.

4. The variable phase control is adjusted such that commutation will not change the setting of the R voltmeter. This will be discussed in detail in paragraph 2.12.

The equipment is now ready for making the measurement. The magnetic field could be set at the desired value and the readings of the voltmeter could be taken before and after commutation of the sample. Instead of doing this, the magnetic field is slowly varied from zero to maximum with the sample in one coil, at maximum field the sample is commutated and the field strength is reduced to zero. The sample is again commutated and the initial starting con-

dition is reached again. The dc voltages from the synchronous detectors are recorded on an X-Y writer, providing a permanent record of each measurement. The voltage across the shunt of the amperemeter, indicating the current through the solenoid, is applied to the horizontal amplifier which is adjusted that 1 cm equals 250 Oe (100 Oe on an extended scale). The output voltage of the synchronous detectors is applied to the vertical amplifier, after passing through two calibrated attenuators (fig. II-24). These attenuators are constructed such that a 500 mV excursion on the voltmeter corresponds with 15 cm deflection on
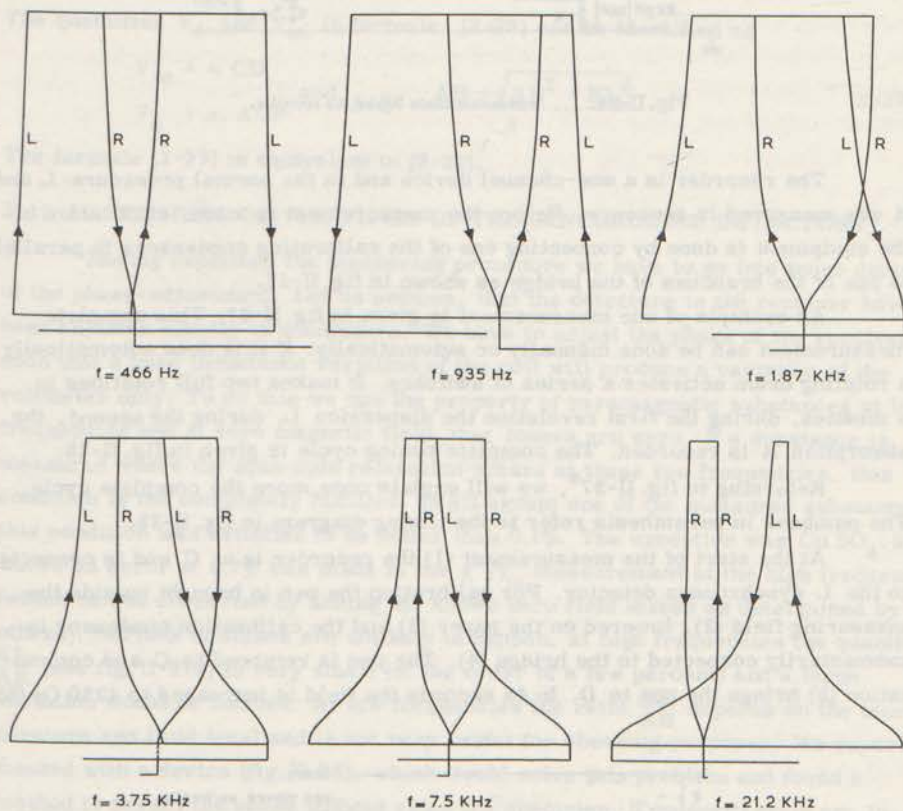
complete set of relaxation measurements of $Mn(NH_4)_2(SO_4)_2 \cdot 6H_2O$; $T = 20.3\ °K$

Fig. II-23.

the recorder at a predetermined sensitivity. Both the R and L channel of the receiver have a separate input attenuator and the gain of each channel can be individually multiplied by a factor 3 or 10 (switch S_1). The switch S_2 controls a calibrated attenuator with steps of 0.1 db.
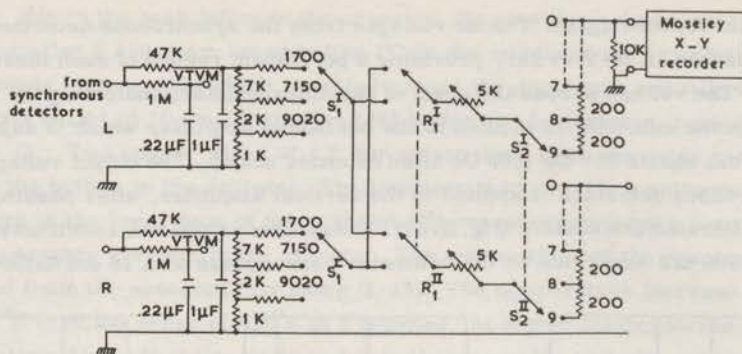
Fig. II-24.   Attenuator chain before the recorder.

The recorder is a one-channel device and in the normal procedure L and R are measured in sequence. Before the measurement is made, calibration of the equipment is done by connecting one of the calibrating condensors in parallel to one of the branches of the bridge as shown in fig. II-17.

An example of one measurement is given in fig. II-27. This complete measurement can be done manually or automatically. If it is done automatically a rotating drum activates a series of switches. It makes two full rotations in 5 minutes, during the first revolution the dispersion L, during the second, the absorption R is recorded. The complete timing cycle is given in fig. II-25.

Returning to fig. II-27[a], we will explain once more the complete cycle. The numbers in parenthesis refer to the timing diagram in fig. II-25.

At the start of the measurement (1) the recorder is at C and is connected to the L synchronous detector. For calibration the pen is brought outside the measuring field (2), lowered on the paper (3) and the calibration condensor is momentarily connected to the bridge (4). The pen is returned to C and commutation (5) brings the pen to D. In 45 seconds the field is increased to 4250 Oe (6)

timing diagram

Fig. II-25.

64
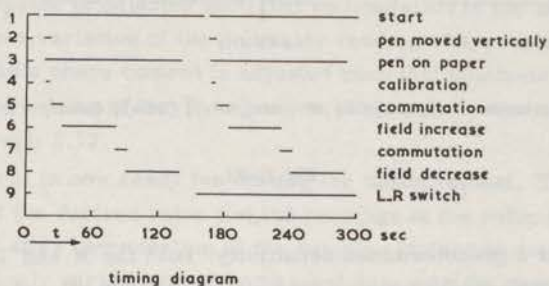
and the curve DF is obtained. Commutation (7) gives FG and reducing the field (8) produces GC, after which the pen is lifted. The recorder is next connected to the R synchronous detector (9) and in the same manner the R curve is produced.

The quantities χ'/χ_o and χ''/χ_o at a field H_c ($H_c \propto UT$) can be determined in the following simple manner

$$\left(\frac{\chi'}{\chi_o}\right)_{H_c, f} = \frac{EH}{DC} \quad (2\text{-}26a) \quad \text{and} \quad \left(\frac{\chi''}{\chi_o}\right)_{H_c, f} = \frac{NQ}{DC} \quad (2\text{-}26b)$$

The quantities V_c and V_m in formula (2-23) can be identified as

$$V_m = \alpha. \, CD$$
$$V_c = \alpha. \, A'B' \quad \text{and} \quad A'B' = \frac{AB + \sqrt{AB^2 + KL^2}}{2} \quad (2\text{-}27)$$

The formula (2-27) is equivalent to (2-22).

2.12 ADJUSTMENT OF THE PHASE OF THE SYNCHRONOUS DETECTORS

Having explained the measuring procedure we have to go into more detail of the phase-adjustment. Let us assume, that the detectors in the receiver have been adjusted exactly in quadrature. We have to adjust the phase of the receiver such that a pure inductance variation of the coil will produce a variation of the L voltmeter only. To do this we use the property of paramagnetic substances at low frequencies and at zero magnetic field that losses are zero. If a substance is measured where the spin-spin relaxation occurs at these low frequencies, this condition is not completely fulfilled. In all except one of the measured substances this condition was satisfied to be better than 0.1%. The exception was $Cu\,SO_4 . 5H_2O$ where an error of 0.7% was made in the χ''/χ_o measurement at the high frequencies (which can be corrected by adding the known zero field losses as determined by others). Serious mistakes are unlikely to happen, at high frequencies the quantity $\frac{KL}{AB}$ (see fig. II-27a) is very small (of the order of a few percent) and a large deviation would be noticed. At low frequencies the ratio $\frac{KL}{AB}$ depends on the temperature and fluid level and is not very useful for checking purposes. We experimented with a device (fig. II-26), which would solve this problem and found a method to preset the phase without using the specimen. Two small coils are in-

Fig. II-26.

from cryostat   to bridge
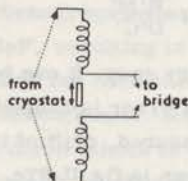
apparatus to adjust
phase of the receiver

serted in series with the bridge leads and a ferrite core is moved from one coil into the other by mechanical means at a 10 Hz rate. The moving core produces practically a pure inductance variation in the branches of the bridge containing the cryostat coils. The phase of the receiver should be adjusted such that the R synchronous detector shows a zero deviation, corresponding to a maximum deviation of the L detector. We tried such an experimental device and the phase we obtained was for all frequencies within 2 degrees of the correct one.

An actually operating unit has not been made, during our measurement we did not feel the need for it and to obtain good stability would require a mechanically well designed unit.

If the phase of the receiver is not exactly correct, a measurement as shown in fig. II-27b is obtained. Applying general rotation transformation formulas to fig. II-27b gives:

$$NQ = N'Q' \cos \varphi + E'H' \sin \varphi \quad (2\text{-}28)$$
$$EH = E'H' \cos \varphi - N'Q' \sin \varphi \quad (2\text{-}29) \qquad tg\varphi = \frac{R'M'}{D'C'} \quad (2\text{-}30)$$

no phase error, no drift   small phase error φ drift $R'M'$ and $I'C'$
$$tg\varphi = \frac{M'R'}{C'D'}$$

relaxationcurves at constant frequency with varying field   Fig. II-27.

in which the unprimed letters give the corrected values and the primed letters the measured values. For small phase errors $(<5^{\circ})$ the formulas can be simplified to:

$$NQ \approx N'Q' + E'H' \cdot \frac{R'M'}{D'C'} \tag{2-31}$$

$$EH \approx E'H' - N'Q' \cdot \frac{R'M'}{D'C'} \tag{2-32}$$

Adjusting the phase to $\frac{1}{2}^{\circ}$ is very easy. It can be pointed out, that in any normal ac bridge a similar type of error is caused by impurity of elements.

If small effects are measured, drift of the balance of the bridge will produce a measurement as shown in fig. II-27c. The simplest assumption one can make, is that the drift rate is constant in time and then the following correction can be made:

$$NQ \approx N''Q'' - \frac{H_{max} - H}{H_{max}} M''R'' \qquad (2-33)$$

$$EH \approx E''H'' - \frac{H_{max} - H}{H_{max}} C''I'' \qquad (2-34)$$

If both drift and phase error are present, the drift correction should be made first, followed by the angle correction.

In the above we supposed that the carrier phase of the synchronous detectors was adjusted such that the phase difference was exactly $\frac{\pi}{2}$.

To control this a rude check can be made by adjusting the common phase control such that a certain given variation in the bridge causes no difference on the voltmeter of one of the synchronous detectors and simultaneously a maximum deflection on the voltmeter connected to the second synchronous detector. This is a crude check because, although the zero-determination can be done with high accuracy, the determination of the maximum is not accurate due to a flat top of the cosine function ($\cos 90^o = 1,00$, $\cos 85^o = 0.996$).

To improve this we made a very simple tool. The circuit of fig. II-28a is attached in parallel to one of the branches of the bridge. The bridge is adjusted to an operating frequency of 15 kHz. If C is a pure capacity and R a
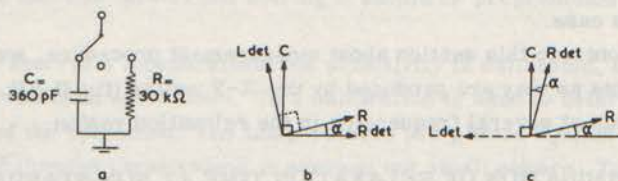
Circuit to adjust phase difference in synchronous detectors and associated vector diagrams

Fig. II-28.

pure resistor, the disturbances produced by these elements are in quadrature, i.e. the phase difference of the vectorial components is $\frac{\pi}{2}$. The values of the elements and the operating frequency are so selected that this condition is practically fulfilled. The condensor is a mica condensor and normally one can expect a tg δ better than 0.001 at these frequencies. The capacity of the 30 kΩ resistor can be of the order of 2pF, resulting in 0.3 degree difference in phase angle. The individual elements have not been checked, but the assumptions made have been confirmed in a measurement. Assuming first of all, that the C and R from fig. II-28 produce disturbances in quadrature, the adjustment of the synchronous detectors is very simple. The condensor is switched in and the phase control is set such that the switching of the condensor effects the L synchronous detector only, i.e. the response of the R detector is made zero.

Next we switch the condensor off and switch in the resistor. The requirement is now that the response of the L detector is zero. If this is not the case the phase relationship between the two synchronous detectors should be altered. (Trimmer 40 pF in fig. II-14).

If, however, the initial disturbances are not in quadrature, but are as indicated by the solid lines in the vector diagram of fig. II-28b, the phase of the synchronous detectors will be adjusted according to the dotted lines. Switching the condensor will affect the L synchronous detector only, switching the resistor will effect the R synchronous detector only. By means of a simple trick we can measure the angle α of the quadrature network (fig. II-28b, c).

To do this, we change the phase of the detector by about 90° and adjust the phase such that switching the condensor affects the R uetector only. Switching the resistor will affect, however, both the L and R detectors which produce respectively l and r mV. The angle α can be computed from the following relation: $\sin \alpha = \frac{r}{2l}$ (2-35). We found that the quadrature network was ideal to within 0.5° and the phase adjustment of the synchronous detectors can be expected to be correct within 1° after adjustment. This error will effect only the shape of the χ'/χ_o curve, at the field values where χ''/χ_o is large. The maximum discrepancy to be expected is 0.005 of the maximum of χ'/χ_o. The curves, from which the $\frac{b}{C}$ values are determined are not effected, because the χ''/χ_o is very small in this case.

To conclude this section about measurement procedure, we give a set of measurements as they are produced by the X-Y writer (fig. II-23). This set shows measurements at several frequencies in the relaxation region.

2.13 DETERMINATION OF RELAXATION TIME AT NON-STANDARD TEMPER-ATURES

The measurement of a complete set of curves, from which the relaxation parameters, as a function of the magnetic field can be determined should be done at a constant temperature, as provided by a bath of cooling liquid, boiling under a constant pressure. From a series of these measurements a ρ-T dependency in the standard temperature ranges can be established. If these results can be described by a straight line, knowledge of the relaxation time at intermediate temperatures is not necessary. If this cannot be done, a knowledge of the ρ-T behaviour at non-standard temperatures (e.g. between 4 and 14°K) is desirable. This is clearly shown in some of our measurements on manganese tutton salt.

We developed a method to make a reasonably accurate determination of relaxation times at any temperature between 1° and room temperature. The basic assumption for this procedure is that the relaxation can be approximated by a Debye relaxation. This should be determined in advance at some fixed temperatures and a knowledge of the $\frac{b}{C}$ value is useful. As is shown in section 1.4.1, χ'/χ_o and χ''/χ_o can be represented on an Argand diagram at any given

constant magnetic field. For a pure Debye relaxation this Argand diagram is a semi-circle. It is also shown in section 1.4.1 that for a pure Debye relaxation, the shape of the χ''/χ_o curve as a function of frequency, if plotted on a double logarithmic scale, is uniform. The full curve is determined in principle, if two values of χ''/χ_o at different frequencies are known. To obtain good accuracy, one frequency should be preferably below the relaxation frequency and the other above it. In some measurements, given in this thesis, we have used the first and in others the second method. We constructed a standard χ''/χ_o curve and made at a certain temperature the standard measurements as shown in fig. II-23 at at least two frequencies. From these we calculated the χ''/χ_o at one or more fields and plotted these values on a double logarithmic scale. The standard curve was brought through the points and the position of the peak determined. If the $\frac{b}{C}$ value of the specimen is known, the value of χ''/χ_o at this peak can be computed and can be used as a third point. Obtaining too low a value for the peak of the standard curve, if fitted through the two points, can be an indication that the relaxation is not a Debye relaxation. One can also plot the several sets of values for $\frac{\chi''}{\chi_o}$ and $\frac{\chi'}{\chi_o}$ in one Argand diagram. Drawing a semi-circle through these points is not necessarily the best solution, as the measuring frequencies give an extra condition to be fulfilled. It is probable that this method is more accurate, but solving it should be programmed for a computer.

At the start of a measurement the sensitivity is calibrated, and the time of the measurement is noted down. This calibration is used to determine the temperature of the specimen. The temperatures are plotted against time and a curve is fitted through these values to average out small errors. To determine the relaxation frequency two sets of measurements can be used at two different frequencies. The difference in time between the two measurements will introduce an error, but it can be shown that the error will be reduced if the relaxation frequency obtained is associated with the average temperature of two measurements. This procedure, followed at non-standard temperatures, we will call the "running method". The accuracy of the determination of the relaxation frequency is estimated to be in the order of 10%. As can be seen from fig. III-1, the relaxation frequencies determined at the standard temperatures fall nicely on the curve produced with the running method. The accuracy of the standard method is estimated to be between 2% and 5%, depending on the susceptibility, the filling factor of the sample, etc.

The running method could undoubtly be improved. A rough ρ versus T graph could be used to predict from the measurement of χ''/χ_o at the second frequency, the value of χ''/χ_o at that frequency at the same time as the χ'/χ_o measurement for the first frequency was taken.

In our measurements we have been more interested in the overall behavior than in precise values, no second order correction has been performed in

using the running method.

One remark should conclude this paragraph. If a specimen does not follow Curie's law accurately, the temperature will not be correctly determined. The measurements taken at standard temperatures serve to check this and the temperature computed by formula (2-25) can be checked at the standard temperature points. If the deviation from Curie's law is known, a slightly different method can again be used to determine the temperature. The only correction we made was using a Curie-Weiss law if applicable. No corrections have been made for diamagnetic effects.

2.14 MEASURING LONG RELAXATION TIMES

To measure long relaxation times, a bridge capable of handling very low frequencies should be used. Technically this gets complicated and VAN DEN BROEK[8] used a method in which the magnetic field is suddenly increased and the magnetization is studied as a function of time. The methods of studying the response of a sinusoidal variation of H or the response to a step ΔH in H_c are basically identical which can be shown by means of Fourier transforms. Analyzing the response to a step in H is, however, not easy and not so accurate. By means of sine waves the system can be probed with a measuring system having practically zero bandwidth; in the pulse method a wide bandwidth is essential, so a large number of repetitions are necessary to eliminate the noise in the "time-domain".

Our bridge is very suitable for the step method. A dc output is available from the synchronous detectors, the output of which is proportional to the susceptibility of the sample. The band-width of this channel can be easily reduced if desired for noise consideration by means of a simple RC filter.

The fast variation of the magnetic field is obtained as indicated in paragraph 2.9 by commutation of a current in an auxiliary coil, contained in the main magnet. In experimenting with this system we discovered that the time constant of this coil was the limiting factor to measuring fast relaxation processes, so instead of using a 24 Volt supply, we used a 100 Volt supply with a large series resistor, thereby reducing the time constant $\tau = \frac{L}{R}$ of the switching circuit. Manual switching was too irregular and too slow; switching by means of a relay improved the overall performance. A large condensor across the coil reduced transients. The complete response including the switching of the coil and the electronic equipment has a time constant τ of 3 msec.

Four different values of the current through the solenoid can be selected by means of switches. The field-strength in the middle of the coil is reported to be 53.40 Oe/Amp. A large field strength variation will increase the sensitivity, but the field variation ΔH ought to be small compared with the constant field H_c (see section 1.4.2).

70

Initially our measurements were done by making Polaroid photographs of the response of the magnetization to a step in the magnetic field strength. Analyzing these small photographs is, however, not easy. First we tried to analyze the photographs with a measuring microscope; afterwards we projected them with an epidascope onto a screen on which e-curves were drawn. The latest
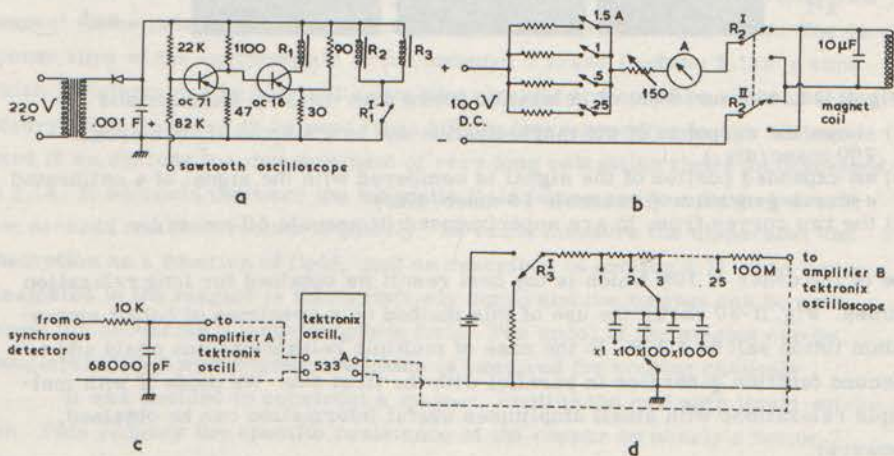

Fig. II-29.   Equipment for measurement of long relaxation times.

improvement we have made is shown with the complete experimental arrangement in fig. II-29.

The oscilloscope, a Tektronix 533, is free running such that the B-sweep triggers the A-sweep and introduces a waiting period for the A-sweep. The saw-tooth voltage derived from the A-sweep, available at an output on the front of the oscilloscope, is amplified in the power amplifier (fig. II-29a). The first transistor inverts the saw-tooth, the second activates a relay R_1. The bias voltages are arranged such that shortly after the beginning of the saw-tooth the relay R_1 is activated and is de-activated after the end of the saw-tooth. The relay R_1 switches two relays R_2 and R_3. By means of this cascade switching, the speed of R_2 and R_3 is independent of the rate of change of the saw-tooth. The relay R_2 is used to commutate the current in the coil (fig. II-29b), the relay R_3 is used in an RC comparing circuit (fig. II-29d). In this comparing circuit e-curves can be generated with a known time constant.

The actual response of the magnetization is compared with the generated e-curve by means of the electronic switch, built-in in the Tektronix dual-trace pre-amplifier, type CA. The generator for e-curves has four decades, which can be selected by a 4-position switch (fig. II-29d). Each decade is logarithmically divided into 25 steps, each step giving a 10% increase. In practice, it is found that for single relaxations one is usually able to select one of the steps as

71

the best fitting and that neighboring positions would be only just acceptable. This indicates that the accuracy of determining relaxation times by this method would
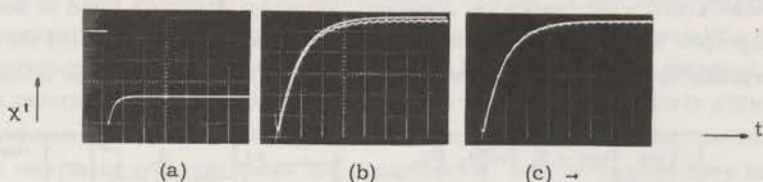

Fig. II-30. Measurement of relaxation times with the step-field method
a) shows the response of the magnetization due to a step in H_c (timescale 200 msec/div.)
b) an expanded portion of the signal is compared with the signal of a calibrated e-curve generator (timescale 50 msec/div.)
c) the two curves from b) are superimposed (timescale 50 msec/div.)

be of the order of 10% which is the best result we obtained for long relaxation times. Fig. II-30 shows the use of this method on a specimen of cobalt ammonium tutton salt at 4.2°K. In the case of multiple relaxations one could add a second function generator in parallel with the first one. We doubt if with multiple relaxations with small amplitudes useful information can be obtained, however.

2.15 CONSTRUCTION OF A MAGNET WITH A HIGH MAGNETIC FIELD (MAXIMUM 30 kOe)

Most of the measurements reported in this thesis have been made with the described magnet, producing a maximum field of 4500 Oe. Quite often the need was felt for a higher magnetic field.

Initially we contemplated construction of a super-conductive magnet. The system of the measuring coils used in this method for measuring paramagnetic relaxation is small in comparison with the Hartshorn system and it would probably be possible to construct a working ensemble, fitting inside a super-conductive coil.

To increase and decrease the magnetic field, flux pumping is considered as the best method, but a time interval in the order of 10-15 minutes is estimated to bring the field strength to a value of 30 kOe. In general we measure χ''/χ_o and χ'/χ_o at a constant temperature with f and H_c as parameters. In our measuring system, it is very convenient to vary H_c, keeping f constant. This would require nearly constant flux pumping. It is reported that excessive flux pumping uses much liquid helium and the pumping mechanism causes splashing. Another disadvantage is that one is practically restricted to helium temperatures. A separate hydrogen cryostat in the helium cooled super-conductive magnet requires a large inner diameter for the magnet and the magnetic field obtained would be reduced.

An all together different approach was tried. In our adopted measuring technique, all the data at one measuring frequency can be obtained in a short interval of time. It is limited by the relaxation time and the speed of the electronic equipment. Roughly speaking, one can say that the observation of dispersion and absorption should be made with a quasi-stationary magnetic field, i.e. the time during which the magnetic field can be considered constant should be long with respect to the relaxation time and the response time of the equipment. The response time of the equipment is of the order of 3 m sec (section 2.14), a time which is determined by bandwidth-limiting circuits and could be reduced if necessary. The bridge can be used from 200 Hz (corresponding to 1 m sec) upward if we exclude the measurement of very long relaxation times as described in 2.14. If we could increase the magnetic field from zero to a large value in a few seconds and then reduce it quickly, we could measure the dispersion and absorption as a function of field, just as described in section 2.11. The power dissipated in the magnet is then relatively small and the magnet can be optimized for producing a large magnetic field. The spool of the magnet can be completely filled with copper, no space is required for cooling channels.

It was decided to construct a magnet, cooling the coil with liquid-nitrogen. This reduces the specific resistance of the copper by nearly a factor 7, giving an increase of a factor 2.6 in field for the same power dissipation. The spool of the magnet is made of brass, a shorted turn is avoided by making one cut in a plane through the rotation-axis of the spool. This is done to keep the
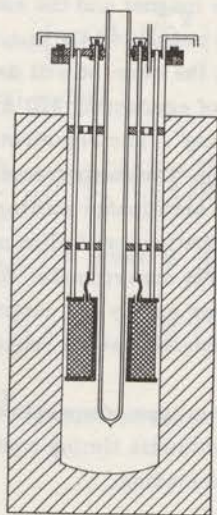

Fig. II-31.

▨ copper winding
▨ tempex insulation

sketch of the nitrogen-cooled magnet

time-constant of the magnet itself as high as possible. The spool is filled with copper band, cross-section of 4.5 mm x 2 mm and contains approximately 1900 turns. The wire is isolated with "Duroflex". The magnet is inserted in a stainless steel tank of 23 cm diameter. This cylinder is insulated at the outside by means of foam plastic insulation (Tempex). The field strength has been measured to be homogeneous with 2% in a vertical range of 10 cm. No deviation in a horizontal direction could be found inside the inner-diameter of the glass (45 mm). Our best estimate of the field strength is 75 Oe/Amp. measured by means of one of the anomalous absorptions of the cobalt salt described in section 3.7.

A sketch of this magnet is given in fig. II-31. A cryostat filled with helium or hydrogen just fits inside the magnet, the spool having an inner diameter of 65 mm; an outer glass is not needed because the whole magnet being immersed in liquid nitrogen.

The measurements reported, have been done by using the rectifier and stabilizer used for the water cooled magnet. Due to a different impedance the stabilizer oscillated occasionally, which produced irregularities in our measurements. The results obtained on some manganese, copper and cobalt specimens have been encouraging, however, for a first attempt and are given. The maximum field obtained was 15 kOe. For each measurement (cycle time 90 seconds) we used 2 liters of liquid nitrogen and a waiting time of 20 minutes was needed between measurements in order to cool the magnet.

The intention is ultimately, to operate the magnet on a 136 V battery. The magnet will be connected to the battery by means of a relay activated switch, the time constant of the magnet and the associated supply is estimated to be 0.7 sec. and the field will reach 30 kOe in 1.5 sec. At that moment the magnet will be switched off and the current will decay in the following second. A large silicon diode, capable of conducting 400 A is connected across the magnet and takes the "back-swing". The registration of the measurements will have to be done photographically. The measurement as proposed would require 0.3 liter liquid nitrogen with an anticipated waiting time between measurements of five minutes. The use of the battery will eliminate the oscillations of the stabilizer encountered in the first experiments. In this manner we hope to obtain 30 kOe with a 50 kW power supply. In contrast a conventional magnet (which could be operated continuously) would require an estimated power of 500 kW.

Control apparatus for this type of operation is under construction. The short time intervals require automatic timing equipment and provisions are nesessary to prevent thermal overloading.

2.16 CORRECTION FOR SPIN-SPIN ABSORPTION PEAKS

In some of our salts we were able to measure spin-spin relaxation phenomena. Spin-spin relaxation appeared in our absorption curves as small peaks

and an associated reduction of the χ'/χ_o could be detected. A typical example is shown in fig. III-14, in which the absorption curve is magnified 3 x in relation to the dispersion. From these curves we can obtain:

a) χ''/χ_o for the peak absorption

b) ΔH defined here as the total width of the absorption curve (expressed in Oersteds) at half of the maximum spin-spin absorption.

c) H' the value of the field (in Oersteds) corresponding to the absorption peak in the χ''/χ_o curve.

In spin-spin relaxation phenomena, the absorption is normally expressed as a fraction of the adiabatic susceptibility:

$$\frac{\chi''}{\chi_{ad}} = \frac{\chi''}{\chi_o} \frac{\frac{b}{C} + H^2}{\frac{b}{C}} \tag{2-36}$$

The value of the field H'' for which $\dfrac{\chi''}{\chi_{ad}}$ is a maximum, does not coincide with the value H' for the peak in the $\dfrac{\chi''}{\chi_o}$ curve for the spin-spin absorption.

In the following, we will calculate the correction for this. In all practical cases spin-spin relaxation occurs in our frequency range at fields $H > b/C$ (2-37).

Assume a Gaussian absorption curve given by:

$$\frac{\chi''}{\chi_{ad}} = K \exp\left[-\left(\frac{H - H''}{a. \Delta H}\right)^2\right] \text{ with } a \approx 0,6 \tag{2-38}$$

Using (2-36) and (2-37) in (2-38) yields:

$$\frac{\chi''}{\chi_o} \approx K \frac{b}{C} \frac{1}{H^2} \exp\left[-\left(\frac{H - H''}{0.6 \Delta H}\right)^2\right] \tag{2-39}$$

$$\frac{\partial}{\partial H}(\chi''/\chi_o) = 0 \text{ gives if } \frac{H''}{\Delta H} \gg 1$$

$$H'' \approx H' \left\{1 + 0,36\left(\frac{\Delta H}{H'}\right)^2\right\} \tag{2-40}$$

A typical value for $0.36\left(\dfrac{\Delta H}{H'}\right)^2$ is of the order of 0.01.

CHAPTER 3

DESCRIPTION OF THE MEASURING RESULTS

3.1 INTRODUCTION

In this chapter we will give the results of some measurements made with the bridge described in chapter 2.

The following specimens have been examined:

1. A series of 26 specimens of $Mn(NH_4)_2(SO_4)_2 \cdot 6H_2O$.
2. Gadolinium sulphate: $Gd_2(SO_4)_3 \cdot 8H_2O$.
3. A series of copper salts
    a. copper ammonium tutton salt: $Cu(NH_4)_2(SO_4)_2 \cdot 6H_2O$.
    b. copper cesium tutton salt: $Cu\,Cs_2(SO_4)_2 \cdot 6H_2O$.
    c. copper sulphate: $Cu\,SO_4 \cdot 5H_2O$.
    d. copper potassium chloride: $Cu\,K_2Cl_4 \cdot 2H_2O$.
4. Cobalt ammonium tutton salt: $Co(NH_4)_2(SO_4)_2 \cdot 6H_2O$.

Unless otherwise specified, all specimens have been prepared from Analar Analytical Reagents.

In several cases we have added impurities to the crystals. If a percentage of impurities is stated, it always refers to the percentage of impurities in the aqueous solution, from which the crystal was grown.

The results of measurements will, in general, be given in graphs. Symbols of different shape will be used to indicate a variation of a parameter, while the following coding will be used to denote the method by which the result was obtained.

    △ Results obtained by "running method" i.e. by slowly warming up the cryostat from a low temperature (open symbols).

    ▲ The specimen has been measured at 6 to 15 frequencies at a constant temperature and the relaxation constants have been derived from these curves (closed symbols).

    ◮ The relaxation time has been measured with the pulse-method (half open symbols).

76

In most of our measurements we obtained good Casimir-Du Pré relaxation curves, which were checked by comparing the curves obtained with a series of standard curves. When the relaxation curves were broadened we used in some cases the parameter d* as used by VAN DEN BROEK [64] to indicate the degree of broadening.

The general symbol used to denote relaxation time is ρ and is expressed in seconds, ρ is the inverse of the frequency at which the absorption coefficient χ''/χ_o in a Casimir-Du Pré curve has its maximum value and the dispersion coefficient χ'/χ_o is at "half value" (paragraph 1.4). If both parameters were available and good C.d.P. curves were obtained we give the average of ρ_a and ρ_d. In other cases we indicate the choice.

The following abbreviations have been used:

ρ, ρ_{sl} = spin-lattice relaxation time

ρ_a = spin-lattice relaxation time determined from the absorption curve

ρ_d = spin-lattice relaxation time determined from the dispersion curve

ρ_{ss} = spin-spin relaxation time

ρ_{hf} = spin-lattice relaxation time constant, used to indicate relaxation time for crystals with poor heat conduction (VAN DEN BROEK [23]).

In the pulse measurements for long relaxation times one obtains directly a time-constant τ, which is converted into ρ by the relation $\rho = 2\pi\tau$. The results have been plotted in the following manner:

1. χ'/χ_o and χ''/χ_o for the standard relaxation curves,
2. $\log \rho$ against $\log T$ and $\log \rho$ against $\log H$,
3. $\log \rho_{ss}$ against H^2 for the spin-spin relaxation.

3.2 MEASUREMENTS ON MANGANESE TUTTON SALT

The following specimens have been measured (all except specimen a, were from analar chemicals):

a) Specimen a, undiluted $Mn(NH_4)_2(SO_4)_2 \cdot 6H_2O$,
b) Specimen b, undiluted $Mn(NH_4)_2(SO_4)_2 \cdot 6H_2O$.
c) Specimen a, recrystallized.
d) Specimen b, with 1% $KMnO_4$ added.
e) Specimen e, undiluted $Mn(NH_4)_2(SO_4)_2 \cdot 6H_2O$.
f) Specimen similar to b, diluted with Zn 1:6.
g) Specimen similar to b, diluted with Zn 1:58.
h) 1% Co^{2+} added to chemicals from the same container as used for b.
i) 0.1% Co^{2+} " " "
j) 1% Fe^{2+} " " "
k) 0.1% Fe^{2+} " " "

l) 1% Co added to chemicals from the same container as used for b measured with the "running method".

m) Control specimen for h through l, similar to b.

n) 1% Cu^{2+} added to chemicals from the same container as used for e.

o) 1% Ni^{2+} added to chemicals from the same container as used for e.

u) A series of four specimens in which different amounts of $KMnO_4$ were added (0.1%, 1%, 3%, 10%) to a solution of specimen b.

v) A series of seven specimens in which the following percentage of the NH_4^+ ions were replaced by K^+ ions: 0%, 1.35%, 10%, 50%, 90%, 99%, 100%. For the 1.35% specimen chemicals from the same container as used for b were used, for the other specimens as used for e.

Manganese tutton salt was selected for the first measurements with the bridge for several reasons. It has a relatively high susceptibility (S = 5/2) and its deviations from isotropy and Curie's law are small; previous measurements showed that in a large temperature interval the relaxation times fall within the range of the bridge.

After the first measurements on specimen a, we decided to continue research on this salt in an attempt to solve some questions which had arisen earlier in the study of paramagnetic relaxation; the magnetic strength and the isotropy made it a good salt for this sequence of experiments.

3.2.1 Measurements on specimens of concentrated manganese tutton salt

In the Netherlands the relaxation phenomena of the salt have been measured by several investigators. BROER [65] measured spin-lattice relaxation at nitrogen and room temperatures. BIJL [6] and VAN DER MAREL [7] measured manganese tutton salt at helium temperatures by means of bridge methods and were able to do a few measurements in the hydrogen range. BÖLGER [9] studied this salt at helium temperatures with the saturation method. VERSTELLE [5] studied spin-spin relaxation.

The agreement between the results at helium and hydrogen temperatures of the different investigators was poor, and the connection between the helium and hydrogen results gave difficulties. The most important prior results have been indicated in our graphs. Combining the high and the low temperature data indicates a S-shaped dependency (GORTER [10]).

Sample a was obtained from Mr.C.VAN RIJN, who had grown large crystals for thermometry purposes. The crystals were made from standard laboratory chemicals (lab. B.D.H. reagent). The crystals were grown at 30°C in a temperature controlled oven and weighed between 5 and 50 grams. We measured several specimens weighing approximately 1 gram each in the temperature range from 4°K - 300°K. The results of a series of measurements on a single crystal (weight 1.13 g) in the K_2 direction are shown in fig. III-1. Three different

crystals have been measured in the K_1, K_2, and K_3 directions; al were cut from the same large crystal.

These measurements all produced a ρ-T dependency as indicated in fig. III-1, with relaxation times differing by less than 10% for the three crystals. In the following description we will combine these results.
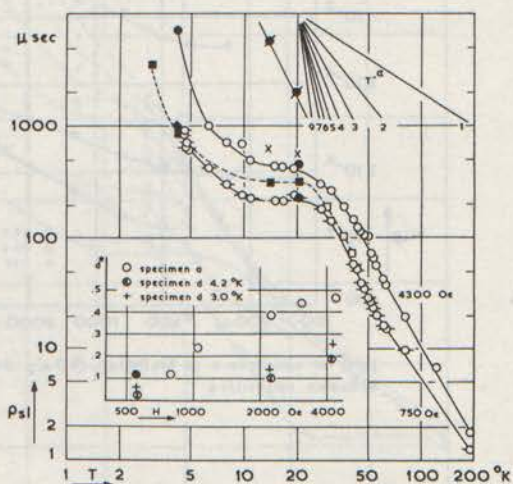

Fig. III-1.

$\rho(T)$ and $d(H)$ for specimens a and d of $Mn(NH_4)_2(SO_4)_2 \cdot 6H_2O$.

	specimen b	
-o-•- " a	750 Oe
o • " a	4250 Oe
□ ■ " d	750 Oe
x " d	4250 Oe

Three different regions can be observed in fig. III-1, two regions with a fairly high temperature dependency (T^{-3} - T^{-5}) connected by a temperature region where the relaxation time is practically independent of temperature.

In fig. III-1 the $\rho(T)$ curve is drawn for two values of the magnetic field (750 Oe and 4250 Oe). These are derived from measurements with the "running method". We made a full set of measurements at $4.2^{\circ}K$ and $20.3^{\circ}K$. On one of the other specimens, we measured two hydrogen and two nitrogen sets.

We will describe the three different regions in more detail.

1. The high temperature region ($T > 30^{\circ}K$) can be described by a dependency of T^{-3} between $30^{\circ}K$ and $50^{\circ}K$, at nitrogen temperatures we measured a $T^{-2,2}$ dependency. The relaxation curves have good C.d.P. shape. The ρ-H dependency at nitrogen temperatures is indicated in fig. III-2. The relaxation cannot be described by the Brons-Van Vleck formula, the best fitting p-value is 0.35, but the field-dependency at high fields is too steep. BROER[65] found p = 0.50 at $90^{\circ}K$.

2. The $\rho(T)$ dependency is fairly weak in the region from $8^{\circ}K$ - $30^{\circ}K$. In the hy-
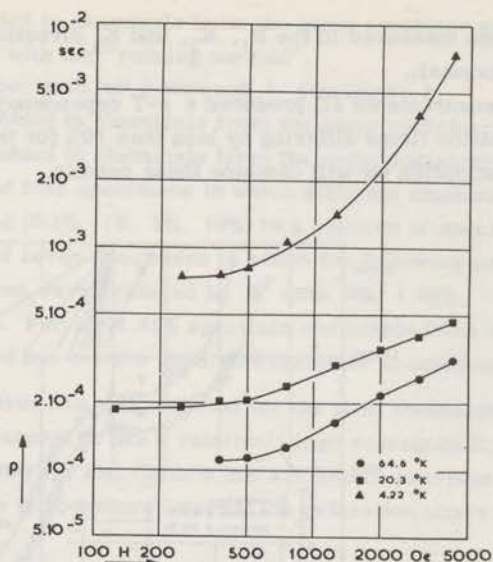
79

Fig. III-2.

$\rho(H)$ for specimen a of $Mn(NH_4)_2 (SO_4)_2 \cdot 6H_2O$ with unknown impurities

drogen range $\rho \propto T^{-0.3}$. The relaxation curves are good C.d.P. curves ($d^* < 0.05$). The $\rho(H)$ curve is given in fig. III-2 and cannot be described by a Brons-Van Vleck formula either.

3. The third region ($T < 8^{\circ}K$) is again characterized by a steep ρ-T dependency. Between $3^{\circ}K$ and $4^{\circ}K$ we find $\rho \propto T^{-\alpha}$, with $3 < \alpha < 4$. We find, however, at these liquid helium temperatures considerable deviations from C.d.P. curves, the deviation is largest at high dc magnetic fields ($H_c > 1250$ Oe). In fig. III-1 we give d^* for different values of the constant field H_c at $4.2^{\circ}K$.

We obtained between 4° and 20° several values for ρ by means of the running method. For low fields ($H_c < 1250$ Oe) good estimates are obtained, for high fields the deviations from true C.d.P. curves for temperatures below $8^{\circ}K$ are so large that the standard absorption curve, if fitted through two points, yields too low a value for χ''/χ_0 and the method cannot be used. The knee of the curve is approximately at $8^{\circ}K$ and the transition in behaviour seems to be fairly sharp. VAN DER MAREL [7] (sample q) reported a T^{-5} dependency and good C.d.P. curves in the helium range. The absolute values of his relaxation times were a factor 10 longer than our values, while the values obtained by BIJL [6] (sample s) were much higher still. Our results (including more measurements to be described) and the results of BIJL and VAN DER MAREL have been given in fig. III-3.

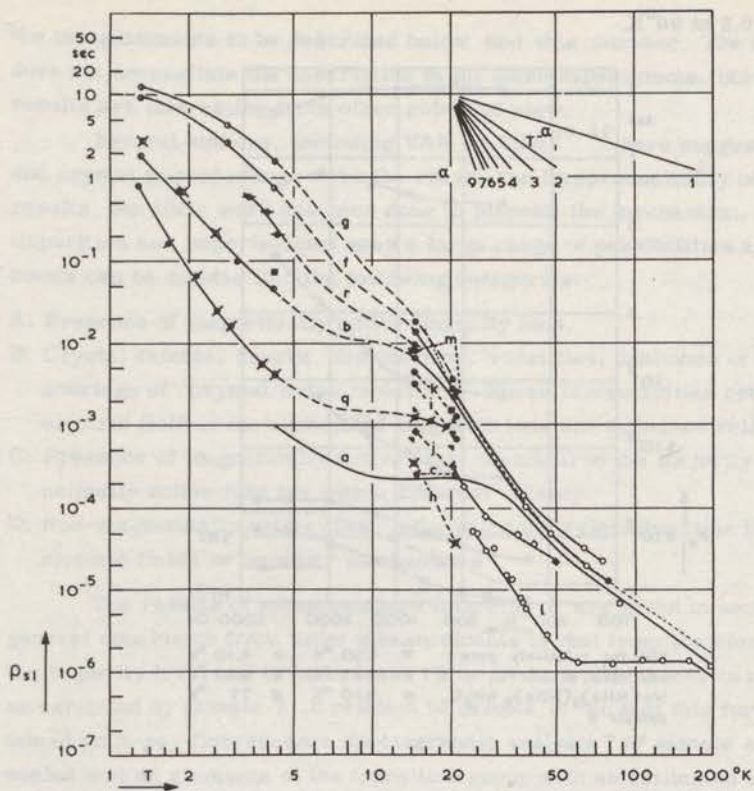Several researchers in this field expected that imperfections would

Fig. III-3.

	H_c in Oe		H_c in Oe
a: concentrated sample	750	k: 0.1% Fe^{++} added	750
b: concentrated sample	900	l: 1% Co$^+$ added, running method	750
c: specimen a recrystallized	750	m: control specimen as b, for h-through L	900
d: as b 1% KMnO$_4$ added, see fig III 1	750	n: 1% Cu added to e	750
e: concentrated sample	750	o: 1% Ni$^+$ added to e	750
f: diluted with Zn (Zn:Mn = 6:1)	900		
g: diluted with Zn (Zn:Mn = 58:1)	900	q: v.d. Marel, undiluted specimen	900
h: 1% Co added	750	r: v.d. Marel, diluted with Zn (1:88)	900
i: 0.1% Co^{++} added	750	s: Byl, undiluted specimen	900
j: 1% Fe^{++} added	750	t: Broer, undiluted specimen	750
		computed using (1.36)	

$\rho(T)$ for different specimens of Mn $(NH_4)_2$ $(SO_4)_2$ $6H_2O$

shorten the relaxation times; mostly they refer to physical imperfections. To check this, we obtained a new specimen (prepared from Analar chemicals) and the measured curve b is also drawn in fig. III-3. The relaxation times obtained are comparable to those obtained by BIJL[6]. At a low hydrogen temperature ($T = 14.4^{\circ}$K) we were able to obtain a good estimate of the relaxation time by extrapolation of our measuring results. At 20°K good C.d.P. curves are obtained; at 14.4°K we cannot determine this due to lack of data. The ρ-H dependency is given in fig. III-4 and can be described very well by the Brons-Van Vleck formula with p = 0.5. At 77°K we also made a complete measurement. In contrast to specimen a we found a Brons-Van Vleck character with p = 0.45 (fig. III-4); this correlates reasonably with measurements done by BROER[65]

81

who finds $p = 0.5$ at $90°K$.

Fig. III-4.

$\rho(H)$ for relatively pure specimen of $Mn(NH_4)_2(SO_4)_2 \cdot 6H_2O$, sample b

▽	1.30 °K	◐	4.10 °K
▲	1.81 °K	●	20.2 °K
▣	3.10 °K	⬈	77 °K
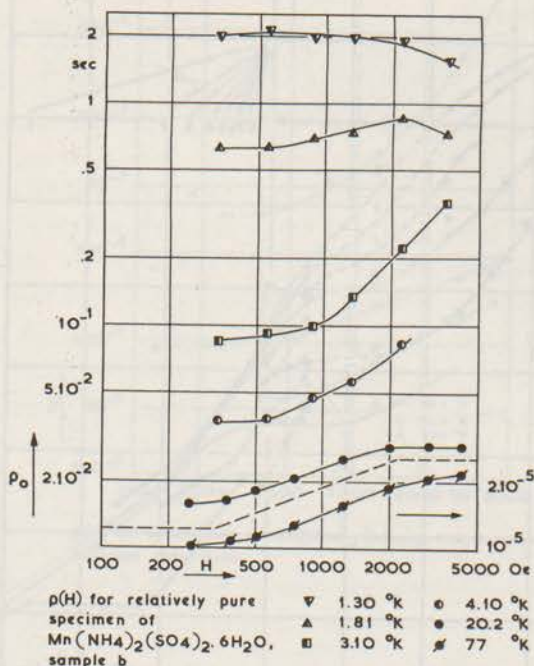
In the helium range we used the pulse method and obtained $\rho \propto T^{-3.5}$. The ρ-H dependency, however, changes drastically at different helium temperatures and is indicated in fig. III-4. The other points in the graph III-3 have been determined by the running method.

The $\rho(T)$ curve can again be divided into three parts:

1) a steep part in the range from $14°-40°K$ ($\rho \propto T^{-5}$), while at nitrogen temperatures the slope is reduced to a value close to T^{-2}.
2) a transition region somewhere between $4°$ and $14°K$ with a small slope.
3) a rather steep part in the helium range ($\rho \propto T^{-3}$).

The difference between the relaxation times in crystals a and b is large at the lower temperatures. In surveying the literature one often finds that different spin-lattice relaxation times are reported for the same salt under more or less identical conditions. Furthermore deviations of C.d.P. relaxation curves are often observed, mainly at low temperatures. In most cases it is not understood why this happens. Here we had measurements available from three specimens, in which the above mentioned difficulties were found in addition to an anomaly in the $\rho(T)$ curve. It was thought that discovering the differences between samples a, b, q, and s might give a clue to the solution of the general problem and

82

the measurements to be described below had this purpose. The final conclusion does not necessitate the description of all these experiments, but some of the results are interesting from other points of view.

Several authors, including VAN VLECK [36, 40] have suggested impurities and crystal imperfections to be the reason for irreproducibility of measuring results, but little work has been done to pinpoint the mechanism. The terms impurities and imperfections span a large range of possibilities and our experiments can be divided into the following categories:

A: Presence of magnetically active impurity ions.
B: Crystal defects, cracks, dislocations, vacancies, inclusion of additional, or shortage of crystal water molecules. These irregularities could change the electric field at the associated magnetic ions and influence relaxation times.
C: Presence of magnetically active ions, identical to the majority of the magnetically active ions but with a different valency.
D: Non-magnetically active ions, influencing the relaxation time by means of electric fields or by other mechanisms.

The results of measurements following A are given in section 3.2.4, the general conclusion from these measurements is that from the elements surveyed, the impurity level had to be at least 1% to produce differences in relaxation time as exhibited by sample a in relation to sample b. To test this further, we obtained an X-ray fluorescence spectographic analysis * of sample a. This revealed that no elements of the transition group with an estimated concentration larger than a few parts per million could be found in the sample.

Only one experiment has been done to try to find if the cause mentioned in B (crystal defects, etc.) could be responsible for the difference between the samples. The only known difference between a and b was the method of growing the samples. Sample a was grown as a large crystal at a controlled temperature of $30^{o}C$, b was grown at fluctuating room temperature. Therefore we dissolved a and grew crystals under the same condition as used for b. We thus obtained specimen c. The measuring results at two hydrogen temperatures are indicated in fig. III-3 and the difference between the relaxation times of c and a is small.

To test possibility C we added $KMnO_4$ to the solution to act as an oxydizer. The addition of $KMnO_4$ is known to produce manganese ions with higher valencies. TREADWELL [66] claims that Mn^{3+} is most likely to form, although higher valencies are possible. We prepared specimen d, made with chemicals used for specimen b and with the addition of $KMnO_4$ such that for each 100 Mn atoms due to manganese sulphate we would expect one Mn atom due to the $KMnO_4$. After the addition of $KMnO_4$ a brown residue appeared which may have been Mn_2O_3; this was removed by filtering. Crystals were grown from the solution.

---

* We are grateful to the University of Durham, England, through the intermediary of Dr. D.A. Curtis for performing the analysis.

These crystals were measured and the results are indicated in fig. III-1. The results for specimen b have also been indicated in fig. III-1 for comparison. At hydrogen temperatures we obtained good C.d.P. curves. With the running method we obtained a few points and the specimen has been measured at $3.0^{\circ}K$ and $4.2^{\circ}K$ with the Hartshorn bridge. In the helium range we again obtained large deviations from C.d.P. curves at high magnetic fields as shown in fig. III-1. The similarity between the results obtained from specimens d and a is striking, especially if one observes the large difference between specimen a and b in fig. III-1 and remembers that d has been derived from b by adding $KMnO_4$. We tried to confirm the existence of Mn^{3+} by means of optical spectroscopy, but were not able to obtain a usable absorption in a solution of either of the two crystals with the spectrometer in the Organic Chemical Laboratory in Leiden. An attempt to reduce Mn^{3+} to Mn^{2+} in sample a by boiling a solution of this sample with alcohol and sulphuric acid added, failed to produce a different relaxation time (after growing a crystal).

It was further thought to be interesting to find the relation between the concentration of the alleged Mn^{3+} ions and the relaxation times. We tried to establish this by adding different amounts of $KMnO_4$ to chemicals from the same container as used for b. The results of these measurements on the samples u are displayed in fig. III-5. Relaxation times were measured at two hydrogen temperatures ($14.4^{\circ}K$ and $20.3^{\circ}K$) at 750 and 4250 Oe. No deviations from C.d.P. curves have been observed in the hydrogen range. The measurements show the relaxation time in this temperature interval to be strongly dependent on the $KMnO_4$ concentration and to be practically temperature independent for all samples except the one with zero and 0.1% $KMnO_4$ added. These last two samples were also measured at helium temperatures. The pulse measurements produced good e-curves indicating that the relaxation mechanism can be described with a single time constant.

After these series of experiments we were fairly confident in having found, at least experimentally, the cause of the anomalous behaviour of the relaxation times as a function of temperature. Together with the samples u we had prepared one sample in which 1.35% K_2SO_4 was added to the basic chemical solution as used for sample b. The purpose of this sample was to show that the K^+ ions in the $KMnO_4$ did not give any changes in the relaxation time. The changes in relaxation times produced by this sample were, however, so large that we made a new series of samples v in which the following percentages of NH_4 in the $Mn(NH_4)_2(SO_4)_2 \cdot 6H_2O$ were replaced by K: 0, 1.35, 10, 50, 90, 99, 100%. To prepare these samples v we had to use a new container of manganese sulphate (Analar, Merck), the old container (also Analar, Merck) being empty. A sample e, made from this material, without any impurities added, was measured and the results are shown in fig. III-3 and fig. III-5. We see that in the hydrogen temperature range, the relaxation time of sample e

84
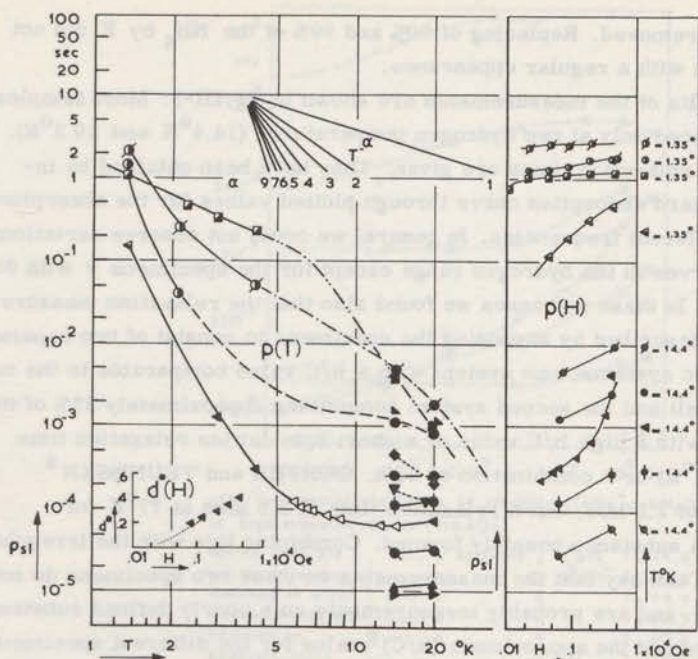
u: indicated percentages $K Mn O_4$
added to specimen b of $Mn(NH_4)_2(SO_4)_2 \cdot 6H_2O$

- - - - ⌀ ⌀ 0%
∘ ● 0.1%
● ● 1%
◆ ◆ 3%
◖ ◖ 10%

v: indicated percentages NH_4^+ ions in
$Mn(NH_4)_2(SO_4)_2 \cdot 6H_2O$ replaced by K ions

◀ ◀ ◁ 1.4%   ▲ 0% (sample e)
▲ 10%
▶ 50%
▼ 90% } formula and structure
◆ 99% } very doubtful
▣ ■ 100% $Mn K_2(SO_4)_2 \cdot 4H_2O$

Fig. III-5.

$p(T), p(H)$ and $d^*(H)$ for specimens u and v of $Mn(NH_4)_2(SO_4)_2 \cdot 6H_2O$

is similar to the values obtained by VAN DER MAREL [7] (fig. III-3 sample q) but, that this sample is somewhat less pure than sample b, if we associate long relaxation times with pure chemicals.

A few comments should be made about the specimens v. Crystals grown from solutions in which up to 50% of the NH_4^+ ions were replaced by K^+ ions, showed a regular crystal habit. The solution in which all the NH_4^+ ions were replaced by K^+ ions produced tiny crystals, except for one larger one. In the literature we were not able to find a manganese potassium tutton salt, but found instead a salt with the formula $Mn K_2(SO_4)_2 \cdot 4H_2O$ [67, 68, 69] (manganese leonite). The amount of crystal water in our sample was probably as given by this formula, being checked by weighing the crystal before and after heating above an open flame. The temperature reached by the specimen is unknown, but 4 water

molecules were removed. Replacing of 90% and 99% of the NH_4 by K did not produce crystals with a regular appearance.

The results of the measurements are shown in fig. III-5. Most samples have been measured only at two hydrogen temperatures ($14.4^\circ K$ and $20.3^\circ K$), and the obtained relaxation times are given. They have been obtained by inserting the standard absorption curve through plotted values for the absorption at four to six different frequencies. In general we could not observe deviations from C.d.P. curves in the hydrogen range except for the specimens v with 90% and 99% K-ions. In these two cases we found also that the relaxation measurements could be described by supposing the specimens to consist of two separate parallel magnetic systems, one system with a b/C value comparable to the manganese leonite salt and the second system comprising approximately 25% of the magnetic ions, with a high b/C value or a short spin-lattice relaxation time ($< 1\,\mu sec$ at $14.4^\circ K$) or a combination of both. GORTER and TEUNISSEN [4] report a $(b/C)^{\frac{1}{2}}$ of 2.5 kOe, but a relaxation time of 3.5 μsec at $77^\circ K$ for $Mn(SO_4).4H_2O$, a substance possibly formed. Combining this with the irregular crystal habit we can say that the measurements on these two specimens do not have much value; and are probably measurements on a poorly defined substance.

We determined the approximate $(b/C)^{\frac{1}{2}}$ value for the different specimens and indicated the values in the following table:

% K^+ ions:	0	1.35	10	50	90	99	100
$(b/C)^{\frac{1}{2}}$ in Oe:	770	770	770	840	1200	1200	1170

Table III-1: $(b/C)^{\frac{1}{2}}$ value of $Mn(NH_4)_2(SO_4)_2 . 6H_2O$ when the indicated percentages of the NH_4^+ ions have been replaced by K^+ ions.

Two of the specimens of the v-series were also measured at helium temperatures. The ρ-T dependency for the $MnK_2(SO_4)_2.4H_2O$ specimen in the helium range can be represented by $\rho \propto T^{-1.3}$ while ρ is at all helium temperatures nearly independent of H_c.

The sample with 1.35% K_2SO_4 added has also been measured at helium temperatures. At $4.2^\circ K$ we measured the sample completely. The dependency is displayed and again we find in this sample large deviations from C.d.P., mainly at high magnetic fields. The parameter $d^*(H)$ is shown also in an insert in fig. III-5. By means of the running method we measured the relaxation time between $4^\circ K$ and $14^\circ K$.

To conclude this section on concentrated manganese tutton salt, we refer to fig. III-6. In this diagram we give some of the initial measuring results on the samples a and b with the nitrogen cooled magnet at two hydrogen temperatures with magnetic fields up to 14 kOe.

Fig. III-6.
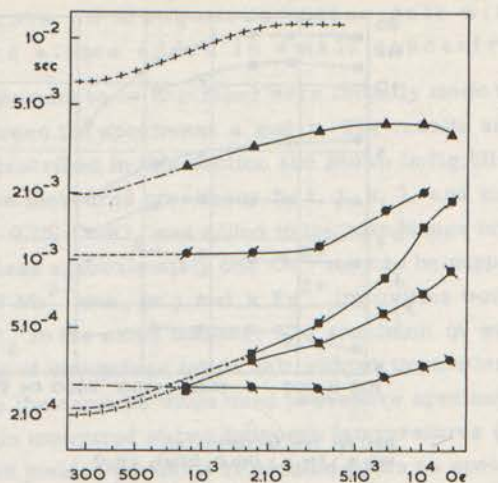
ρ(H) for several specimens of Mn(NH4)2(SO4)2 6H2O
at high magnetic fields (<14 KOe)

dotted lines are ____ ▨ specimen j 1% Fe++ T= 14.4 °K
low field values __ __ ■ " j 1% Fe++ T= 20.3 °K
obtained in other ·—·—· ◪ " a T= 14.4 °K
measurements and –·–·– ■ " a T= 20.3 °K
adjusted in ____ ▲ " b T= 20.3 °K
absolute value +++ " b T= 14.4 °K
(<20%) to
correlate with these measurements (different samples etc)

3.2.2 Measurements on diluted manganese tutton salts

We also measured two specimens, consisting of small crystals, in which
a large part of the Mn^{2+} ions were replaced by Zn^{2+}. The dilution was deter-
mined magnetically, by using the calibration as explained in section 2.8 and by
comparing with a concentrated crystal. The results of these measurements are
also indicated in fig. III-3. At temperatures above $20^{\circ}K$, the difference between
the diluted specimens and the undiluted "pure" specimen b is not very large, at
helium temperatures very long relaxation times are obtained. The field depend-
ency in the helium range, with $\rho \propto H^{\beta}T^{\alpha}$ and $\beta < 0$ at higher values of the constant
magnetic field (fig. III-7) is interesting. The same happened with the undiluted
"pure" sample b, but there only at the lowest temperature of $1^{\circ}K$. The differ-
ence between the 1:6 and 1:58 dilutions seems to be relatively small. These
findings are in fair agreement with the measurements of VAN DER MAREL [7].

3.2.3 The b/C values of manganese tutton salt

The b/C value of the manganese tutton salt has been the subject of some
controversy. BIJL [6] and VERSTELLE [5] both found 0.64×10^{6} Oe^{2}. VAN DER
MAREL [7] reports 0.54×10^{6} Oe^{2}. We have carefully analyzed several measure-
ments, made on our pure samples at several temperatures.

87
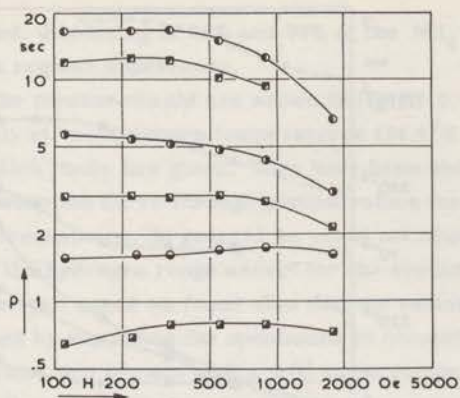
p(H) for two specimens of
$Mn_{(\frac{1}{n+1})} Zn_{(\frac{n}{n+1})} (NH_4)_2 (SO_4)_2 . 6H_2O$

1.32°K f▪ g●, 2.83°K f▪ g●, 4.23°K f▪ g●

f(n_6) and g(n_58)

Fig. III-7.

Specimen	Description	Temperature (°K)	b/C (kOe)^2
a	undiluted	4.2	0.58
b-1	undiluted	4.2	0.55
b-2	undiluted	4.2	0.585
b-1	undiluted	20.3	0.575
b-2	undiluted	20.3	0.575
j	diluted with Zn 1:6	4.2	0.35
k	diluted with Zn 1:58	4.2	0.32

Table III-2. Values of b/C for $Mn(NH_4)_2(SO_4)_2 . 6H_2O$

In general we find only a very small discrepancy between the measured x'/x_o values and values computed from the obtained b/C values. Because of unknown demagnetization factors, the helium results for the undiluted samples should be discarded. From the measurements at hydrogen temperatures our estimate of the b/C value of this salt is $(0.575 \pm 0.005) \, 10^6 \, Oe^2$. VAN DER MAREL[7] found at helium temperatures $0.54 \times 10^6 \, Oe^2$ but perhaps neglected to correct for demagnetization. At our request Mr. J.G.A. HILLAERT measured, in the bridge used by VERSTELLE[5], the material we used, and found at $20°K \, 0.61 \times 10^6 \, Oe^2$ and at 10 MHz. BENZIE et al[70] report b/C = $0.63 \times 10^6 \, Oe^2$ in reference 30, but they state in reference 71 that their values are 5.5 % high, due to an error in the magnet calibration. This brings their b/C value to $0.59 \, 10^6 \, Oe^2$.

88

3.2.4 Measurements on manganese tutton salt with magnetically active atoms added in small concentration

Most measurements to be described were initially made to find the cause of the difference between the specimens a and b. The results are, however, interesting and are described in this section and shown in fig. III-3. In the first set of experiments we measured specimens h, i, j, k, l, and m. In h and i respectively 1% and 0.1% $CoSO_4$ was added to the manganese tutton solution such that in the 1% case approximately one Co^{2+} ion can be supposed to be present for each 100 Mn^{2+} ions. In j and k Fe^{2+} impurities were added by using $Fe(NH_4)_2(SO_4)_2$ in the same manner. The specimen m was a control specimen, consisting of manganese tutton salt without impurities added. The chemicals used were the same as those used to prepare specimen b. The five specimens were again measured at two hydrogen temperatures (14^oK and 20^oK). The control specimen yielded the same relaxation times as specimen b.

The effect of the impurities on the relaxation time is considerable, the effect of about 0.1% of impurities can be clearly demonstrated and shortens the relaxation times by a factor 2 to 5 in the hydrogen range. A 1% impurity changes ρ by a factor 100.

Most salts containing cobalt ions have short spin-lattice relaxation times. VERSTELLE [5], pag. 71, reports $\rho = 0.4$ µsec at 20^oK, for $Co(NH_4)_2(SO_4)_2 \cdot 6H_2O$; a value which correlates with measurements made with our apparatus (section 3.7).

A few additional remarks can be made about the measurements on manganese tutton salt with 1% cobalt impurities (see fig. III-9). At field values up to 2000 Oe we find at 20^oK good C.d.P. curves, with a relaxation time which is practically independent of the magnetic field. At the fields 3000 Oe and 4250 Oe (which we normally choose for analyzing) the relaxation curves appear to be irregular (see χ'/χ_o at low measuring frequencies in fig. III-9) indicating a second relaxation or at least considerable deviations from C.d.P. curves. A standard C.d.P. curve is inserted through the measuring points and the best fit gives the apparant ρ. This phenomenon is somewhat similar to the findings for specimen a at helium temperatures. The field dependency of ρ is given in fig. III-8. The relaxation time is practically independent of the magnetic field. At 20^oK we find a sudden rise of the apparent ρ at high fields.

With Fe^{2+} impurities we did not detect a second relaxation from the curves obtained. The samples were, however, only investigated at three frequencies and the relaxation times determined in the same manner as in the running method; this method does not detect small deviations from C.d.P.-curves. Sample j was also examined by the running method up to 50^oK. Between 30^oK and 50^oK we find again a temperature region where the ρ is relatively constant. Above 50^oK the relaxation time approaches that of pure manganese tutton salt. After having investigated the crystals with 1% cobalt at
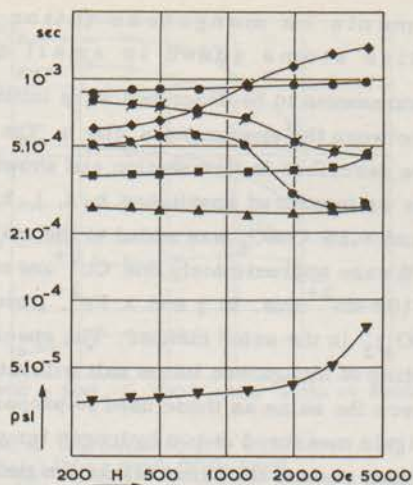
p(H) for four specimens of Mn(NH4)$_2$(SO4)$_2$.6H$_2$O salt with impurities added.

	o: 1 % Ni	h: 1 % Co	j: 1 % Fe	n: 1 % Cu
14.4°	◿	■	●	⎯
20.4°	◤	▼	▲	◆

Fig. III-8.

hydrogen temperatures, we realized that BROER [65] reported a decrease of relaxation time of only 5% at nitrogen temperatures if 1.5% cobalt was added to manganese tutton salt. This indicates that again a temperature region should be found in which ρ varies only a small amount. We used another sample with 1% cobalt and used the running method, starting from hydrogen temperature. The results are also indicated in fig. III-3. The value of the relaxation time at 20°K was different from measurements on sample h, but a slightly different Co^{2+} concentration could easily account for this. The results confirmed those obtained by BROER [65]. We measured the specimen from 20°K to 160°K. At 60°K the relaxation time becomes independent of temperature. The specimen was also measured at room temperature. The value of the relaxation time ρ at room temperature is practically the same as measured for a pure salt. Between 20°K and 60°K, the curves produced, gave large deviations from C.d.P. curves (as was found at 20.3°K, fig. III-9) and a standard $\frac{\chi''}{\chi^o}$ curve could not be fitted through two measuring points. This reduced the accuracy of the determination of the ρ values with the running method and errors of 50% are possible. This will, however, not have a large influence on the overall trend. In the flat part of the ρ(T) curve, the experimental curves indicate a single relaxation, indicating that the grip of the cobalt ions on the relaxation process has been reduced.

The series of measurements on manganese tutton salts with magnetic impurities added was concluded by measuring specimens n and o, containing

90

$$\frac{\chi'}{\chi_0}(f) \text{ and } \frac{\chi''}{\chi_0}(f) \text{ for } Mn(NH_4)_2(SO_4)_2 \cdot 6H_2O$$

salt (specimen h) with 1% Co'' added in
solution T= 20.3 °K

Fig. III-9.

Hc in Oe

1 — 125
2 — 250
3 — 375
4 — 500
5 — 750
6 — 1250
7 — 2000
8 — 3000
9 — 4250
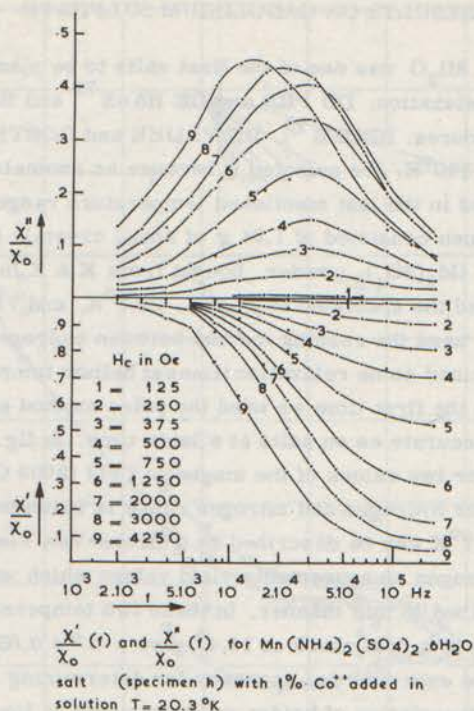
copper and nickel ions. The supply of the manganese sulphate, used for speci-
mens b through m (except e), was exhausted, so we had to use the the same
material as used for specimen e. Adding Cu^{2+} had, at $20^{\circ}K$, only a small ef-
fect on the relaxation time as can be seen in fig. III-3. $\rho(H)$ is given in fig. III-8,
which shows the same trend as for pure manganese salt. It should be noticed
that in $Cu(NH_4)_2(SO_4)_2 \cdot 6H_2O$ the relaxation time $\rho = 2.10^{-4}$ sec. at $20^{\circ}K$, which
is only a factor 10 different from manganese tutton salt (see section 3.2.1). The
addition of Ni^{2+} causes profound changes in the character of the relaxation. The
$\rho(H)$ curve at $14^{\circ}K$ and $20^{\circ}K$ has a part in which $\frac{\partial \rho}{\partial H} < 0$ which is very uncommon
at hydrogen temperatures. At the four highest fields (1250 Oe, 2000 Oe, 3000 Oe,
and 4250 Oe) we find deviations from C.d.P. curves with, at $20^{\circ}K$, values of d*
of respectively 0.01, 0.03, 0.05, and 0.09. The ρ is again the apparent ρ and
can be composed of several contributions if deviations from C.d.P. curves occur.

In measuring these impurities in manganese ammonium tutton salts we
have been studying systems in which cross relaxations and probably spin-diffu-
sion processes play an important role. Large magnetic fields should make
cross relaxation processes ineffective. To check this we have done a few meas-
urements with the new high-field magnet; the results are given in fig. III-6.

91

3.3 MEASURING RESULTS ON GADOLINIUM SULPHATE

$Gd_2(SO_4)_3 \cdot 8H_2O$ was one of the first salts to be measured in the study of paramagnetic relaxation. DU PRÉ and DE HAAS [72] and BIJL [6] measured it at helium temperatures; BROER [73], DE VRIJER and GORTER [74] measured between 77^OK and 290^OK. We selected it because an anomalous part in the $\rho(T)$ curve was reported in the last mentioned temperature range.

Our specimen consisted of 1.84 g of small crystals (< 0.5 mm diameter) crystallized from $Gd_2(SO_4)_3$ powder, bought from K & K Inc. and marked 99.9% pure. We measured the specimen at 14.5^OK, 20.3^OK, and 77^OK completely in the standard manner, used the running method between hydrogen and room temperature, and determined some relaxation times at helium temperature with the pulse method. This was the first time we used the pulse method and the results are not so complete and accurate as on salts at a later time. In fig. III-10 we give the ρ - T dependency for two values of the magnetic field (2000 Oe and 4250 Oe). The relation ρ - H in the hydrogen and nitrogen range is indicated in fig. III-11. The measurement at 77^OK can be described by a Brons-Van Vleck formula with p = 0.35. The hydrogen measurements yield values which were too steep at high fields to be described in this manner. In these two temperature ranges we find good C.d. P. curves, a spot check at 14.4^O gave a d * = 0.03 for 4250 Oe, which is smaller than the experimental accuracy for determining d *. We obtained ρ at 4.2^OK from extrapolation of bridge measurements at low frequencies and found deviations from C.d. P. curves (the standard absorption curve did not fit through the measuring points, the magnitude of the deviation cannot be specified). The pulse measurements at lower helium temperatures gave only approximate relaxation times.

The experimental results of BROER, GORTER and DE VRIJER which are also plotted in fig. III-10, are particularly very interesting to us. They reported that $\left(\frac{\partial \rho}{\partial T}\right)_H > 0$ between 77° and 90^OK. The value of the relaxation times they obtained is a factor 10 smaller than the values we measured. Combining these findings, we expected similar phenomena as found in the manganese tutton salt. To demonstrate possible influences of impurities we measured another sample (from the same supplier) and obtained the same results as shown in fig. III-10 with the relaxation times in the region between 50^OK and 90^OK temperature independent and equal to the values of the first sample within 5%. We dissolved this second sample in water and added 1% Dy^{3+} in the form of dysprosium ethyl sulphate, such that for each hundred gadolinium atom, one dysprosium atom was supposed to be present. The relaxation times have only been measured with the running method, and have been determined by means of an Argand diagram, being nearly out of the range of our bridge. The results are shown in fig. III-10 and are discussed in chapter 4.

From the first set of measurements described we determined the $\frac{b}{C}$ value.

Fig. III-10.

$\rho(T)$ for $Gd_2(SO_4)_3 . 8H_2O$.
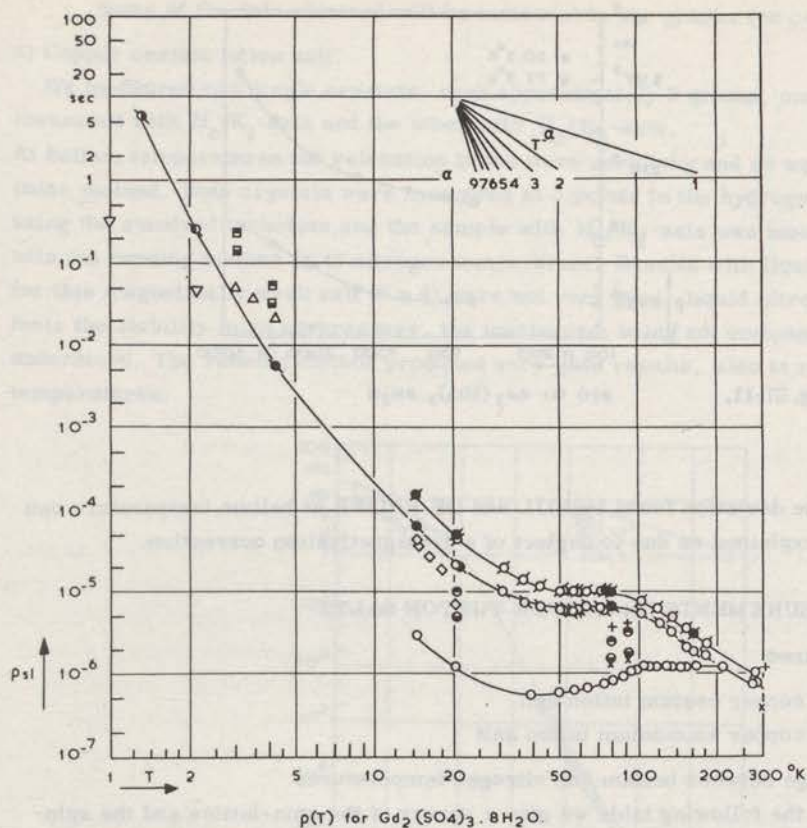
◌ ◖ ◑	de Vries	2000 Oe		⊡	Bijl	2000 Oe (extrapolated)
⊘ ⊘ ⊘	,,	4250 Oe		◼	,,	4000 Oe
○	,,	4250 Oe		x	Broer, Gorter	ρ_0
1% Dy added as dysprosium ethylsulphate						
◕	de Vrijer	2000 Oe (extrapolated)		+	,, ,,	ρ_∞
◔	,,	4000 Oe		△	Du Pré	1000 Oe
◇	,,	3200 Oe		▽	Benzie & Cooke	570-850 Oe

Our helium measurements at $4.2^{\circ}K$ gave $b/C = 3.3\ 10^6\ Oe^2$, a value which should be regarded as an estimate due to an unknown demagnetizing factor. Our value at $20^{\circ}K$ is in good agreement with values found by others listed in table III-3.

	Temperature ($^{\circ}K$)	b/C in Oe^2
De Vrijer	90, 77, 20	3.7×10^6
Broer	77, 90, 290	3.9×10^6
Bijl	4	3.6×10^6
De Vrijer	4.23	3.24×10^6
De Vries	20	3.82×10^6

Table III-3. b/C values of $Gd_2(SO_4)_3 . 8H_2O$

93

Fig. III-11. $\rho(H)$ for $Gd_2(SO_4)_3 \cdot 8H_2O$
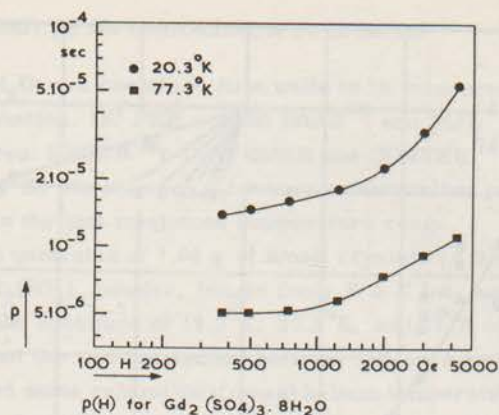
The deviation found by BIJL and DE VRIJER at helium temperature can again be explained as due to neglect of a demagnetization correction.

3.4 MEASUREMENTS ON COPPER TUTTON SALTS

We measured

    a) copper cesium tutton salt

    b) copper ammonium tutton salt

in the range between helium and nitrogen temperatures.

In the following table we give a survey of the spin-lattice and the spin-spin measurements, reported on copper tutton salts (excluding SeO_4 salts).

	Spin-lattice relaxation reported in the indicated temperature range by:		Spin-spin relaxation reported by:
	$1^{\circ}K - 4^{\circ}K$	$60^{\circ}K - 80^{\circ}K$	
$CuCs_2(SO_4)_2 \cdot 6H_2O$	Drewes and Gorter [75]		Ten Hove* Locher [42]
$Cu(NH_4)_2(SO_4)_2 \cdot 6H_2O$	Drewes and Gorter [75] Benzie and Cooke [76] Bölger [9]	Gorter e.a. [4]	Volger [79], Verstelle [5]
$CuRb_2(SO_4)_2 \cdot 6H_2O$	Benzie and Cooke [76]		
$CuK_2(SO_4)_2 \cdot 6H_2O$	Benzie and Cooke [76] Bijl [77], Van den Broek [78] Bölger e.a. [9] Drewes and Gorter [75]		

Table III-4. Survey of measurements on copper tutton salts. * not published

94

Some of the data obtained will be indicated in our graphs for comparison.

a) Copper cesium tutton salt.

We measured two single crystals, each approximately 3 grams, one was measured with $H_c // K_1$-axis and the other with $H_c // K_2$-axis.

At helium temperatures the relaxation times were very long and so we used the pulse method. Both crystals were measured at 3 points in the hydrogen range using the standard technique and the sample with $H_c // K_1$-axis was measured with the running method up to nitrogen temperature.. Results with liquid nitrogen for this magnetically weak salt ($S = \frac{1}{2}$) were not very good, liquid nitrogen affects the stability in an adverse way, the mechanism being not completely understood. The running method produced very good results, also at nitrogen temperatures.

$\rho(T)$ for $CuCs_2(SO4)_2 . 6H_2O$ with $H_c // K_1$ axis

o-●-o 125 Oe ;   o ● o 1250 Oe

——— computed using (1.36)
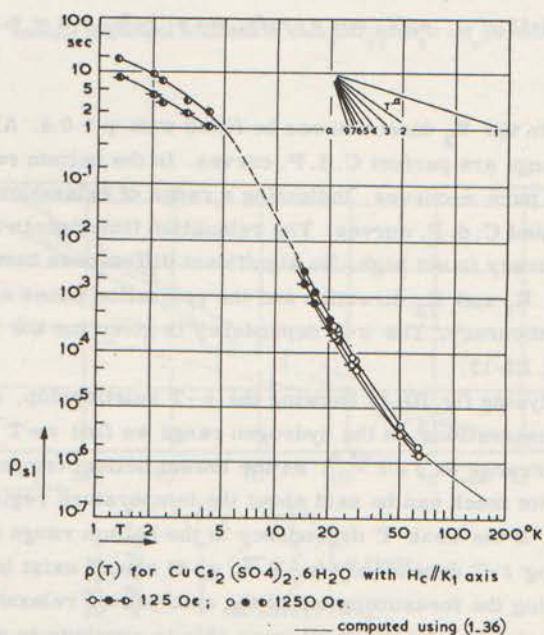
Fig. III-12.

The results of the measurements are displayed in fig. III-12 in which we give $\rho(T)$ for the K_1 direction for H_c = 125 Oe and 1250 Oe. In the hydrogen range the relaxation values stay constant for higher fields. The crystal in the K_2 direction has been measured only at helium and hydrogen temperatures. At hydrogen temperatures the $\rho(T)$ curves for K_1 and K_2 at 125 Oe, coincide at 1250 Oe the curves are slightly different at hydrogen temperatures. This is also obvious by studying the $\rho(H)$ curve, given for the K_1 and K_2 directions in fig. III-13. The $\rho(H)$ dependency in the K_1 direction at hydrogen temperatures can be described excellently by a Brons-Van Vleck formula with p = 0.55, while

95

p(H) for CuCs$_2$ (SO4)$_2$. 6H$_2$O

$T = 20.3\ ^\circ K$
$T = 20.3\ ^\circ K$
$T = 4.2\ ^\circ K$

Fig. III-13. $H_c \parallel K_2$-axis #; $H_c \parallel K_1$-axis ×; $H_c \parallel K_2$-axis or K_1-axis ∘.

the results in the K_2 direction can be fitted with $p = 0.4$. All the curves in the hydrogen range are perfect C.d.P. curves. In the helium range the pulse method did not give pure e-curves, indicating a range of relaxation times, comparable with broadened C.d.P. curves. The relaxation times given are average values and the accuracy is not high. No significant differences have been observed between the K_1 and K_2 direction and the relaxation times are equal within measuring accuracy. The ρ-H dependency is given for the K_1 direction at $4.2\ ^\circ K$ in fig. III-13.
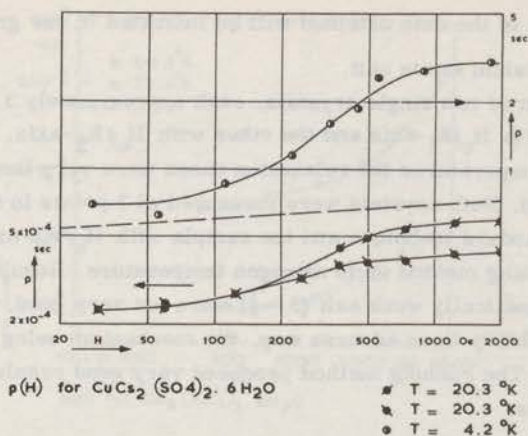
Analyzing fig. III-12 showing the ρ-T relationship, one can make the following observations: In the hydrogen range we find $\rho \propto T^{-6}$, which reduces in the nitrogen range to $\rho \propto T^{-3.5}$. At the lowest helium temperatures we find $\rho \propto T^{-1.5}$. Not much can be said about the temperature region between hydrogen and helium. If the weak T dependency in the helium range continues beyond $5\ ^\circ K$ a strong ρ-T dependency ($\rho \propto T^{-\alpha}$, $\alpha > 6$) should exist in this region.

During the measurements of the spin-lattice relaxation we noticed small absorption peaks which we were able to attribute to spin-spin relaxation. An example is shown in fig. III-14 which gives a measurement on copper cesium tutton salt in the K_1 direction with a frequency of 170 kHz. The absorption values are 3 x magnified relative to the dispersion curve. H_c' could be determined with an accuracy of 1 to 3% depending on the quality of the graph. ΔH and $\chi''_{ss\,max}/\chi_o$ could be determined with an accuracy of 10 to 20%. After applying the correction mentioned in section 2.16 the results were given in fig. III-15. We plotted $\rho_{ss}(H^2)$ for the K_1 and K_2 direction. Data are included for $4\ ^\circ K$, $14\ ^\circ K$, $17\ ^\circ K$, and $20\ ^\circ K$. Also plotted in fig. III-15 are unpublished early results of higher frequency measurements made by Mr. E.A. TEN HOVE. His sample consisted of small crystals. Fig. III-15 shows an anisotropy for the two crystal

96
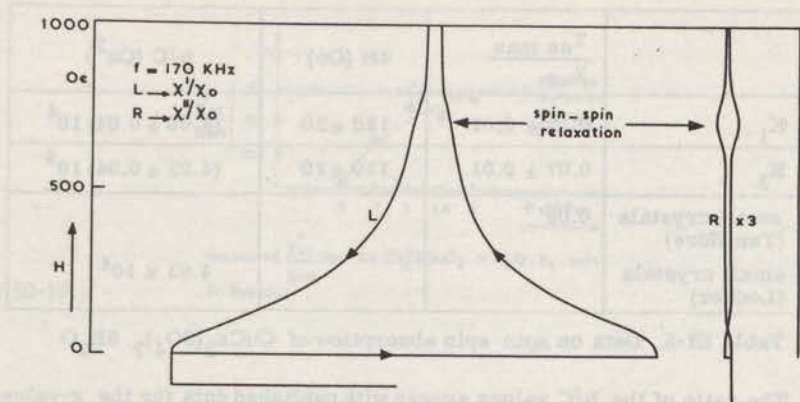
Fig. III-14.   Example of spin-spin relaxation in $CuCs_2(SO_4)_2 \cdot 6H_2O - H_c /\!/ K_1$ axis.

T	$H_c /\!/ K_2$	$H_c /\!/ K_1$	
4 °K			
14 °K			
16.7 °K			< 1 MHz
20 °K			
20 °K		ten Hove (>1MHz)	

$\rho_{ss}(H^2)$ for $Cu\,Cs_2\,SO_4{}_2\cdot 6\,H_2O$.
calculated (Tjon) _ _ _ _ sc (100), _ . _ . _ fcc (100), ... fcc (111)

Fig. III-15.

directions. The average of our measurements agrees with the measurements of
Mr. TEN HOVE. We also found a large anisotropy in the magnitude of
$\dfrac{X''_{ss\ max}}{X_{ad}}$. This, the value of ΔH and b/C are given in table III-5.

97

	$\dfrac{\chi''_{ss\ max}}{\chi_{ad}}$	ΔH (Oe)	b/C (Oe^2)
K_1	0.15 ± 0.02	120 ± 20	$(4.00 \pm 0.04)\,10^4$
K_2	0.07 ± 0.01	130 ± 20	$(4.92 \pm 0.04)\,10^4$
small crystals (Ten Hove)	0.08		
small crystals (Locher)			4.63×10^4

Table III-5. Data on spin-spin absorption of $CuCs_2(SO_4)_2 \cdot 6H_2O$

The ratio of the b/C values agrees with published data for the g-values. Using formula (1-38) from section 1.7, with $g_{//} = 2.43$, $g_\perp = 2.06$ and $\alpha = 40^\circ$ (BLEANEY et al[80]), we computed:

$$\frac{\chi_1}{\chi_2} = 1.22^5 \quad \left(\frac{\chi_1}{\chi_3} = 1.06\right).$$

Experimentally we found:

$$\frac{(b/C)_{K_2}}{(b/C)_{K_1}} = \frac{4.92}{4.00} = 1.23$$

Our values, however, do not agree with the measurements on powders by BENZIE et al[71]. They obtained a b/C value of 4.63×10^4 Oe^2. If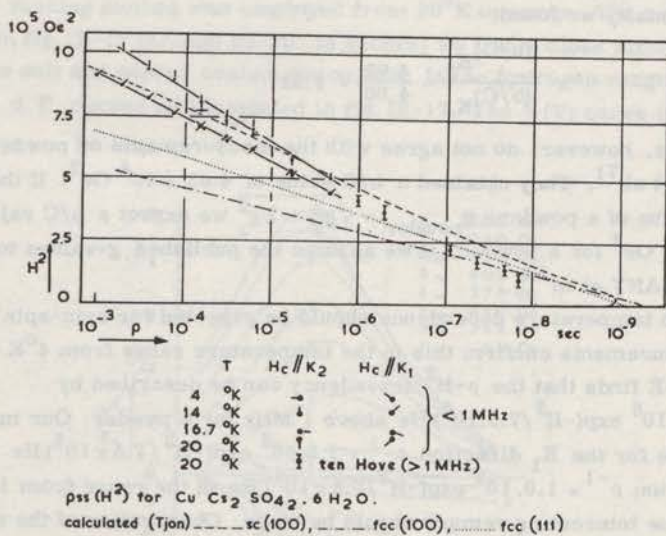 the effective g-value of a powder: $g_{powder} = \sqrt{g_{//}^2 + 2\,g_\perp^2}$ we expect a b/C value of 4.33×10^4 Oe^2 for a powder, if we assume the published g-values to be correct (BLEANY et al[80]).

No temperature dependence should be expected for spin-spin relaxation. Our measurements confirm this in the temperature range from 4°K - 20°K. TEN HOVE finds that the ρ-H^2 dependency can be described by $\rho^{-1} = 2.1.10^8 \exp(-H^2/7.9.10^4)$ Hz above 1 MHz for a powder. Our measurements would give for the K_1 direction $\rho^{-1} = 1.8.10^8 \exp(-H^2/7.5 \times 10^4)$ Hz and for the K_2 direction $\rho^{-1} = 1.0.10^8 \exp(-H^2/9.5 \times 10^4)$ Hz in the range from 1 kHz - 1 MHz.

One interesting remark should be made. Observation of the spin-spin absorption of some specimens gave an indication that if the spin-lattice relaxation time ρ_{sl} got shorter than the anticipated spin-spin relaxation time ρ_{ss}, the absorption due to the spin-spin relaxation disappeared. The observation is not easy. A small spin-spin absorption (a fraction of a percent) is masked by a large spin-lattice relaxation (50%). Results of measurements on $CuCs_2(SO_4)_2 \cdot 6H_2O$ in the K_1 direction are shown in fig. III-16. This shows that the apparent spin-spin absorption definitely reduces if $\rho_{ss} > \rho_{sl}$. Our observations indicate that the spin-spin absorption peak disappears, although if the spin-spin absorption smears out over a large field-range (for some unknown reason) it could stay unnoticed.

.15
.10
.05

$\dfrac{\chi''_{ss}}{\chi_{ad}}$

average
value for
$\dfrac{\rho_{sl}}{\rho_{ss}} \gg 1$

.5 .7 1 1.4 2 ρ_{sl}/ρ_{ss}

measured $\dfrac{\chi''_{ss}}{\chi_{ad}}$ for Cu Cs$_2$(SO$_4$)$_2 \cdot$ 6H$_2$O. K$_1$ .axis

if $\rho_{sl} \approx \rho_{ss}$.
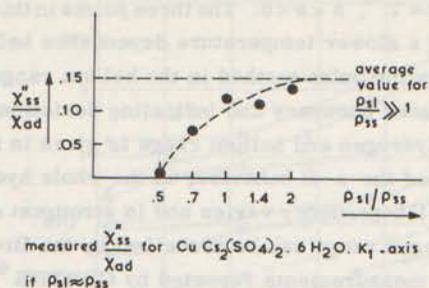
Fig. III-16.

b) copper ammonium tutton salt.

Crystals of copper ammonium tutton salt do not grow easily and no large single crystals were available. We measured 3 gram of small crystals (1-3 mm diameter) of this salt. The specimen was measured at helium temperatures with the pulse method and at three temperatures in the hydrogen range. The running method was employed from 20°K upwards. The results are shown in fig. III-17 through III-20. In general we find a close similarity between this salt and copper cesium tutton salt. In the hydrogen range we find excellent C. d. P. curves as illustrated in fig. III-17. The ρ (T) curve is shown

.5
.4
.3
.2

8 — 2000 Oe
7 — 1250 Oe
6 — 750 Oe
5 — 500 Oe
4 — 375 Oe
3 — 250 Oe
2 — 125 Oe
1 — 62 Oe

$\dfrac{\chi''}{\chi_o}$

.1

.0

.9
.8
.7
.6
.5
.4
.3
.2
.1

$\dfrac{\chi'}{\chi_o}$

T = 20.3 °K

5.10^2 10^3 2.10^3 5.10^3 10^4 2.10^4 5.10^4 10^5 Hz

f
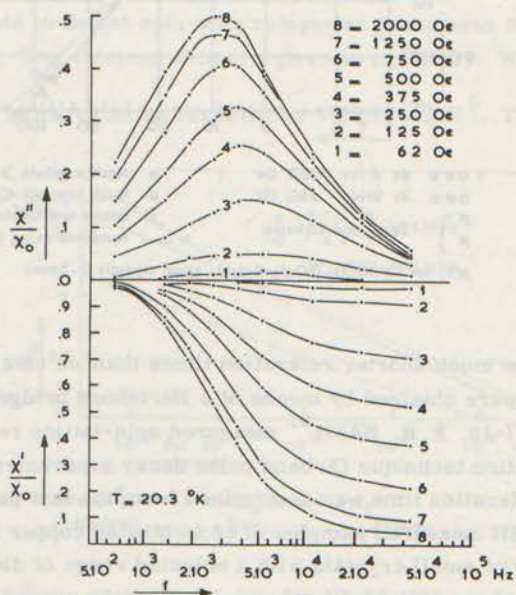
$\dfrac{\chi'}{\chi_o}(f)$ and $\dfrac{\chi''}{\chi_o}(f)$ for Cu (NH$_4$)$_2$ (SO$_4$)$_2 \cdot$ 6H$_2$O

Fig. III-17.

in fig. III-18 and gives $\rho \propto T^{-\alpha}$, $5 < \alpha < 6$. The three points in this range are not on a straight line, indicating a slower temperature dependence below $14^\circ K$. The relaxation curves produced by the pulse method in the helium range were poor e-curves, resulting again in a reduced accuracy and indicating deviations from C.d.P. The ρ-H dependency in the hydrogen and helium range is given in fig. III-19. The curve at $20.3^\circ K$ described the ρ-H behaviour in the whole hydrogen range; in the helium range the ρ-H dependency varies and is strongest at low temperatures. The results in the hydrogen range can be described by the Brons-Van Vleck formula with $p = 0.5$. The measurements reported by GORTER [4] fall on an extrapolated part of our curve. The measurements of BENZIE and COOKE [76] give in

Fig. III-18. $\rho(T)$ for $Cu(NH_4)_2(SO_4)_2.6H_2O$. small crystals (1-3mm)
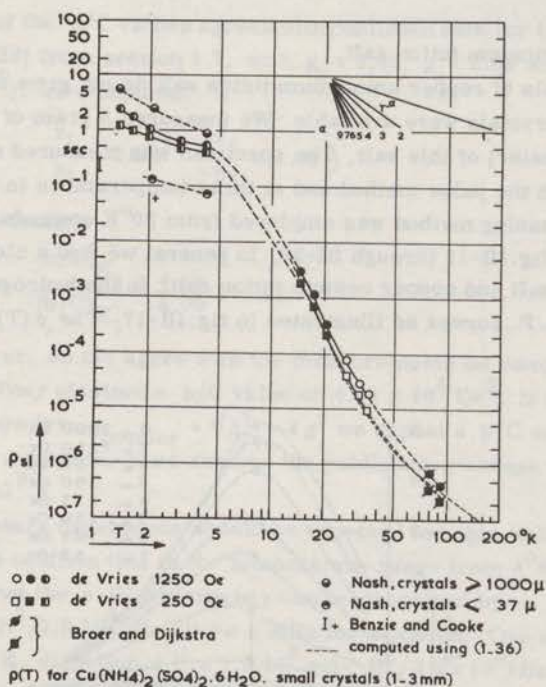
the helium range much shorter relaxation times than we obtained. These measurements were obtained by means of a Hartshorn bridge and are also indicated in fig. III-18. F.R. NASH [81] measured spin-lattice relaxation by means of a spin saturation technique (X-band pulse decay superheterodyne spectrometer). The relaxation time was determined from the last part of the relaxation curve. NASH measured samples of concentrated copper ammonium tutton salts consisting of small crystals with a selected range of diameters. Some of his results have been indicated in our graph III-18 for comparison. He found that the relaxation time was strongly dependent on the size of the crystals and

Fig. III-19.

p(H) for Cu (NH4)2 (SO4)2 6H2O

- ● 20.3 °K (right hand scale)   ■ 4.22 °K
- ◀ 2.00 °K   ▶ 3.06 °K
- ▼ 1.60 °K   ▲ 1.33 °K
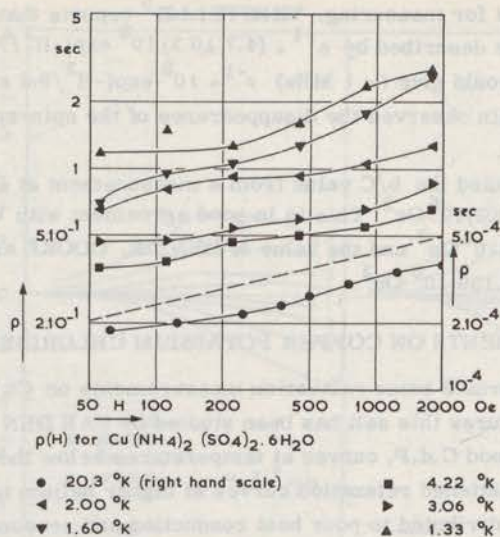
attributed this to bottleneck phenomena. He claimed that the relaxation time was constant for crystal diameters larger than 1 mm. No difference was observed between cooling by liquid helium or helium gas. The absolute magnitude and the temperature dependence of the relaxation times obtained by us are in good accordance with the measurements obtained by NASH.

We were able to detect spin-spin relaxation phenomena in copper ammonium tutton salt. The obtained data are given in fig. III-20. We found $\frac{\chi''_{ss\ max}}{\chi_{ad}} = 0.10$, the same value as reported by VERSTELLE [5]. The spin-spin

Fig. III-20.

Pss (H²) for Cu (NH4)2 (SO4)2 6 M2O
calculated ‑‑‑‑‑‑‑‑ Tjon ‑ ‑ ‑ ‑ ‑ Caspers

- ● 20.3 °K < 1 MHz
- ○ 4.2 °K
- —— > 1 MHz _Verstelle.

data of VERSTELLE [5] are also indicated in fig. III-20. We see that we found a different ρ-H^2 relationship, but that the measurements results coincide at

101

1 MHz, our limit for measuring. VERSTELLE[5] reports that his measurements
(> 1 MHz) can be described by $\rho^{-1} = (4.7 \pm 0.2) 10^8 \exp(-H^2/7.4 \times 10^5)$ Hz. Our
measurements would give (< 1 MHz) $\rho^{-1} = 10^8 \exp(-H^2/9.3 \times 10^5)$ Hz. In this
specimen we again observed the disappearance of the spin-spin relaxation if
$\rho_{ss} > \rho_{sl}$.

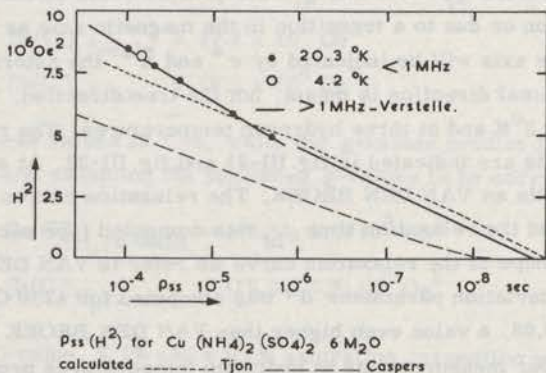We computed the b/C value from a measurement at $4^\circ K$ and obtained
$b/C = (0.151 \pm 0.002)10^6 Oe^2$. This is in good agreement with VERSTELLE's value
of $(0.152 \pm 0.005)10^6 Oe^2$ and the value of BENZIE, COOKE and WHITLEY[71] who
obtained $b/C = 0.150 \ 10^6 Oe^2$.

3.5 MEASUREMENTS ON COPPER POTASSIUM CHLORIDE

We performed some relaxation measurements on $Cu K_2 Cl_4 . 2H_2O$. At
helium temperatures this salt has been studied by VAN DEN BROEK et al [19, 8].
They reported good C.d.P. curves at temperatures below the λ-point of helium,
but found very flattened relaxation curves at higher helium temperatures. This
effect has been attributed to poor heat conduction and reasonable correlation
was obtained between the theory of EISENSTEIN[18] and the obtained results.
VAN DEN BROEK[8] studied also paramagnetic saturation effect in this salt.

Two crystals were obtained from Dr. MIEDEMA, and the intention was
to measure these crystals with the field parallel to the c-axis in one and par-
allel to the a-axis in the other. The crystals consisted of slabs respectively
6 mm and 4 mm thick and weighed 1.3 g and 0.8 g. The crystal axis could not
be recognized from the crystal habit and we tried to find the axis of maximum
susceptibility by suspending the crystal on a thin nylon wire and observing its
rotation in a strong magnetic field produced by an iron magnet. This was done
at room temperature. After working out the results, the relation between the
susceptibilities is not as predicted by the published g-values. (BOWERS and
OWEN[51] reported $g_{/\!/} = 2.06$ and $g_\perp = 2.27$). This could be due to a mistake in
the orientation or due to a transition in the magnetic axis as the temperature
changes. The axis will be indicated by c^* and a^*, the asterisk indicating that
the experimental direction is meant, not the true direction. We measured both
crystals at $4.2^\circ K$ and at three hydrogen temperatures. The results of these
measurements are indicated in fig. III-21 and fig. III-22. At $4.2^\circ K$ we find
similar results as VAN DEN BROEK. The relaxation curves were extremely
broadened and the relaxation time ρ_{hf} was computed (see section 1.4.3). For
the typical shape of the relaxation curve we refer to VAN DEN BROEK[19, 8].

The deviation parameter d^* was computed for 4250 Oe. At $4.2^\circ K$ we
found $d^* = 0.68$, a value even higher than VAN DEN BROEK[19] reports
($d^* = 0.5$). Our measurements at hydrogen temperatures produced irregular
relaxation curves, a set of which is shown in fig. III-21 for $T = 14.25^\circ K$. The
deviations from a pure C.d.P. curve were still large ($d^* = 0.47$ for $H_c/\!/c^*$-
axis and $d^* = 0.42$ for $H_c/\!/a^*$-axis), but it was possible to give an estimate

102
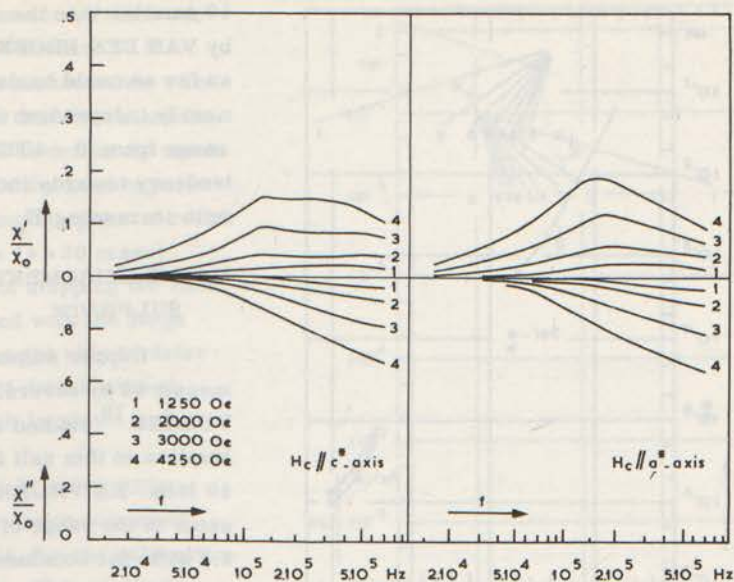
Fig. III-21. $\frac{\chi'}{\chi_o}(\uparrow)$ and $\frac{\chi''}{\chi_o}(\uparrow)$ for Cu K_2 Cl$_4$.2H$_2$O   T = 14.25 °K

for the peak of the absorption. We see that the relaxation curves for the crystal with $H_c /\!/ c^*$-axis are different from $H_c /\!/ a^*$-axis. The difference may be inherent to the crystal, instead of to the direction. It may be that cracks and irregularities of the crystals influence the heat flow and the distribution of temperature. The crystals are difficult to grow and they have an uneven color.

The b/C values were computed from a measurement at 4.2°K. We found:

$$[b/C]_{c^*\text{-axis}} = 17.4 \times 10^6 \text{ Oe}^2$$

$$[b/C]_{a^*\text{-axis}} = 16.5 \times 10^6 \text{ Oe}^2$$

The ratio between these values is 1.06, while the g-values predict 1.16. Combining these results and assuming the published g-values to be correct, we can state that:

$$[b/C]_{H_c /\!/ c\text{-axis}} = (18.3 \pm 1.0)\, 10^6 \text{ Oe}^2$$

$$[b/C]_{H_c /\!/ a\text{-axis}} = (15.8 \pm 0.8)\, 10^6 \text{ Oe}^2$$

In computing the b/C value, a 1% and a 0.5% saturation correction is applied to the χ-values at respectively 4250 Oe, and 3000 Oe. For the details of the correction we refer to VAN DEN BROEK [9,23].

The relaxation times obtained are indicated in fig. III-22. In the hydrogen range we obtained $\rho_a \propto T^{-5}$; the value for the relaxation time at 4.2°K is a factor

103

$\rho(T)$ for $Cu_2 K_2 Cl_4 . 2H_2O$ at 4250 Oe.   x v.d. Broek

■ $H_c \parallel c^*$ axis
● $H_c \parallel a^*$ axis

Fig. III-22.

10 smaller than the value obtained by VAN DEN BROEK [19]. The ρ is, as far as could be determined, nearly independent of H_c in the range from 0 - 4000 Oe, with a tendency towards increasing ρ with increasing H_c.

3.6 MEASUREMENTS ON COPPER SULPHATE

Copper sulphate has been measured by several investigators. VOLGER [79] studied spin-spin relaxation in this salt from 3 MHz - 40 MHz. DE VRIJER [82] did the same in the range of 150 kHz - 9.3 MHz but concluded that no spin-lattice relaxation could occur at $20^{\circ}K$ below 11 MHz (although the beginning of the spin-lattice relaxation is indicated by his abso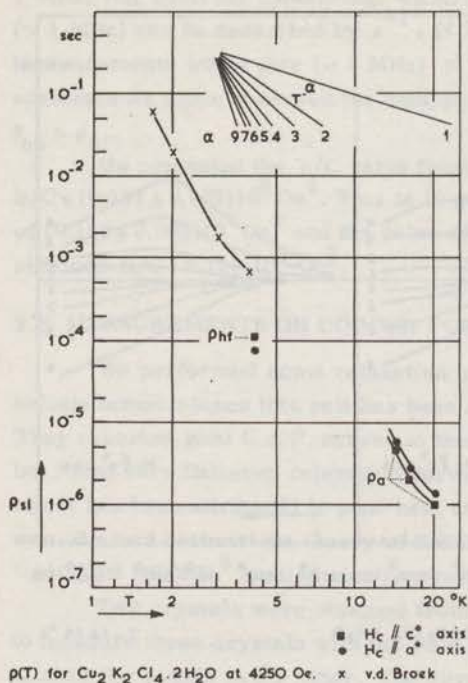rption measurements). LOCHER [42] measured at microwave frequencies and came to the conclusion that, on the contrary, spin-lattice relaxation had to exist at low frequencies.

We have made two sets of measurements. The first measurement was done on approximately 3 grams of small crystals with the 4 kOe magnet. A spin-lattice relaxation was detected in the temperature range from $4^{\circ}K$ - $20^{\circ}K$. The available field was, however, small compared to the $(b/C)^{\frac{1}{2}}$ field of approximately 14 kOe and a field dependency could not be established. The relaxation times obtained are shown in fig. III-23. In copper sulphate the spin-spin absorption is still significant at frequencies below 1 MHz. DE VRIJER's measurement indicates this, but the absolute value of his measurement is disputed by LOCHER who claims that the relaxation in zero field can be described by a Debye-relaxation with $\rho_{ss} = 6.5 \times 10^{-9}$ sec. In adjusting the phase of the measuring apparatus, we assumed the absorption to be zero in zero magnetic field. Our measured curves and the ones corrected for spin-spin absorption at zero field H_c are shown in fig. III-24 for $T = 14.4^{\circ}K$ with $\rho_{ss} = 6.5 \times 10^9$ sec used for the correction. With the new magnet we did some prelimenary measurements on a single crystal of approximately 4 grams, with $H_c \parallel c$-axis. The results obtained were not yet ideal, some of the curves showed large disturbances, which could be due to the oscillating power supply of the magnet or to other unknown reasons.
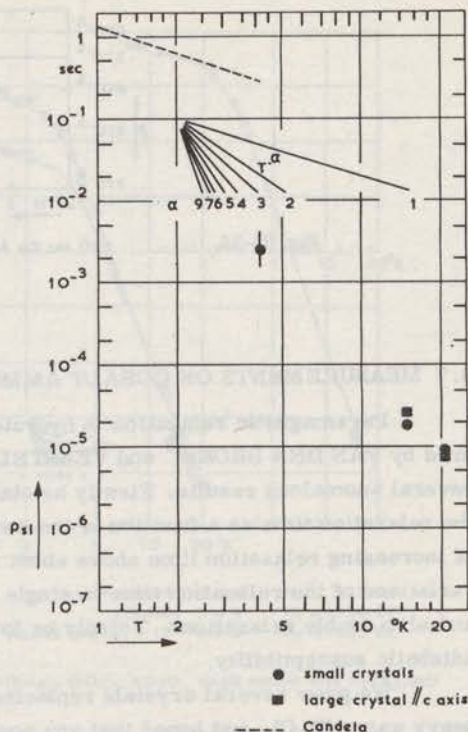
104

The relaxation times obtained, were close, however, to the first set of measurements with the exception that the relaxation time at $4.2°K$ is definitely much longer than in the first experiment and completely out of reach of our bridge ($\rho > 30$ msec). The method of stepping the field cannot be used with the large magnet. We were able to determine the field dependency at $14.4°K$, which is shown in fig. III-25.

The b/C value with $H_c \parallel c$-axis has been computed, using 75 Oe/A for the calibration of the magnet. This yielded a preliminary value of b/C of $(1.92 \pm 0.08).10^8 \, Oe^2$. The effect of saturation has been computed and we have corrected for it (VAN DEN BROEK[9]). At $14.4°k$ and at 14 kOe a correction of only 0.5% in $\chi_b(H)/\chi_0$ is calculated. Results of spin-lattice relaxation measurements reported by CANDELA[83] have been indicated in fig. III-22. They were obtained by measuring the direct current susceptibility as a function of microwave power absorbed at electron spin resonance.

Fig. III-23.

$\rho(T)$ for $Cu SO_4 . 5 H_2O$

● small crystals
■ large crystal $\parallel$ c axis
---- Candela

Fig. III-24.

$\frac{\chi'}{\chi_0}$ and $\frac{\chi''}{\chi_0}$ for $Cu SO_4 . 5 H_2O$ _ small crystals

□ 2000 Oe
○ 4250 Oe
----- calculated correction for spin-spin relaxation with $\rho_{ss} = 65 \, 10^9$ sec
---- corrected curves
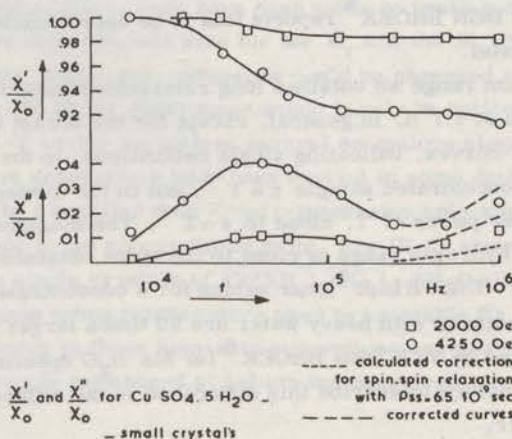
105

Fig. III-25.

$\rho(H)$ for $Cu\,SO_4.5H_2O$ $H_c \parallel C\text{-axis}$
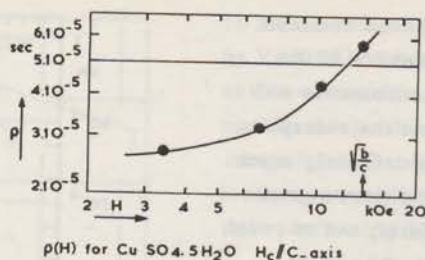
3.7 MEASUREMENTS ON COBALT AMMONIUM TUTTON SALTS

Paramagnetic relaxation in hydrated cobalt tutton salts has been measured by VAN DEN BROEK [8] and VERSTELLE [5]. VAN DEN BROEK obtained several anomalous results. Firstly he obtained a sharp decrease in the value of the relaxation time as a function of the magnetic field H_c followed by a region of increasing relaxation time above about 1 kOe. Secondly he reported rapid variations of the relaxation time in single crystals as the field was increased, and also double relaxations. Thirdly he found an anomalous behaviour of the adiabatic susceptibility.

We grew several crystals replacing the normal crystal water (H_2O) with heavy water (D_2O), and hoped that any possible changes might give a better understanding of the anomalous results. Although the measurements are not finished, we will give a report of the initial findings. To compare some of our measurements with a salt with H_2O as crystal water, we remeasured old specimens, but we do not know whether these are the same specimens measured by VAN DEN BROEK [8]. Fig. III-26 shows the relaxation time ρ as a function of temperature for a concentrated crystal with D_2O as crystal water, and one which has been diluted 1:12 with Zn. The figure mentioned is the dilution in solution, but VAN DEN BROEK [8] reports this to be approximately equal to the dilution in the crystal.

In the helium range we obtained long relaxation times; for the diluted sample 40 seconds at $1.1^{\circ}K$. In general, except for the lowest temperatures, we found very good e-curves, indicating single relaxations. In the hydrogen range we found for the concentrated sample $\rho \propto T^{-6}$, but in the diluted sample there is definitely a lower power of T, close to $\rho \propto T^{-4}$. The magnitude of the relaxation times in the hydrogen range is close to the value obtained by both VAN DEN BROEK [8] and VERSTELLE [5], our values for a concentrated sample at low helium temperatures with heavy water are 50 times larger than the relaxation times reported by VAN DEN BROEK [8] for his H_2O specimens. It would be, however, premature to ascribe this difference to the different character of the crystal water.

106

Fig. III-26.

concentrated ⎫ ♂ ♂ ♂ H_c = 225 Oe
crystal ⎬ o ⊙ ● H_c = 1350 Oe
diluted with Zn 1:12   ♭ ♭ ♭ H_c = 225 Oe
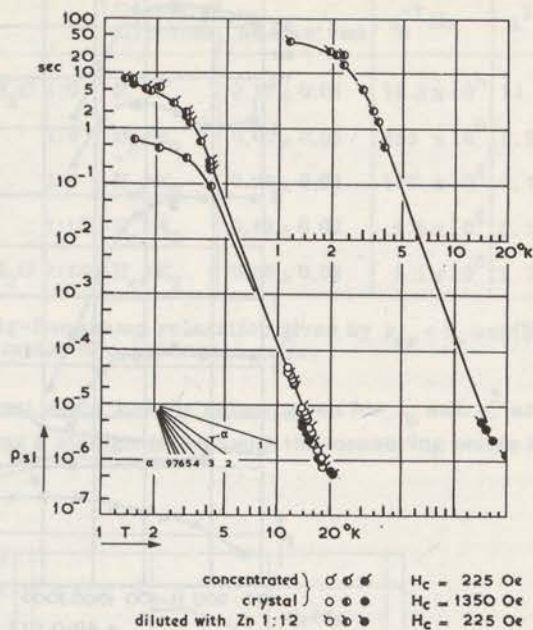
ρ(H) for Co(NH4)$_2$ (SO4)$_2$. 6 D$_2$O. single crystal with $H_c \parallel K_2$-axis

     The ρ-H dependency for a number of cases is given in fig. III-27. At helium temperatures the trend is the same as reported by VAN DEN BROEK [8]. In fields above 500 Oe we find $\rho \propto H^{-3}$. The ρ-H relation is determined by means of stepping the dc field, no measurements could be taken at magnetic fields higher than 1500 Oe. In the hydrogen range for the concentrated sample ρ(H) can be described by a Brons-Van Vleck formula with p = 0.6, for the diluted samples not enough measurements have been made to reach a conclusion. Relaxation times have been obtained also for the K_1 and the K_3 directions in concentrated D_2O salts. Very little difference could be observed and if the results were plotted in fig. III-26 the differences would barely be noticed. In the graphs produced by the X-Y writer we noticed several anomalous absorptions at different fields. These absorptions have been studied in some detail. One of these absorptions could be classified as a Kronig-Bouwkamp spin-spin relaxation, similar to that found in the copper tutton salts. Fig. III-29 shows some of the results from three single crystals of $Co(NH_4)_2(SO_4)_2 \cdot 6H_2O$. Measurements at three different helium temperatures were used to assemble fig. III-29. Some further data pertaining to these spin-spin absorptions and some additional data for two diluted crystals (measured at helium temperatures) are given in table III-6.
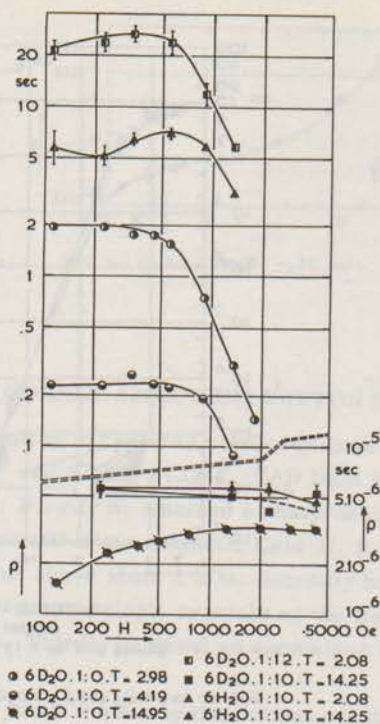
$\rho(H)$ for several samples Co$(NH_4)_2$ $(SO_4)_2$ $6H_2O$ or $6D_2O$; single crystals with $H_c \parallel K_2$ axis. temperatures in $^\circ$K.

- ◨ $6D_2O.1:12.T = 2.08$
- ◐ $6D_2O.1:O.T = 2.98$
- ◓ $6D_2O.1:O.T = 4.19$
- ◙ $6D_2O.1:O.T = 14.95$
- ■ $6D_2O.1:10.T = 14.25$
- ▲ $6H_2O.1:10.T = 2.08$
- ▲ $6H_2O.1:10.T = 14.25$

Fig. III-27.
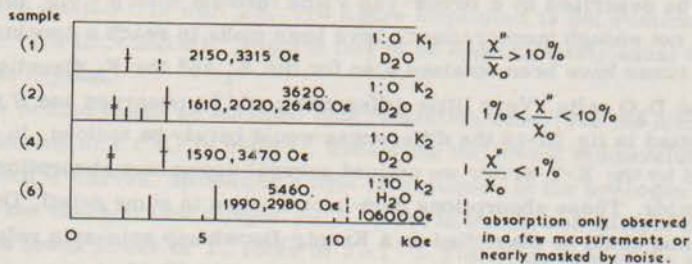
location and strength of field independent absorptions in Cobalt tuttonsalt. for the description of the samples the reader is referred to the text; the numbers in the figure indicate the value of the magnetic field Hc at which the absorption has its peak.

Fig. III-28.

108

Sample	Substance	Crystal direction	$\chi''_{ss\,max}/\chi_{ad}$	ρ_o^{-1} Hz	Δ^2 Oe^2
1	$Co(NH_4)_2(SO_4)_2 \cdot 6D_2O$ 1:0	$H_c /\!/ K_1$	0.17 ± 0.01	18.3×10^6	11×10^5
2, 4	" " 1:0	$H_c /\!/ K_2$	0.07 ± 0.01	256×10^6	6.9×10^5
3	" " 1:0	$H_c /\!/ K_3$	0.09 ± 0.01	107×10^6	7.7×10^5
5	" " 1:12	$H_c /\!/ K_2$	0.12 ± 0.02	4.5×10^6	2.3×10^5
6	$Co(NH_4)_2(SO_4)_2 \cdot 6H_2O$ 1:10	$H_c /\!/ K_2$	0.08 ± 0.02	3.1×10^6	2.1×10^5

Table III-6. Data for Kronig-Bouwkamp relaxation given by $\rho_{ss} = \rho_o \exp(H^2/\Delta^2)$ for several samples of cobalt tutton salts.

It should be pointed out again that the values given for ρ_o and Δ^2 are the values determined by drawing a straight line through the measuring points in a $\log \rho - H^2$ graph.
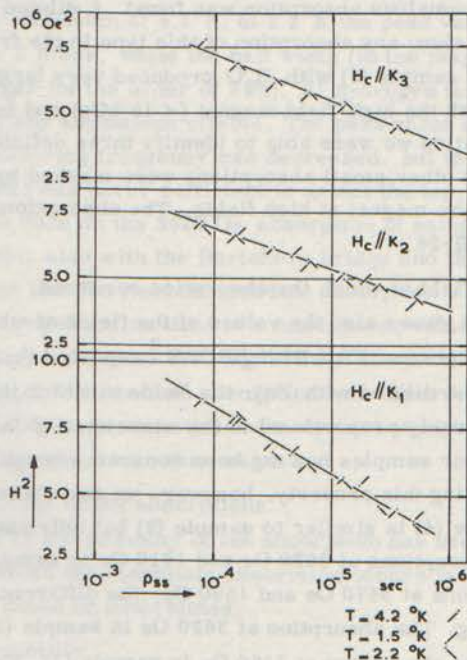

Fig. III-29. $\rho_{ss}(H^2)$ for $Co(NH_4)_2(SO_4)_2 \cdot 6D_2O$.

The main characteristic of the other absorptions was their independence from field as a function of temperature and measuring frequency. Although many measurements have been done there are not enough data yet to describe adequately

109

the phenomena observed. At present we will describe the general line of our observations. The following properties of the field independent absorptions will be considered:

a) The type of sample measured.
b) The fields at which the absorption occurred.
c) The intensity of the absorptions and the dependence on the measuring frequency.
d) The temperature dependency.
e) The adiabatic susceptibility.

a) The types of samples used.

All measurements were done on single crystals of cobalt ammonium tutton salt with D_2O and occasionally H_2O as crystal water. The samples (1), (2), and (3) (see table III-6) have been measured in the K_1, K_2, and K_3 directions respectively. (1) and (2) showed a field independent absorption, (3) has not been completely examined (only with measuring frequencies above 7.5 kHz), but no trace of anomalous absorption was found. A diluted sample (5) with D_2O did also not show any absorption of this type in the frequency range of the bridge. A diluted sample (6) with H_2O produced very large absorptions; it was also examined with the high-field magnet (< 15 kOe) and besides the Kronig-Bouwkamp relaxation we were able to identify three definite absorptions, but it is possible that other small absorptions were masked by instabilities of the power source of the magnet at high fields. The absorptions are schematically indicated in fig. III-28.

b) The magnetic field at which the absorption occurred.

Fig. III-28 shows also the values of the fields at which we found the field independent absorptions. VAN DEN BROEK[8] reported that in the single crystal he measured (1:9.5 diluted with Zn), the fields at which the first absorption occurred were inversely proportional to the associated g-factor. Unfortunately the mounting of our samples has not been accurate enough to confirm this completely. By assuming this property, however, we can classify some of the absorptions. Sample (4) is similar to sample (2) but only smaller. There is little doubt that the absorptions at 3620 Oe and 1610 Oe in sample (2) correspond with the absorptions at 3470 Oe and 1590 Oe, the difference being due to differences in mounting. The absorption at 3620 Oe in sample (2) can probably be connected with the absorption at 2150 Oe in sample (1). From values of the adiabatic susceptibility on the samples (1), (2), and (3) we calculated the b/C values and found respectively 13.5×10^4 Oe^2, 40.4×10^4 Oe^2, and 19.8×10^4 Oe^2. The ratio's of the effective g-values are thus:

$$\frac{g_{K_1}}{g_{K_2}} = 1.73, \quad \frac{g_{K_1}}{g_{K_3}} = 1.21 \text{ and } \frac{g_{K_2}}{g_{K_3}} = 0.70$$

110

For cobalt ammonium tutton salt with H_2O as crystal water, BLEANEY and INGRAM [84] report

$$\frac{g_{K_1}}{g_{K_2}} = 1.86, \quad \frac{g_{K_1}}{g_{K_3}} = 1.31 \quad \text{and} \quad \frac{g_{K_2}}{g_{K_3}} = 0.70$$

An error in the mounting of sample (1) could explain the differences. The ratio of the fields at which the absorptions occur is

$$\frac{(H_c)_{K_2}}{(H_c)_{K_1}} = 1.69$$

which is close to the 1.73 found for the ratio of the effective g-values. Our initial conclusion is that the absorptions in 1 and 2 are connected, and we indicate this by a small bar in fig. III-28.

c) The intensity of the absorptions.

The intensity of a particular absorption depended on the measuring frequency and the temperature. We found the absorption, expressed in χ''/χ_0, in the helium range to be maximum at $4.2^{\circ}K$; at $2.2^{\circ}K$ the peak value of χ''/χ_0 was approximately a factor 2 lower, while the half width (in the magnetic field) of the absorption was larger (of the order of 20%). At hydrogen temperatures we were not able to detect any anomalous effects. The peak value of the absorptions increased when the measuring frequency was decreased, but the measuring range of the bridge (f > 180 Hz) was never sufficient to detect the top. The most complete measurement was done on the 3620 Oe absorption of sample (2) at $4.2^{\circ}K$. We measured this sample also with the Hartshorn bridge and the combined measurements indicated that the field independent absorption was due to a decrease of the spin-lattice relaxation time to a much lower value at a particular field. In fig. III-28 we have indicated the magnitude of the maximum absorptions observed by us. The largest anomalous absorption was observed with the nitrogen cooled magnet at 5400 Oe in an initial measurement at high fields. Sample (6) is the only sample examined with this magnet.

d) Temperature dependence of the absorptions.

The dependence of the intensity of the absorption has been mentioned in c). The field value at which the maximum absorption occurs is temperature independent, as far as could be determined.

e) The adiabatic susceptibility.

In some of the samples we noticed that the adiabatic susceptibility was larger than in others. The adiabatic susceptibility could be represented in these cases by

$$\chi'_T(H) = \chi'_c + \chi'(H)$$

in which χ'_T represents the total measured susceptibility, consisting of a con-

stant part χ'_c and a part $\chi'(H)$ fulfilling the relation $\dfrac{\chi'(H)}{\chi_o} = \dfrac{b}{b + CH_c^2}$ reasonably well.

In sample (1) the quantity $\dfrac{\chi'_c}{\chi'_T(H=0)}$ was of the order of 0.03 and was temperature independent between 2°K and 4°K. In sample (6) $\dfrac{\chi'_c}{\chi'_T(H=0)} = 0.15$ and also temperature independent in the same temperature range. In the other samples this value was 0.01 or less. The value of χ'_c/χ_o has been observed at frequencies up to 250 kHz and is independent of frequency.

112

CHAPTER 4

THE DISCUSSION OF THE RESULTS

4.1 DISCUSSION OF THE MEASURING APPARATUS

In chapter 2 we have shown in detail the construction of the bridge and the associated detector circuit, while in chapter 3 we have shown measuring results obtained with the bridge. In this section we will make a few additional remarks and suggestions for improvements.

The basic system of measuring paramagnetic relaxation described in this thesis is identical to that of the Hartshorn bridge or the Twin T bridge[5], the magnetization is measured by introducing a sample into a coil. The main advantage of this general system is the freedom to use the dc magnetic field as a completely independent parameter.

Our method of detection enabled us to obtain the values of X'' and X' proportional to a dc voltage, which in turn made it possible to record these values as a continuous function of H. Besides a considerable time saving, it enabled us to detect the spin-spin relaxations at low frequencies and we were also able to detect the small absorptions in the cobalt tutton salts. These phenomena would have been very difficult to detect by means of a normal "hand operated" bridge. The graphs produced by the XY writer also give a fast indication during the measurements of the trend and type of results. A disadvantage is the greater complexity of the measuring system in comparison with e.g. the Hartshorn bridge.

It should be pointed out that the system of synchronous detection is usable for most types of a.c. bridges. It is however the first time it has been applied to a bridge for paramagnetic relaxation in Leiden. Synchronous detection in general is applied in many forms, mainly because it can reduce signal to noise ratios in transmissions of signals. It is widely used in modern communication-systems (television, frequency-modulation, carrier-telephony, space communications, etc.). The essential principle in synchronous detection is to use all the knowledge available about the signal. In our application, the problem is rather simple. The operating frequency of the bridge is exactly

known and the output signal of the bridge is compared in two synchronous de-
tectors with the input signal, which has a very good signal to noise ratio. The
band-width of the output signal of the synchronous detector can be limited to any
desired value, providing it is wide enough to follow variations of the bridge out-
put signal fast enough. One can state that our system, from the signal to noise
standpoint, is optimum. Presently the main limitation in the sensitivity of the
bridge is drift of components and is as such still open for improvements.

In electron- and nuclear spin resonance, synchronous detection methods
have been used for many years, and we will not attempt to review all the sys-
tems used. FEHER [85] has analyzed several and computed the sensitivity ob-
tainable. In the systems used in Leiden for paramagnetic resonance experi-
ments the total magnetic field consists in general of three components. For
electron-spin resonance, the sample is usually in a micro wave cavity and is
subject to an R F field with an angular frequency ω. Perpendicular to this field
is a constant field H_c on which is superimposed a relatively small alternating
field ΔH_c, usually with a frequency of the order of 30 Hz. At resonance, deter-
mined by the condition $\hbar\omega = g\mu_\beta H_c$, energy will be absorbed by the sample. A
part of the RF energy is coupled to an RF detector (occasionally after a heter-
odyne operation and amplification) and the absorption influences the output sig-
nal of the RF detector. The alternating field ΔH_c will effectively modulate the
detected signal and this modulation contains the desired information about the
resonance. This information is then abstracted from the detected signal by
means of synchronous detection (phase sensitive detection).

This short description shows some of the differences. In our system we
have one ac signal, the measuring signal of the bridge, and this signal is sepa-
rated into two components by means of synchronous detection. In electron-spin
resonance the RF signal acts as a carrier which is modulated by the absorption
of the sample in the rhythm given by the small alternating field ΔH_c. This mo-
dulation is most effectively demodulated by phase sensitive detection.

Returning to the system used by us, the following improvements could
be suggested. It might have advantages to build a complete bridge inside the
cryostat, with the supply and detector leads as connections. The output of a
second bridge, supplying merely a correction to balance the main bridge,
should be added to the output of the main bridge and could be located outside
the cryostat. At present the connections from the two coils in the cryostat to
the bridge probably form the main source of instability. The length of the meas-
uring cycle is presently dictated by the speed of the regulating mechanism for
the magnet current. Shortening the time interval would improve the stability.
In association with the nitrogen cooled magnet (paragraph 2.15) a regulating
mechanism is being constructed which can bring the magnetic field to a value
of 15 kOe within 5 seconds, maintain the field long enough for commutation
(3 seconds) and bring the field down in 5 seconds. A lead battery will be used

114

as the power source, the regulating unit will be transistorized and we hope to obtain a very smoothly varying field, without transients.

It should be pointed out that these techniques, by which a relatively high magnetic field can be obtained at low cost, can be used because of the fast method of measuring χ' and χ''. Finally it can be remarked that the method of measuring relaxation phenomena in between the standard temperature regions is again applicable due to the fast operation of the equipment.

4.2 DISCUSSION OF THE MANGANESE TUTTON SPECIMENS AND GADOLINIUM SULPHATE

4.2.1 Discussion on the manganese tutton specimens without magnetic impurities added

The purpose of most of the experiments on the manganese tutton specimens was to find an answer to the question: Why are the spin-lattice relaxation times in the three specimens a, b and q so different? In searching for the answer we hoped to obtain also the answer to the following two questions:

    1. Why do relaxation curves deviate occasionally from C.d.P. curves?
    2. How can the flat part in the $\rho(T)$ characteristic be explained?

As indicated in chapter III the investigations followed four different "roads" A, B, C, D, which will be listed in short for convenience:

    A. Magnetic impurity ions.
    B. Crystal defects, cracks, etc.
    C. Ions with a different valency.
    D. Non-magnetic impurity ions.

We will first consider A. From the experiments in section 3.2.3 we learned that some impurities (such as Co^{2+} and Fe^{2+}) have a strong influence on the relaxation time. 1% Co^{2+} reduces the relaxation time in the hydrogen range by a factor of 100. This result shows that one cannot possibly see the manganese and the cobalt ions as separate systems, not even in the fairly diluted salts such as the tutton salts. In that case addition of 1% Co^{2+}-ions could only produce a small second relaxation which we would barely detect. Apparently the cobalt atoms act as "relaxation pockets" with a short relaxation time (see section 1.5) and the majority of the manganese atoms are tightly coupled to these cobalt ions, giving the complete crystal a short relaxation time (VAN VLECK[60], BÖLGER[22]). With 1% Co^{2+} added we also found a part in the $\rho(T)$ characteristic where ρ was independent of temperature, showing that this phenomenon can be caused by impurities. Furthermore we learned from these experiments with magnetic impurities added to the manganese crystal that the relaxation time always decreases, with some elements having more effect than others. From the results obtained it was evident that the

115

magnetic impurities surveyed did not produce effects as found in sample a. The spectrographic analysis confirmed that no unwanted transitions metals were present in appreciable quantities.

Although we will return to A later in this discussion we will continue with B. We only did one simple experiment following this line (recrystallized a sample at a different temperature) and obtained a negative answer. In our experiments (also on different salts) we have not seen any correlation between the relaxation time and the crystal defects but did no experiments in which crystal defects etc. were on purpose induced.

We tested the possibility indicated in C by adding $K MnO_4$, which is known in chemistry as an oxydizer, raising for instance the valency of Mn from two to a higher value. It is reported [66] that Mn^{3+} is mainly formed, but that higher valencies are possible. The resemblance between the relaxation times with 1% $KMnO_4$ added and the specimen a was so close that we believed we had found the cause for the differences between a, b and q but a few points needed an explanation. Mn^{3+} would not fit naturally in the crystal but one could assume vacancies to maintain electrical neutrality. Furthermore Mn^{3+} would not be detected by X-ray spectroscopy. The main question was to explain why the reduction experiment as described in section 3.2.1 did not produce any effect. This difficulty was solved with the unexpected result of experiment v, which showed that K^+ions alone produced the same effects as the $KMnO_4$. Our conclusion is that there is no evidence to prove that different valencies of Mn play a role in effecting the relaxation time of manganese tutton salt, but that the introduction of K^+ions affect the relaxation time strongly. In the following part we will use some of the results obtained with the addition of $KMnO_4$ by only considering the K^+ ions added. It should be pointed out that addition of 2% $KMnO_4$ is equivalent of adding 1% K_2SO_4, the percentages for the $KMnO_4$ were related to the Mn atoms. Comparing the measurements from fig. III-3 and III-5 shows that adding 0.1% of $KMnO_4$ to specimen b produces relaxation times very close to those of specimen q, while addition of 1% of $KMnO_4$ to specimen b, gives results comparable to those obtained with specimen a. The measurements on the specimen with 1.4% K_2SO_4 added ($\equiv$ 2.8% $KMnO_4$) produced results very similar to specimen a, but again changed in absolute value due to a different K^+ concentration. The occurrence of deviations of relaxation curves from C.d.P. curves in all these specimens at high magnetic fields is also a point of resemblance.

Our conclusion is therefore that the differences observed in the relaxation time of the specimens a, b, q, u and v may very well all be due to the same cause: alkaline impurities. We will mention in the following only K^+ impurities, but it is quite possible that other alkaline impurities have similar effects.

In very recent experiments, not described in chapter 3, we have measured

ammonium manganese tutton specimens in which the following percentages of ammonium were replaced (in the solution) by impurities: 10% Cs, 10% Li, 1% Na. We have not analyzed if these impurities were present in the crystals, with the exception of sodium. Burning the crystal produced a yellow flame, indicating qualitatively the presence of sodium. None of these impurities had an appreciable effect on the relaxation time. We also replaced 1% and 10% of the $(NH_4)^+$ ions by K^+ ions in copper ammonium tutton salt, and the relaxation time decreased an order of magnitude for each step. The experiments, up to the present, show that potassium apparently is the only alkaline impurity found which affects the relaxation time so strongly in the tutton salts. The label on the Analar manganese sulphate, produced by Merck, states the maximum limit of alkaline impurities to be less than 0.25%; addition of 0.1% of $KMnO_4$ changes specimen b into specimen q. Specimen a was not made from Analar chemicals.

The next question is why the K^+ ions have such a large influence on the relaxation time of the manganese ions. On this important question we can only make a few comments. Of all processes suggested to explain the spin-lattice interaction, one of the most important ones is the mechanism suggested by KRONIG-VAN VLECK. In this mechanism the electric crystal field is modulated by the crystal vibrations, this modulated field acts on the orbital momentum and produces spin transitions through the spin-orbit coupling. Mn^{2+} is an S-state ion, the orbital momentum is zero in the ground state and this mechanism can operate only by taking into account higher orbital states with nonzero orbital momentum, i.e. higher order perturbation calculations are needed to calculate relaxation times. These higher order processes are not so effective, giving Mn^{2+} long relaxation times (the manganese tutton salts can be measured up to $300^{\circ}K$ in our bridge).

Our best explanation at present is to suggest that the presence of the K^+ ions modifies the electric field, thereby improving the efficiency of the relaxation process. Potassium tutton salt apparently does not exist, but a salt with four water molecules is formed with the formula $MnK_2(SO_4)_2.4H_2O$. In the copper tutton salts Bleaney et al[45] find that the angle ψ (see section 1.7) in the ammonium copper tutton salt is 65° while in similar salts with K, Cs and Rb the angle is of the order of 110°. We do not know how far the structure changes on inclusion of a small percentage of K^+ ions. The b/C value is approximately 1200 Oe versus 770 Oe for the tutton salt. This together with the four instead of the six water molecules suggests that the manganese atoms are closer together in the leonite salt. PAULING[86] gives the following ionic diameters: Li^+ 0.60, Na^+ 0.95, K^+ 1.33, $(NH_4)^+$ 1.48, Rb^+ 1.48, Cs^+ 1.69, all expressed in Angstroms.

If the percentage of K^+ ions is not too large it could be possible that a K^+ ion takes the place of an $(NH_4)^+$ ion. Even for 10% K^+ ions, we find no change

117

in b/C value and 50% K^+ ions produce a change in $(b/C)^{\frac{1}{2}}$ of only 10%. Of all specimens in v we find in the hydrogen range the shortest relaxation time (fig. III-5) for the case in which 50% of the $(NH_4)^+$ ions are replaced by K^+ ions. The pure manganese leonite salt has relative long relaxation times; replacing K^+ ions by $(NH_4)^+$ ions again reduces relaxation times, but we have indications of a poor crystal structure with $(NH_4)^+$ ions present in the solution. One can imagine that the larger $(NH_4)^+$ does not fit in the space allotted to the smaller K^+ ion.

In the following discussion we will assume that a manganese tutton molecule, in which one of the two $(NH_4)^+$ ions is replaced by a K^+ ion, has a short relaxation time. We will indicate these molecules by adding a K to the symbol as e.g. Mn_K^{2+}. We do realize that the last few paragraphs are speculative and more investigations are necessary.

Returning to the results of the measurements of fig. III-3 we note that if a small amount of K is added to a pure manganese tutton salt we can clearly separate the $\rho(T)$ characteristic into three parts (as in specimen a) and from the measurements in fig. III-3 we can see that the high temperature branches of the curves for different amounts of impurities are close together. The temperature independent part of the $\rho(T)$ curve is interesting, a second observation is the large deviation from C.d.P. curves shown in the low temperature region at high magnetic fields. If one tries to explain the anomalous $\rho(T)$ curves for specimens a or q, one has first to find a reason why the efficient relaxation process at low temperatures ($\rho \propto T^{-5}$) gives way to a less efficient process ($\rho \propto T^o$). This could be explained by supposing two processes to be in series, in which the inefficient process blocks the efficient one. We therefore suggest the following thermodynamic model in which the specimen contains two different types of ions, symbolically represented as system 1 and system 2 (fig. IV-1).
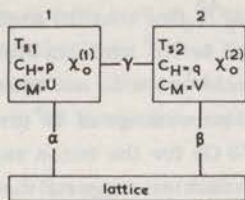
thermodynamic model to describe relaxation
phenomena with two different magnetic systems.

Fig. IV-1.

By a similar method as used in section 1.4 we can derive

$$\chi' = \frac{\chi_o^{(1)}[A^2 + \omega^2(BD-AE-AG) + \omega^4 EG] + \chi_o^{(2)}[A^2 + \omega^2(CD-AF-AG) + \omega^4 FG]}{A^2 + \omega^2(D^2 - 2AG) + \omega^4 G^2}$$

$$\chi'' = \frac{\chi_o^{(1)}[A(D-B)\omega + (BG-DE)\omega^3] + \chi_o^{(2)}[A(D-C)\omega + (CG-DF)\omega^3]}{A^2 + \omega^2(D^2 - 2AG) + \omega^4 G^2}$$

in which the following abbreviations are used:

$A = \alpha\beta + \alpha\gamma + \beta\gamma$

$B = \beta u + \alpha q + v\gamma + u\gamma$

$C = \alpha v + \beta p + v\gamma + u\gamma$

$D = \alpha q + \beta p + p\gamma + q\gamma$

$E = uq, F = vp, G = pq$

χ' and χ'' are related to the dispersion and absorption of the total system.

We computed the relaxation times one can expect for this model. We associated the magnetic properties of the Mn^{2+} ions with system 1, in which the relaxation to the lattice and bath is determined by the constant α. System 2 represents the Mn_K^{2+} ions, with the associated coefficient β. The two systems are coupled by an energy link with a coefficient γ. Presently we think that this link represents cross relaxation processes which connect the Mn^{2+} system to the Mn_K^{2+} system and with perhaps spin diffusion processes transporting the energy through the Mn^{2+} spin system. Both are spin-spin processes which are temperature independent.

By means of the equation (4-2) we computed χ''/χ_o for several cases, trying to choose the parameters so as to obtain a curve similar to a. The purpose of the calculations was twofold. Firstly we wanted a $\rho(T)$ curve such as those of a, q and b. Secondly we wanted to see if large deviations from C.d.P. curves could occur as found in specimen a at low temperatures. Equation (4-2) contain terms to a higher power of ω than in the case of a single relaxation. We have tried several sets of parameters (assuming a concentration of Mn_K^{2+} of 1%). To do these calculations we assumed a few general properties of α, β and γ. Our measurements gave $\rho \propto T^{-5}$ for the temperature range from $20^oK - 40^oK$ for the Mn^{2+} system. VAN DER MAREL[7] has done the most complete measurements and finds in the helium range also $\rho \propto T^{-5}$. Formula (1-19) gives $\rho = 2\pi C_H/\alpha$, C_H is proportional to T^{-2} in the temperature region where Curie's law applies well, so we assumed both α and β to be proportional to T^3. To obtain a temperature independent process, representing spin-spin processes, we assumed γ proportional to T^{-2}. For the quantities C_H and C_M we tried several choices, representing cases in which the measuring fields were of the order of, or large compared to the $(b/C)^{\frac{1}{2}}$ value.

In all cases evaluated we were only able to obtain very small deviations from C.d.P. curves. An example is shown in fig. IV-2; the deviations from C.d.P. are so small that they would escape attention in a normal measurement. Physi-

$$\alpha = 1.5\,10^{-4}\,T^3 \qquad p = \frac{1}{2\pi}\,T^{-2} \qquad \left.\begin{array}{l} H_c \cong 7\left(\frac{b}{c}\right)^{\frac{1}{2}} \\[4pt] \text{for system 1} \end{array}\right.$$

$$\beta = C\,T^3 \qquad u = \frac{1}{\pi}\,10^{-2}\,T^{-2}$$

$$\lambda = C.5.10^3\,T^{-2} \qquad q = \frac{1}{2\pi}\,10^{-2}\,T^{-2} \qquad \left.\begin{array}{l} H_c = 10\left(\frac{b}{c}\right)^{\frac{1}{2}} \\[4pt] \text{for system 2} \end{array}\right. \quad \text{computed } \frac{X''}{X_0} \text{ curves for model of fig. } IV.1$$
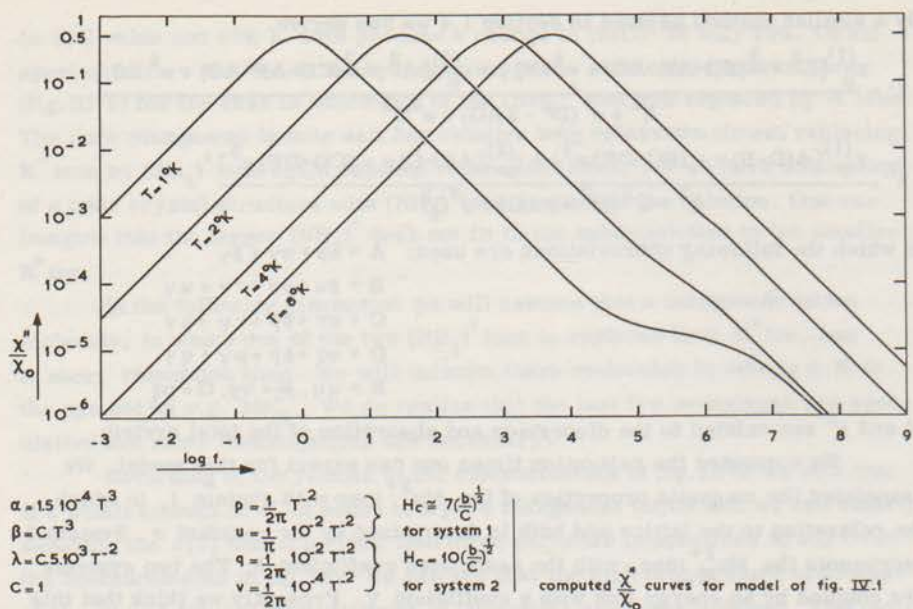
$$C = 1 \qquad v = \frac{1}{2\pi}\,10^{-4}\,T^{-2}$$

Fig. IV-2.

cally this is not too amazing. For an impurity of 1%, the quantities C_H and C_M of system 2 are small and can be neglected in comparison with system 1 and the system then degenerates into a lower order system with a single relaxation time determined by α, β and γ.

The calculations for computing relaxation times following formulas (4-1) and (4-2) are very lengthy but if the system degenerates into a simpler system by neglecting the specific heat of system 2 it can be easily shown that we can make a simplification as shown in fig. IV-3. With these simplifications

Fig. IV-3. simplified model for computing relaxation times

we found the parameters for α, β and γ which would approximate curve a. It can be seen from fig. IV-4 that the agreement between the measured curve a and the calculated curve I is good, which is not too astonishing, 3 parameters being available. If the concentration of the Mn_K^{2+} is reduced, the assumption is made that both β and γ will be reduced by the same ratio z. We computed the χ''/x_0 characteristic for two additional cases II and III. The curves II and III

120

were calculated by selecting such values of a single parameter z that good matching with the measured curves b and q was obtained. These curves also are plotted in fig. IV-4 and a reasonable agreement can be observed between b and III, and q and II. The parameter z would in our model be associated with the concentration c of the Mn_K^{2+} ions. The deviations between the calculated and measured curves are larger for the lower helium temperatures. At very low temperatures a deviation can be expected due to the influence of a direct process. This direct process would affect mainly the relaxation times which are long, as observed experimentally. We do not have enough data available to make a meaningful calculation, in which a direct process could be thought to be in parallel with the process represented by β in fig. IV-4.

From the experimental results u and v, we were able to determine the relationship between the parameter z and the percentage c of the $(NH_4)^+$ ions replaced by K^+ ions. The parameter z is calculated from that part of the $\rho(T)$ curve where ρ is independent of T (in the hydrogen temperature range). This experimentally determined relationship is shown in fig. IV-5. The line drawn through the experimental points can be represented by $Z = 1.6\ C$ and a reasonable fit is obtained up to a value of C of 10%. One should keep in mind that the K^+ ions are added to the solution, and the percentage of K absorbed in the crystal could possibly deviate from the percentage K added to the solution, with fluctuations possible, due to temperature, amount of solution etc. It can be remarked that the deviation of the experimental curve from the calculated one above $35^{\circ}K$ is due to the fact that the slope of the χ'/χ_o curve decreases towards the Debije temperature, while a T^{-5} dependency is assumed for the calculated curve.

The model can also be used to explain the effects of addition of 1% Co^{2+} on the relaxation time. The effect is large at temperatures between $14^{\circ}K$ and $180^{\circ}K$, (curve 1), but measurements at helium temperatures (h) failed to show a significant difference. In fig. IV-4 we also indicated the relaxation time of cobalt ammonium tutton salt. We see that it intersects the curve b at $6^{\circ}K$. At that temperature the cobalt has ceased to provide an easy relaxation path and the measurements at helium temperatures can be explained.

We have not been able to give an explanation for the large deviations from C. d. P. curves found in specimen a below $8^{\circ}K$ at large magnetic fields. The distribution of the impurities through the crystal will not be very regular and it could be supposed that a few Mn_K^{2+} atoms in a cluster have a different relaxation time from a single one. However, the efficient cross relaxation process would tend to equalize these differences. One additional comment could be made in association with deviations from C. d. P. curves. VAN DER MAREL[7] reported good C. d. P. curves while measuring q, our measurements of the oxydized sample d showed large deviations from C. d. P. curves at helium temperatures but with a value of the deviation parameter d^* of only 40% of the

Fig. IV-4.

```
C_H = 1/(2πT')
α = 1.5 10^-4 T^3
β = 1.2 T^3 z
γ = 3.5 10^3 z / T^2

I   z = 1.0
II  z = 0.2
III z = 0.02
```
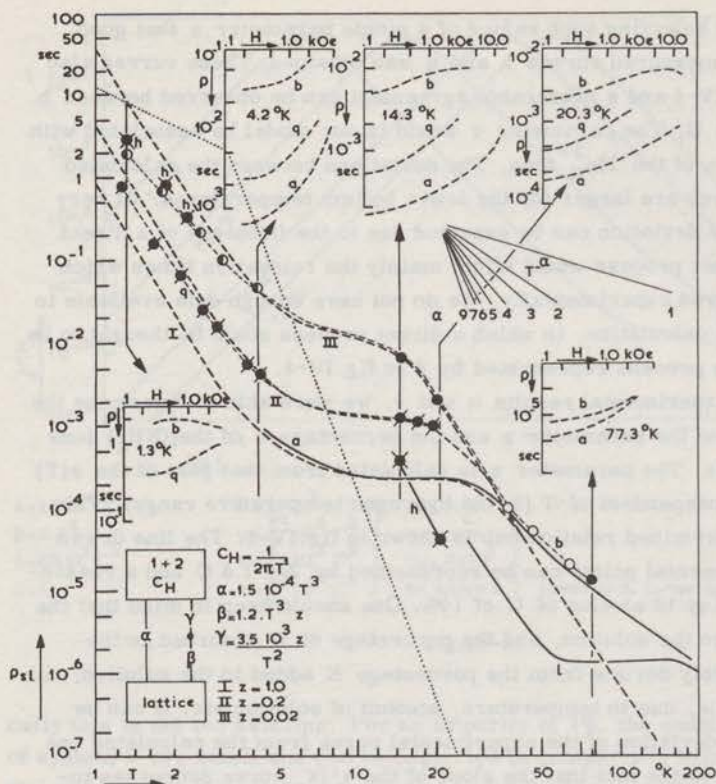
- - - - calculated curves I, II and III.   ✱ van den Marel (q)
——— de Vries (a) ○ ◑ ● de Vries (b)   ✖ 1% cobalt (h)
· · · · · · · Co(NH₄)₂(SO₄)₂·6D₂O at 750 Oe from III.25 and III.26

comparison of measured and computed relaxation times using model.

value obtained from sample a (fig. III-1). The value of the relaxation times in the middle region (relaxation time ρ independent of T) obtained with the oxydized sample are nearly 2 times smaller than these of sample a. This could indicate that these deviations from C.d.P. curves only occur with relatively high concentration of Mn_K^{2+}.

Fig. IV-4 has been drawn for a constant magnetic field of 750 Oe. Similar plots could be made as a function of H_c, and if an H_c axis were chosen per-

experimentally determined ratio between the parameter Z and the percentage C of NH₄⁺ ions replaced by K⁺ ions in Mn(NH₄)₂(SO₄)₂·6H₂O. symbols as in fig III-5.
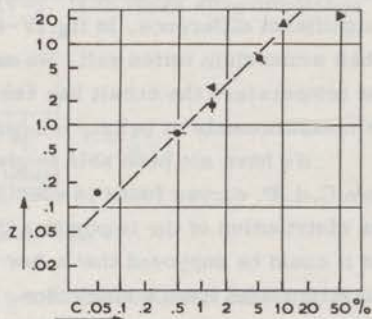
Fig. IV-5.

122

pendicular on the ρ-T plane one would obtain a three dimensional ρ-T-H_c diagram for each of the specimens a, b and q. In fig. IV-4 we have included graphs which show the measured $\rho(H)$ relationship at five different temperatures, representing intersections of the three dimensional ρ-T-H_c graphs with a plane perpendicular to the H_c-axis. The general observation is that the differences between the curves a, b and q are considerably reduced by applying high fields. Cross relaxation processes are strongly dependent on the value of the constant magnetic field (PERSHAN [87]), and it is reasonable to expect that the high magnetic fields reduce the interaction between the Mn^{2+} and Mn_K^{2+} ions caused by the cross relaxation.

The efficiency of the diffusion process must also be expected to depend strongly on the value of the magnetic field H_c. An order of magnitude estimate of the distance 1, over which energy can be transported in a time $\frac{1}{2\rho_{sl}}$ is given by

$$1 \approx \sqrt{\frac{D}{\rho_{sl}}} \approx a\sqrt{\frac{\rho_{sl}}{\rho_{ss}}} \qquad \text{(see 1-38)}.$$

For H_c = o, typical values of ρ_{sl} and ρ_{ss} could be 10^{-3} sec and 10^{-9} sec respectively giving 1 = 1000 a, but for a field $H_c = 5(b/C)^{\frac{1}{2}}$ this distance 1 could be reduced to the order of one lattice constant.

We will discuss below the effect of the magnetic field in some more detail and show the result of some calculations made to test the consistency of the model of fig. IV-1 for different magnetic fields. To be able to do a calculation we have to make assumptions about the dependencies of α, β, γ and C_H on the magnetic field. We assume that the dependency of the relaxation time of pure Mn-tutton sample in the Raman region can be given by a Brons-Van Vleck dependency with p = 0.5 which is confirmed by measurements on sample b at $20.3^{\circ}K$ and $77.3^{\circ}K$. This determined the coefficient $C_H\alpha^{-1}$ (section 1.4.1 formula 1-19). In the model shown in fig. IV-4, the relaxation time of specimen a is at $14.3^{\circ}K$ nearly completely determined by $C_H\gamma^{-1}$. The field dependency of $C_H\gamma^{-1}$ is assumed to be identical to the $\rho(H_c)$ relationship of specimen a at $14.3^{\circ}K$. Similarly the $\rho(H_c)$ relationship of sample a at $4.2^{\circ}K$ should give information about the field dependency of β, and again we assumed $C_H\beta^{-1}$ to be proportional to the $\rho(H_c)$ relationship of specimen a at $4.2^{\circ}K$.

Having assumed these relations for $C_H\alpha^{-1}$, $C_H\beta^{-1}$ and $C_H\gamma^{-1}$, we have computed the relaxation times as functions of the field H_c for $4.2^{\circ}K$, $14.3^{\circ}K$ and $20.3^{\circ}K$. The calculated values together with the actual measured values are given in fig. IV-6. In the same figure we also gave the assumed relation between $C_H\alpha^{-1}$, $C_H\beta^{-1}$, $C_H\gamma^{-1}$ and C_H as a function of H_c with

$C_H = C_M(1 + \frac{C H_c^2}{b})$ using $(b/C)^{\frac{1}{2}}$ = 750 Oe. There is only fair agreement between the calculated and measured curves. Qualitatively the computed curves show at hydrogen temperatures a similar trend as experimentally found e.g. a reduction

comparison of measured
values of ρ(H) with calculated relaxation times from model of fig. IV-4

I   Z = 1.0   ⚡ sample a
II Z = 0.2   ⚡ sample q (v.d. Marel)
III Z = 0.02   ● sample b
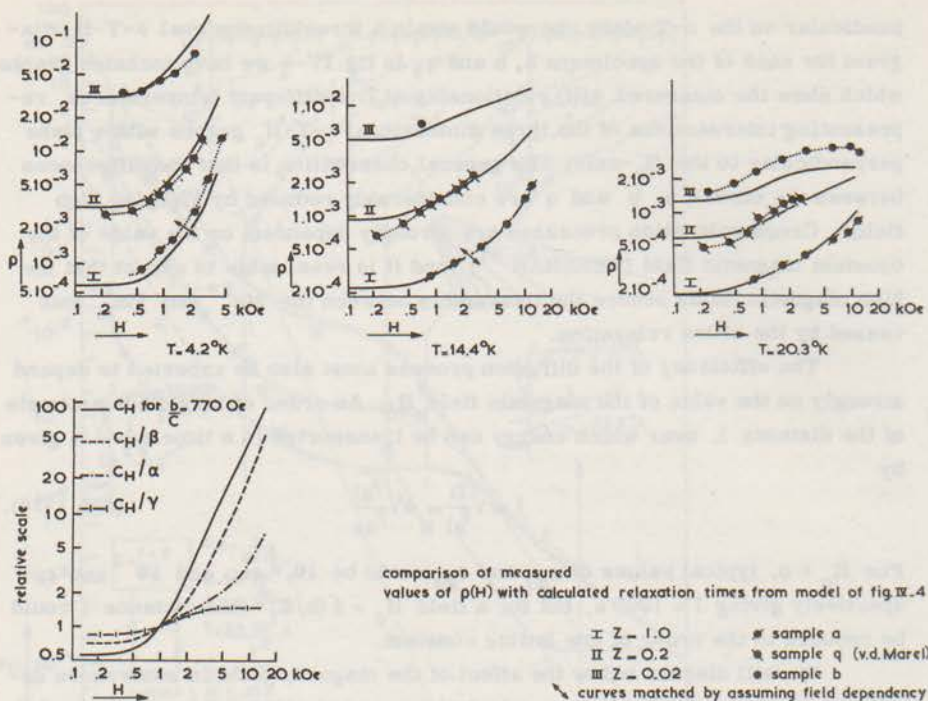   ╲ curves matched by assuming field dependency

Fig. IV-6.

of the spread of the relaxation times of the curves a, b and q at high magnetic fields. At helium temperatures the calculation does not show this trend at low field (< 5000 Oe, but experimentally it is found, see fig. IV-4). At low helium temperatures one will likely have to include a direct process, but not enough experimental data are available to make a calculation feasible. The same comment is valid in the nitrogen range. Here we find again that high magnetic fields decrease the difference between specimen a and b, but the model would have to be made more complex to account for the different ρ-T relation in this temperature range.

Up to this point we have assumed that at low temperatures the relaxation time is controlled by the relaxation of the Mn_K^{2+} ions. The associated field dependency is shown in fig. IV-6 by the curve β but no process is known to exhibit that field dependency coupled with a ρ(T) relationship given by $\rho \propto T^{-5}$. As such the problem is not different from that of most relaxation measurements with concentrated crystals using the bridge method in the helium temperature range [7,8].

In the model of fig. IV-1 we have supposed that cross relaxation processes and perhaps spin-diffusion processes form the link between the Mn^{2+} and Mn_K^{2+} ions.

124

We are not able to substantiate this with other evidence or to show that the field dependency is in agreement with theoretical calculations. Summarizing we can say that the model of fig. IV-1 provides, at present, only a tool to describe the majority of the experimental results.

In the following lines we will compare some of our results with the theoretical predictions, which are $\rho^{-1} \propto H^2 T$ for a direct process and $\rho^{-1} \propto T^7$ for a Raman process (ORBACH[32], LEUSHIN[33,34]). The influence of the impurities makes it impossible to estimate the relaxation time of pure manganese tutton salt below hydrogen temperatures. In the diluted salts we obtain long relaxation times and between 1°K and 2°K we find $\rho \propto T^{+\alpha} H^\beta$ with $\alpha \approx -1.5$ and $\beta < 0$ for $H_c > 500$ Oe and $T < 3^\circ$K (fig. III-9). The relaxation times for the concentrated crystals are still shorter than those for the diluted salts, thus no indications for a bottleneck process are found. In the temperature range between 14°K and 40°K we find $\rho \propto T^{-5}$ with a Brons-Van Vleck field dependency. The correlation between measurements of BROER and GORTER[65,4] and our measurements is excellent at nitrogen temperatures and higher. We compared our measuring results on manganese tutton salt with the predictions for a Raman process by matching our experimental curve with a standard ρ-T curve (see section 1.5). This curve is also indicated in fig. III-3 and good matching is obtained if we assume $\theta_D = 180^\circ$K.

It is interesting to note that relaxation times of Mn^{2+} with a concentration of 5.10^{-4} in SrS reported by MANENKOV and MILYAEV[88] are close to our values although the salt is different ($\rho = 10^{-5}$ sec at 77°K and $\rho = 3.10^{-7}$ sec at 300°K).

The relaxation measurements on $MnK_2(SO_4)_2 \cdot 4H_2O$ gave in the hydrogen range $\rho \propto T^{-5}$ with a Brons-Van Vleck dependency with $p \approx 0.5$. In the helium temperature range we find $\rho \propto T^\alpha H^\beta$ with $\alpha \approx -1.3$ and $\beta \approx 0$. The temperature dependence is close to that for a direct process, a field dependency $\rho \propto H^{-2}$ associated with a direct process for fields above the internal field $H_i [(b/C)^{\frac{1}{2}} \approx 1200$ Oe] is not observed.

Shortly before the completion of this thesis our attention was drawn to a paper by Zverev et al[89]. They measured spin-lattice relaxation of 0.01 % Cr in Corundum with 0.1 % V added, using a pulse method at 9.4 GHz. The ρ-T dependency they obtain is somewhat similar to that found by us for the manganese tutton salt with impurities. They explain their experimental results by considering the probability of simultaneous spin lattice relaxation of a vanadium and a chromium spin (Bloembergen[90]). By using a combination of cross-relaxation and spin lattice relaxation processes, with a possible inclusion of spin diffusion they give as an estimate for the ρ-T dependency of the spin lattice relaxation time of the chromium ion: $\rho \propto e^{\frac{\Delta}{T}}$. The formula for the relaxation time is so somewhat similar to that of an Orbach process.

This interpretation has several aspects in common with our description

as given in section 3.2.1 and in this section and the impurities could also be called "relaxation centers" (Van Vleck [36, 40]).

Very recently a paper was published by CHAO-YUAN HUANG in Phys. Rev. 139A (1965) 241 with a reference to a paper by BIERIG, WEBER and WARSHAW in Phys. Rev. 134A (1964) 1504. In these papers ρ is reported to be proportional to T^{-5} for Gd^{3+} and Eu^{2+} in CaF_2 in a temperature interval of approximately $15^\circ K$ - $30^\circ K$. A Debye temperature of approximately $350^\circ K$ is reported for this salt. This relaxation process is apparently identical to that predicted by ORBACH and BLUME [31]. With a lower Debye temperature ($\approx 180^\circ K$) the manganese tutton salt can be best described by a T^{-7} relationship.

4.2.2 Ammonium manganese tutton salt with magnetic impurities

Addition of other impurities of the iron group elements all changed the relaxation time of the crystal. Addition of 1% of Ni^{2+}, Fe^{2+} and Co^{2+} had a large effect on the relaxation time at hydrogen temperature. The results with 1% Ni^{2+} are anomalous, we only measured this salt at $14.4^\circ K$ and $20.3^\circ K$ (fig. III-3 and fig. III-8). Specimen 1 (1% Co^{2+}, fig. III-3 and fig. III-8) was measured from the hydrogen temperature range to room temperature and the relaxation time was found to be independent in the range from $60^\circ K$ to $170^\circ K$. The same type of calculation as done for the Mn_K^{2+} case, could be tried for the cobalt impurities. For this sample the dependency of ρ on the magnetic field is only measured completely at two hydrogen temperatures, the data at higher temperatures are obtained with the "running" method. If we again use the model of fig. IV-1 to explain the $\rho(T)$ and $\rho(H)$ relationship, the $\rho(H)$ at hydrogen temperatures would be determined by the relaxation of the cobalt ion at the hydrogen temperatures. The prediction would be a Brons-Van Vleck dependency. Experimentally we find that ρ is independent of H_c for $H_c < 3000$ Oe. Variations of the relaxation time below 200 Oe are, however, difficult to observe, because the χ'/χ_o and the χ''/χ_o are as a function of H similar to that of manganese tutton salt with a value of $b/C = 750$ Oe. At fields above 4000 Oe we see the onset of a sharp increase in relaxation time, which could be quantitatively explained by the fact that at these fields the quantity γ has the same order of magnitude as β. For the specimen j (1% Fe^{2+}) the same comments can be made. Here we do not find a part in the $\rho(T)$ characteristic where ρ is independent of T. The difference in relaxation time between the curves j and b is not so large and the situation is similar to that of curve III in fig. IV-4. The measurement on this sample (fig. III-5) shows that at high magnetic fields the trend is to equalize the relaxation time of specimen j with that of specimen b.

4.2.3 Gadolinium sulphate. $Gd_2(SO_4)_3 \cdot 8H_2O$

In the following section we will discuss the measurements on Gadolinium sulphate. We feel that in this salt we have observed similar phenomena as in the case of the manganese tutton salts (see fig. III-10), although it is probable that a second anomaly complicates the picture. We have shown that 1% impurities change relaxation times by a factor 10. The differences between the value of relaxation times obtained by GORTER and BROER [73] and by us at nitrogen temperatures is likely to be due to a different amount or different nature of impurities. In our initial measurement we obtained between 40^oK and 100^oK relaxation times independent of temperature which was confirmed by three measurements on two samples (from the same source). A 1% Dy^{3+} impurity gave a relaxation time independent from T between 100^oK and 200^oK, and nearly independent between 20^oK and 100^oK but with a clear minimum. One can observe that similarly shaped curves could be drawn through the measurements of BROER and GORTER [73]. Our present opinion is that the relaxation time below 100^oK in our initial sample is effected by impurities, with a mechanism similar to that in the manganese tutton salt, but with an unknown impurity. The minimum in the relaxation time cannot, however, be explained in this manner. A possible explanation is a change in crystal structure between 50^oK and 100^oK. Anomalies have been reported in gadolinium ethyl sulphate between 20^oK and 290^oK, [98,99,100] but we did not find anomalies in the literature for $Gd_2(SO_4)_3 \cdot 8H_2O$ except an anomaly in the susceptibility between 160^oK and 255^oK (Williams [91]). As a second reason the possibility of (anomalous) expansion could be mentioned. Exchange and dipole-dipole interaction depend strongly on the spacing of the ions. The spin-diffusion efficiency would be reduced if the distance between the magnetic ions increases, resulting in longer relaxation times, as experimentally found.

The value of the relaxation time between 100^oK and 300^oK obtained in our first measurement is likely to be the relaxation time for pure $Gd_2(SO_4)_2 \cdot 8H_2O$, the measurement of GORTER [73] at 300^oK coincides with our value. The value of all data below 100^oK are doubtful in our opinion, representing relaxation times of unknown substances. To describe the ρ-H relationship the following measurements have been reported. GORTER and BROER [73] find at 300^oK a Brons-Van Vleck dependency with $p = 0.36$. Our measurement at 77.3^oK gave $p = 0.35$ (fig. III-11). This value is so close to the transition between the temperature independent portion of $\rho(T)$ and the high temperature region that little information can be gained about the field dependency of the relaxation time in the first mentioned region. The results of the running method, however, indicate a decrease of p. At 20^oK and also at 14.3^oK the slope of the $\rho(H)$ curve is steeper (fig. III-11), a behaviour similar to that of specimen a.

4.2.4 Summary of the discussion on manganese tutton salts and gadolinium sulphate

In the preceding section we have discussed in detail our experimental results. We can recapitulate and generalize the discussion in the following 6 points:

1. It is shown in these two type of salts that small amounts of impurities can have a strong effect on the relaxation time, the relaxation times are shortened by impurities which could be called relaxation centers (VAN VLECK[36,40]).

2. The influence of the impurity on the relaxation time ceases above a certain temperature, which can, according to our measurements, have any value between helium temperature and room temperature.

3. Probably more salts can be found.showing this behaviour and not unlikely relaxation times of most salts can be affected, the type and the sort of effective impurity could be different in each salt.

4. These mechanisms effecting the relaxation times have the tendency to become ineffective in high magnetic fields,the relaxation times approach thereby these of the original salt. The net effect is a distortion of the ρ-H relationship of the original salt by the impurities with a tendency in general to increase $\left(\frac{\partial \rho}{\partial H}\right)_T$.

5. The influence of the impurities further complicates the relaxation phenomena at the helium temperatures. Bottleneck processes increase the relaxation time due to the direct process, impurities can, in some cases, bypass the bottleneck process and cause a complete distortion of the field dependency of the direct process.

6. It has been shown that impurities in some cases do cause deviations from C.d.P. curves.

4.3 DISCUSSION OF THE RELAXATION MEASUREMENTS ON COPPER TUTTON SALTS

Comparing the results, one finds that the absolute value of the relaxation time for the copper cesium tutton salt and the copper ammonium tutton salt are less than a factor 2 different, making the graphs nearly identical. The presence of impurities is not obvious, and it has meaning to compare our ρ-measurements with the theoretical predictions ($\rho^{-1} \propto H^4 T$ for a direct process and $\rho^{-1} \propto T^9$ for a Raman process). In the helium range we find $\rho^{-1} \propto T^\alpha H^\beta$ with $1 < \alpha < 2$ and $\beta < 0$. The temperature and field dependency of ρ is not that of a direct process.

The order of magnitude of the relaxation times obtained by us for the two tutton salts correlate reasonably well with the measurements of DREWES and GORTER[75]. They also find for the cesium tutton salt a longer relaxation time than for the ammonium salt. The results of NASH[81] for relatively large crys-

tals of ammonium copper tutton salt are also of the same order of magnitude as our experimental values. It would be interesting to repeat his experiments in our bridge, the methods of determining the spin-lattice relaxation being different.

Again we have matched the ρ-T curve with a standard curve and obtained a good match for the NH_4-tutton salt with $\theta_D = 180^\circ K$ and a reasonable match for the Cs-tutton salt with $\theta_D = 160^\circ K$. The experimentally determined $\rho(T)$ relationship in the hydrogen range ($\rho^{-1} \propto T^6$) thus correlates reasonably with the expected dependency ($\rho^{-1} \propto T^7$) using $\theta_D = 180^\circ K$ (see table I-4).

In association with this we wish to make a few comments about the Debije temperature θ_D. The Debije temperature is usually computed from the relation $C_1 = \frac{12}{5}\pi^4 aNk\left(\frac{T}{\theta_D}\right)^3$. In this equation C_1 is the lattice specific heat/mole while aN represents the number of independent oscillators. Unfortunately we were not able to find in the literature the value of C_1 of the salts described in this thesis. If one uses the value of C_1 determined by HILL and SMITH[92] for $Zn(NH_4)_2(SO_4)_2 \cdot 6H_2O$ who found at $20^\circ K$ $C_1 = 15.3 \, 10^7$ erg/mole, the following values can be computed for θ_D: $100^\circ K$ (a = 1), $220^\circ K$ (a = 11), $280^\circ K$ (a = 31) and $340^\circ K$ (a = 39). In the first case (a = 1) the complete molecule is considered as one oscillator, for a = 11 each group (as H_2O, NH_4, Zn) is counted separately, while for a = 31 and a = 39 each atom is counted in the cesium and (NH_4) tutton salts respectively.

Apparently the measuring results are best described by the assumption that each group in the molecule is an independent oscillator. The difference between the experimentally observed values for the cesium and the ammonium salt could be explained by the difference in molecular weight and the resulting difference in C_1.

The spin-spin measurements are discussed in section 4.6.

4.4 DISCUSSION OF THE MEASUREMENTS ON COBALT TUTTON SALT

The discussion of the measuring results on cobalt tutton salt can be divided into three parts.

a) Spin-lattice relaxation.

The shape of the spin-lattice relaxation curves and the order of magnitude is in fair agreement with the data of VAN DEN BROEK[8] and VERSTELLE[5]. In the helium temperature range we had to use the pulse method, which limited the fields at which we could measure the relaxation to 1500 Oe. This is for the K_2 sample just below the value at which VAN DEN BROEK[8] obtained the anomalous results. The number of electrons in the 3d shell is odd, making the cobalt tutton salt a so-called Kramers salt. The prediction is that at low temperatures a $T^{-1}H^{-4}$ dependency should occur for the relaxation time ρ at field values above the internal field H_i. In the Raman region we would

expect $\rho \propto T^{-9}$ with a Brons-Van Vleck dependency on H_c. In the helium
range below $2^{\circ}K$ we find $\rho \propto T^{-\alpha}H^{-\beta}$ with $1 < \alpha < 2$ and $\beta \approx 3$, closer to the
prediction than mostly observed in other salts with a bridge method. From
$4^{\circ}K$ - $14^{\circ}K$ we find for both samples, for which the results are shown in
fig. III-26, approximately a ninth power if we calculate the average slope be-
tween these two temperatures.

b) The field independent absorptions.

The discussion on the anomalous absorptions must be incomplete. The method
of operation of the bridge makes it an excellent tool to study these phenomena,
because the peak value of the absorptions and the associated magnetic fields
can be readily obtained from charts; the frequency range does not extend far
enough downwards, however, to measure the phenomena sufficiently completely.
In the single case we used the Hartshorn bridge to gain more complete informa-
tion, it was found that the anomalous absorption was due to the spin-lattice
relaxation whose characteristic time decreased sharply at certain magnetic
fields. If one assumes that all the absorptions are due to this phenomenon, one
can make an estimate of the spin-lattice relaxation time by computing the ρ_{sl}
from data about the absorption $\frac{\chi''}{\chi_0}$ (by using formula 1-21). It should be pointed
out that this assumption is erroneous in the presence of double relaxations such
as found by VAN DEN BROEK[8] in some of his (1:9.5) diluted samples. With this
assumption we have computed the relaxation curve for sample (2) at $4.2^{\circ}K$ and
$2.2^{\circ}K$ and for sample (6) at $4.2^{\circ}K$. These results are shown in fig. IV-7 and the
curves are quite similar to those obtained by VAN DEN BROEK[8]. We also
checked in a few cases if the (much smaller) increase in χ'/χ_0 at these parti-
cular magnetic fields correlated with the increase in χ''/χ_0 by using an Argand
diagram and found that the increase of χ'/χ_0 was as could be expected. VAN
DEN BROEK[8] measured the curves, shown at page 133 of his thesis, at 2000 Hz
or 3000 Hz far into the measuring range of our bridge, but in our specimens we
have not noticed any indication of a third relaxation, as VAN DEN BROEK[8]
observed in the 1:9.5 salt.

The measurements done by us on the Hartshorn bridge were only per-
formed at one field. Concerning these anomalous absorptions we can state that
at present our high frequency results are not so complete as those by VAN DEN
BROEK[8] but show the same trend. We plan, however, to continue research on
3 samples mounted as closely as possible in the K_1, K_2, and K_3 directions with
high magnetic fields and also at low frequencies with a method similar to the
one used in this high frequency bridge.

The initial measurement has shown that some of these absorptions occur
at fields above 4500 Oe. We do not have at present any definite explanation why
the spin-lattice relaxation becomes more efficient at certain specific fields. The
only comment one could make at present is that in addition to the normal energy
level pattern, additional energy levels must play a role in the relaxation process.
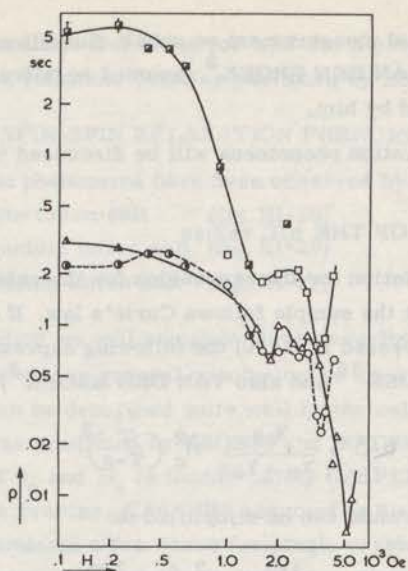
Fig. IV-7.

$\rho(H)$ for Cobalt ammonium tutton salt

			measured	computed from high frequency absorptions
a			⊕	○
b			⊡	□
c			▲	△
a	sample (2)	4.2°K	Co(NH$_4$)$_2$(SO$_4$)$_2$ 6D$_2$O K$_2$	1:0
b	(2)	2.2°K		
c	(6)	4.2°K	Co(NH$_4$)$_2$(SO$_4$)$_2$ 6H$_2$O K$_2$	1:10

One could visualize one or more sets of exited energy levels of a non magnetic origin, possibly due to impurities. At specific values of $g\mu_B H_c$ cross relaxation processes, affecting the relaxation time, could take place. More information about the number of the absorptions and the magnetic fields at which they occur may give some additional information. Another important point in searching for an explanation may also be the fact that no abnormal absorptions were found in the 1:10 diluted D$_2$O sample, while the 1:10 diluted H$_2$O sample showed large absorptions in our frequency range. The fact that we did not see an absorption in the K$_3$ direction should be examined further. In association with this, it can be remarked that the anomaly in the χ'/χ_0 reported by VAN DEN BROEK[8], was small in the K$_3$ sample.

In searching for an explanation, one should not exclude the possibilities of impurities, which at certain magnetic fields could decrease the relaxation time. The phenomena observed by VAN DEN BROEK[8], and by us are similar in certain aspects. There are, however, enough differences, even in a case where we prepared a specimen similar to VAN DEN BROEK[8] (1:10; H$_2$O). The anomalously high adiabatic susceptibilities reported by us for some cases can at present be only ascribed to impurities. There is some, but not a definite, correlation between this last mentioned anomaly and the field independent absorptions.

131

An initial measurement on cobalt fluosilicate produced also anomalous absorptions. VAN DEN BROEK [8] reported negative results in the frequency range examined by him.

c) Spin-spin relaxation phenomena will be discussed in 4.6.

4.5 DISCUSSION OF THE b/C values

In the deviation for the expression for the value of b/C in formula (1-24), it is assumed that the sample follows Curie's law. If deviations from Curie's law occur as expressed in (1-10) the following expression can be derived (BENZIE and COOKE [70] and also VAN DEN BROEK [8])

$$b/C = \frac{\chi_{ad}}{\chi_0 - \chi_{ad}} \, H_c^2 \left(\frac{T}{T-\theta}\right)^3$$

For $\theta < T$ this formula can be simplified to:

$$b/C = \frac{\chi_{ad}}{\chi_0 - \chi_{ad}} \, H_c^2 \left(1 + \frac{3\,\theta}{T}\right)$$

If an accuracy of 1% is desired for b/C, $\frac{\theta}{T}$ has to be less than 0.0033. This requires $\theta < 0.014\,^{\circ}K$ for a temperature T of $4.2\,^{\circ}K$ and $\theta < 0.066\,^{\circ}K$ for T = $20\,^{\circ}K$. Several causes contribute to θ as is mentioned in section 1.2. If we concentrate on the contribution to θ due to the difference in the local field H_1 and the applied field H_c, we see that in salts with a large Curie constant, a sizable contribution to θ can be expected, if the demagnetization factor α is not equal to $\frac{4\pi}{3}$. If we take for example $\alpha = \frac{2\pi}{3}$, we find that for an accuracy of 1% for the value of b/C, the Curie constant C has to be less than 0.007 deg cm^{-3} and 0.032 deg cm^{-3} if the measurement for the b/C value is done at $4.2\,^{\circ}K$ and $20\,^{\circ}K$ respectively.

From table I-1 we see that the Curie constant for manganese tutton salt can expected to be 0.020 deg cm^{-3} while a value of 0.108 deg cm^{-3} has been calculated for gadolinium sulphate. This explains at least partly the deviations of the b/C value reported earlier in these two salts. We believe that we have with our measurements reduced the uncertainty about the b/C value of the manganese tutton salt. Earlier measurements indicated a range of $(0.55 - 0.64)\,10^6\,Oe^2$, the evidence given reduces this range to $(0.57 - 0.60)\,10^6\,Oe^2$. Our measurements indicate $(0.575 \pm 0.005)\,10^6\,Oe^2$ and we do not have any explanation for the differences observed within this last mentioned range of values.

For the copper cesium tutton salt (section 3-4) we determined the b/C value in the K_1 and the K_2 direction, which we found to be consistent with each other, using the published g-values [80]. If we assume a random distribution of the particles we computed from these values a b/C for a powder of $4.33\,10^4\,Oe^2$ while BENZIE [71] et al found $4.63\,10^4\,Oe^2$. A lack of random orientation could

132

be the reason for this difference. Our value for b/C for a powder of copper ammonium tutton salt gives the same value as published by BENZIE[71] et al.

4.6 DISCUSSION OF THE SPIN-SPIN RELAXATION PHENOMENA

Spin-spin relaxation phenomena have been observed by us in
- a) Copper cesium tutton salt   (fig. III-15)
- b) Copper ammonium tutton salt (fig. III-20)
- c) Cobalt ammonium tutton salt   (fig. III-29)

In the following section we will compare our measuring results with the theoretical predictions. As a very general conclusion we see that in all three salts our measurements can be described quite well by the relation $\rho_{ss} = \rho_0 \exp(H_c^2/H_0^2)$ (1-37) as predicted by KRONIG and BOUWKAMP[41] and no temperature dependence of ρ_0 and H_c is found. Lately CASPERS[43] and TJON[44] have made the theory more precise. CASPERS assumed in his calculations an isotropic g-value, and calculated a few cases for single crystals with cubic symmetry. Our measurements are on tutton salts with a monoclinic crystal symmetry, while the g-factor is somewhat anisotropic in the copper tutton salts ($g_{//} = 2.44$ and $g_{\perp} = 2.06$) and very anisotropic in the cobalt tutton salts ($g_{//} = 6.45$ and $g_{\perp} = 3.06$). The situation is furthermore complicated by a sizable h.f.s. (hyper fine structure) interaction not taken explicitly into account by CASPERS (but lately studied by TJON)[93]. Fortunately we have for all salts $S = \frac{1}{2}$ of $S' = \frac{1}{2}$, eliminating zero field splittings due to crystal field.

CASPERS[43] and TJON[93] compared their results with the original spin-spin relaxation measurements done by VERSTELLE[5] on ammonium tutton salt, our measurements on this same salt extend the former measurements and our values on the cesium tutton salt together with (unpublished) measurements from Mr. E.A. TEN HOVE will also be compared.

The ratio between the exchange and dipole-dipole interaction is completely different in the two copper salts, making the set of salts valuable for comparison with the theory.

From the measurements of BENZIE, COOKE and WHITLEY[71] the total internal magnetic field $H_{i\,tot.}$ [which equals $(2\,b/C)^{\frac{1}{2}}$] can be separated into H_{idd} (due to dipole-dipole interaction), $H_{i\,ex.}$ (due to exchange interaction), $H_{i\,hfs}$ (due to nucleus-spin interaction) and $H_{i\,el.}$ (associated with zero field splittings). In table IV-1 we list these values, calculated from the data of BENZIE et al[71].

Our measurements have all been made for high values of H_c ($H_c \gg H_{i\,tot}$) and we can obtain with a good accuracy the value of H_0 (formula 1-37), but an extrapolation of our measurements to give an estimate of ρ_0 can produce large errors. Besides, studies of VERSTELLE[5] and TJON[92] have indicated the relationships between ρ_{ss} and H_0^2 to be more complex than indicated in for-

	H^2_{idd} (Oe^2)	H^2_{ihfs} (Oe^2)	H^2_{iex} (Oe^2)	b/C (Oe^2)
CuCs$_2$ tutton	4.47 10^4	4.10 10^4	0.74 10^4	4.60 10^4
Cu(NH$_4$)$_2$ tutton	4.84 10^4	4.46 10^4	21.2 10^4	15.2 10^4
Co(NH$_4$)$_2$ tutton	18.3 10^4	15.7 10^4	2.6 10^4	18.3 10^4

Table IV-1: Values of H^2_{idd}, H^2_{ihfs}, H^2_{iex} and b/C for three tutton salts.

mula (1-37). If we substitute the quantities of table IV-1 in the formula indicated in table III, page 802 of CASPERS [43], we obtain the values for H_o shown

in table IV-2. In this last table we also indicate our measuring results.

	Calculated values (formulas from Caspers)			Experimental data			
	s.c. (100)	f.c.c. (100)	f.c.c. (111)	powder	K_1	K_2	K_3
CuCs$_2$ tutton	6.1 10^4	3.2 10^4	4.3 10^4	7.9.10^{4*}	7.5 10^4	9.5 10^4	
Cu(NH$_4$)$_2$ tutton	61 10^4	50 10^4	62 10^4	{74 10^4 93 10^{4**}}			
Co(NH$_4$)$_2$ tutton	24 10^4	11 10^4	17 10^4		110 10^4	69 10^4	77 10^4

Table IV-2. Experimental and calculated values (following Caspers) of H^2_o (in Oe^2) for three tutton salts. * Ten Hove. ** Verstelle

Before comparing the calculated and experimental data the following remarks should be made.
1) The effect of the sizable nuclear interaction (H^2_{ihfs}) is not taken into account in table IV-2.
2) It is very doubtful if the theory of CASPERS can be applied to the cobalt ammonium tutton salts in view of the highly anisotropic g-values.

Comparing the calculated and experimental data of table IV-2 shows that the calculated values for the simple cubic lattice (s.c. (100)) come closest to the experimental values. CASPERS [43] remarks, however, that the values for ρ_o found for the s.c. (100) case deviate more from the experimental data than for the other two cases computed. The order of magnitude is quite good for the copper tutton salts, but poor for the cobalt tutton salt. As pointed out, our measuring results are not too suitable for predicting a value of ρ_o. Some additional comments will be made for the two copper tutton salts.

VERSTELLE [5] pointed out that a term should be added to formula (1-37) taking into account the contribution of the second Larmor line. The expression he predicts (following CASPERS [43]) is

$$\rho^{-1}_{ss} = 1.1\ 10^8 \exp(-H^2/0.56\ 10^6) + 2.8\ 10^8 \exp(-4H^2/0.56\ 10^6)$$

and is indicated in fig. III-20. TJON [93] has in a recent paper taken into account
the influence of the hyperfine interaction on the spin-spin relaxation for the same
salt and finds

$$\rho_{ss}^{-1} = (1 + H^2/0.13 \ 10^6) \, [\rho_o^{-1} \exp(-H^2/H_o^2) + 1.5 \ 10^8 \exp(-H^2/0.3 \ 10^6) +$$
$$+ 4 \rho_o^{-1} \exp(-4H^2/H_o^2) \,]$$

(we assume that in reference [93] the term 10^8 in the second exponential is acci-
dentily omitted).

    We have plotted the relaxation time computed by this formula in fig. III-20,
using the same values as suggested by TJON [41] for H_o^2 and ρ_o

$$(H_o^2 = 0.56 \ 10^6 \text{ Oe}^2 \ , \ \rho_o^{-1} = 1.1 \ 10^8 \text{ sec}^{-1})$$

In absolute value, the predictions by TJON agree reasonably well with the experi-
mental value, however, the curvature in his graph at higher field valués is just
apposite to the curve found experimentally. It can be seen from fig. III-20 that
the extrapolation of our measurements does not coincide with the measurements
by VERSTELLE [5]. At present it is difficult to say if this curvature is inherent
to the salt or due to measurements on two different specimens. It would be
worthwile to measure the same specimen in the two measuring systems.

    For the cesium tutton salt the extrapolation of our measurements could
be in agreement with the data obtained by TEN HOVE (not published), a complete
comparison being difficult; we measured single crystals while TEN HOVE meas-
ured a powder. For this salt VERSTELLE [5] has computed, following TJON's [93]
technique

$$\rho_{ss}^{-1} = (1 + H^2/1.5 \ 10^4) \, [\rho_o^{-1} \exp(-H^2/a) + 0.43 \ 10^9 \exp(-H^2/0.3 \ 10^5) +$$
$$+ 4 \rho_o^{-1} \exp(-4H^2/a') \,]$$

The values for a, a' and ρ_o are determined from the expressions of CASPERS [43]
and TJON [93] and are given in table IV-3. As TJON has done in ammonium copper
tutton salt, we have taken for the "double flip" terms the same value for the mo-
ment as found for the "dipole-dipole" term.

	s.c. (100)	f.c.c. (100)	f.c.c. (111)
$\rho_o/2\pi$	$2.4.10^{-9}$	$0.5.10^{-9}$	$0.77.10^{-9}$
a	$6.1.10^4$	$3.2.10^4$	$4.3.10^4$
a'	$14.1.10^4$	$5.5.10^4$	$7.4.10^4$

Table IV-3. Values of $\rho_o/2\pi$, a and a' for $CuCs_2(SO_4)_2 . 6H_2O$.

The calculated values for the three cases have been plotted in fig. III-15. The
actual measurements are closest to the values computed for the simple cubic

lattice, as was also the case in the ammonium salt. The difference between the predicted value of the relaxation time at low fields H_c and the extrapolated value of the measuring results is of the order of a factor 3.

We have been able to determine the quantity $x''_{ss\,max.}/x_{ad.}$ with reasonable accuracy and the results are assembled in table IV-4.

	powder	K_1	K_2	K_3	Caspers
$CuCs_2(SO_4)_2 \cdot 6H_2O$	0.08 [1)]	0.15 ± 0.02	0.07 ± 0.01		0.16
$Cu(NH_4)_2(SO_4)_2 \cdot 6H_2O$	0.3				0.39
$Co(NH_4)_2(SO_4)_2 \cdot 6D_2O$		0.17 ± 0.01	0.07 ± 0.01	0.09 ± 0.01	0.12

TABLE IV-4. Magnitude of $x''_{ss\,max.}/x_{ad.}$ for three tutton salts.   1) Ten Hove

CASPERS [94] showed that for powders the reduction $\Delta x_{ad.}$ of the adiabatic susceptibility $x_{ad.}$ due to the spin-spin relaxation is given by:

$$\frac{1/5\,H^2_{idd} + 1/3\,H^2_{ihfs} + H^2_{ex}}{H^2_{i\,tot}}$$

If the spin-spin relaxation has a Debije character, the maximum absorption $x''_{ss\,max.}$ will be given by 50% of that amount. The quantity is indicated in the last colum of table IV-4. The spin-spin absorptions are so small, that we cannot determine, whether they have a Debije character. It is therefore not possible to check the predictions of CASPERS [94]. No calculations are available to predict the anisotropy in the spin-spin absorption.

4.7 THE RELATION BETWEEN SPIN-LATTICE AND SPIN-SPIN RELAXATION PHENOMENA

In the copper tutton and cobalt tutton salts we were able to do measurements in a condition where the spin-spin relaxation time would be longer than the spin-lattice relaxation time. In all these cases we noticed the disappearance of the spin-spin absorption. This can be qualitatively explained by the establishing of the equilibrium through the spin-lattice contacts, which is under these conditions more efficient. We have tried to observe deviations of C.d.P. when the spin system is not in equilibrium. If the two ions in the unit cell in the tutton salt have a different relaxation time, a deviation from C.d.P. curves would result. We have not noticed this but it should be said that the differences should be sizable before an effect of this type would be noticed (VAN DEN BROEK [8]).

CHAPTER 5

APPENDIX A:

MECHANICAL VIBRATIONS IN THE MEASURING SYSTEM

During the design of the measuring system, we found severe field effects. These effects were found to be proportional to H^2 and showed a typical resonance character. Some actual measurements are shown in fig. II-20. It was found that they were due to electro-mechanical coupling of a mechanical resonator with the measuring coils which vibrated when a dc magnetic field was present. In the following we analyze this system. The analysis is partly the well known mechanical couplings of resonators, the magnetic field, however, enters into equations, and produces a variable coupling. The full analysis is given, because these parasitic phenomena may be quite severe in high magnetic fields.

In this chapter, we will denote complex quantities by $\overline{P}$, $\overline{P}$ represents a vector in the complex plane. Real vectors are denoted by $\underline{B}$.

A few calculations have been made on a model which gives a good explanation of the phenomena observed. The coil is wound on a glass cylinder with N turns/cm. The total length of the coil is 1 cm. If a steady magnetic field B is present the Lorentz force on a sinusoidal current $I = \hat{I}\cos \omega t$ in the coil will, (if the system is linear) tend to expand and contract the cylinder and result in sinusoidal variations $X_1 \cos(\omega t - \varphi)$ of the radius X_0. The Lorentz-force will be uniformly distributed over the circumference and is given by:

$$\frac{dF}{ds} = 0.1 \; \underline{I} \times \underline{B} N l \quad \text{(fig. V-1)} \qquad (5-1)$$

If a uniform pressure is present in a ring, a force $\underline{P}$ will be found given by $\underline{P} = \frac{dF}{ds} X_0$ (5-2) or $\underline{P} = 0.1 X_0 \underline{I} B N l$ (5-3) if $\underline{I} \perp \underline{B}$. The result of the force P will be to increase and decrease the coil-diameter X_0 by an amount X_1. Fig. V-2 shows two coupled mechanical oscillators. The system with indices 1 represents the coil, the system with the indices 2 re-presents the coil, the system with the indices 2 re-
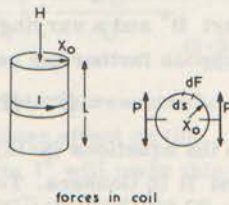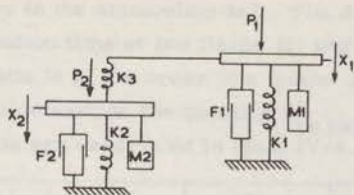

forces in coil

Fig. V-1.

Fig. V-2.   diagram for two mechanically coupled harmonic oscillators.

presents any mechanical resonator coupled by a (weak) spring to coil. P_1 represents the driving force (Lorentz force). The equations governing the system are:

$$P_1 - P_2 = M_1 \ddot{X}_1 + F_1 \dot{X}_1 + K_1 X_1 \qquad (5\text{-}4)$$

$$P_2 = K_3 (X_1 - X_2) \qquad (5\text{-}5)$$

$$P_2 = M_2 \ddot{X}_2 + F_2 \dot{X}_2 + K_2 X_2 \qquad (5\text{-}6)$$

If the driving force is sinusoidal, i.e. $P = \hat{P}\cos \omega t$, the steady state solutions can be found by introducing the following complex quantities:

$$P_1 = \mathrm{Re}\,[\,\overline{P}_1 e^{j\omega t}\,], \quad X_1 = \mathrm{Re}\,[\,\overline{X}_1 e^{j\omega t}\,] \quad \text{and} \quad I = \mathrm{Re}\,[\,\overline{I}\, e^{j\omega t}\,] \quad \text{etc.} \qquad (5\text{-}7)$$

Substitutions of (5-7) into (5-4), (5-5) and (5-6) yields

$$\overline{P}_1 - \overline{P}_2 = -\omega^2 M_1 \overline{X}_1 + j\omega F_1 \overline{X}_1 + K_1 \overline{X}_1 \qquad (5\text{-}8)$$

$$\overline{P}_2 = K_3 (\overline{X}_1 - \overline{X}_2) \qquad (5\text{-}9)$$

$$\overline{P}_2 = -\omega^2 M_2 \overline{X}_2 + j\omega F_2 \overline{X}_2 + K_2 \overline{X}_2 \qquad (5\text{-}10)$$

Solving these three linear equations and expressing $\overline{X}_1$ in terms of P_1 yields

$$\overline{X}_1 = \cfrac{\overline{P}_1}{(K_1 + K_3) + j\omega F_1 - \omega^2 M_1 - \cfrac{K_3^2}{K_2 + K_3 + j\omega F_2 - \omega^2 M_2}} = \frac{\overline{P}_1}{D} \qquad (5\text{-}11)$$

The total magnetic induction B_t inside the coil consists of two parts, a steady part $B^{=}$ and a varying part $B^{\sim}$ (the coil is supposed to be a long thin coil) and suppose further the permeability $\mu = 1$. Then

$$\overline{B}^{\sim} = \overline{H}^{\sim} = 0.4\pi N \overline{I} \quad (5\text{-}12)\ , \quad B_t = B^{=} + 0.4\pi N \hat{I}\cos \omega t \qquad (5\text{-}13)$$

In the equations (5-12) and (5-13) I is expressed in Amperes, H in Oersteds and B in Gausses. To compute $\overline{P}$ we neglect the ac field and obtain:

$$\overline{P} = 0.1\, X_o \overline{I} B^{=} N1 \qquad (5\text{-}14)$$

Substitution of (5-14) into (5-11) gives $\overline{X}_1 = \dfrac{0.1\, X_o B^{=} N1 \overline{I}}{D} \qquad (5\text{-}15)$

138

with $\bar{D} = De^{j\varphi}$ (5-16).

In our measuring system we measure the impedance of the coil. The impedance can be calculated by computing the induced voltage when a current $I\cos\omega t$ passes through the coil. The ratio between $\bar{E}$ and $\bar{I}$ will give the impedance $\bar{Z}$ (neglecting losses of the coil itself). The induced voltage will have non-linear terms and the complex notation cannot be used.

$$e_{ind} = -10^{-8}\frac{d\phi}{dt} = -10^{-8}\frac{d}{dt}(S B_t N1) \tag{5-17}$$

The factor S represents the surface of the coil.

$$e_{ind} = -10^{-8}\frac{d}{dt}[\pi(X_o + X_1)^2(B^= + 0.4\pi N \hat{I}\cos\omega t)N1] \tag{5-18}$$

Substitution of (5-15) into (5-18) gives after differentiation of (5-18) with $B^= \gg 0.4\pi NI$ e.g. $(B^= \gg B\tilde{\ })$ and $\frac{0.1 B^= I N1}{D} \ll 1$ $(X_o \gg X_1)$

$$e_{ind} = 10^{-8}\pi N1\left[\left\{0.4\pi\omega N\hat{I}(X_o^2\sin\omega t + \frac{0.2 X_o^2 B^= \hat{I}\cos(\omega t - \varphi)\sin(\omega t).N1}{D} + \frac{10^{-2} X_o^2 B^{2=} N^2 1^2 \hat{I}^2\cos^2(\omega t - \varphi)\sin\omega t}{D^2}\right)\right\} + \frac{0.2 X_o^2 B^{2=}\omega N1\hat{I}\sin(\omega t - \varphi)}{D}\right] \tag{5-19}$$

The measuring equipment measures only components with a frequency ω. The second term of equation (5-19) contains only terms with frequencies 2ω and o and can be neglected. By means of

$$\sin\omega t.\cos^2(\omega t - \varphi) = \frac{\sin\omega t}{2} + \frac{\sin(3\omega t - 2\varphi)}{4} - \frac{\sin(\omega t - 2\varphi)}{4}$$

and dropping also the terms with a frequency 3ω we obtain, after returning to the complex notation:

$$\bar{E} = 10^{-8}\pi N1\bar{I}\left[j\omega.0.4 N\left\{X_o^2 - \frac{0.25\ 10^{-2} X_o^2 B^{2=} N^2 1^2(1 - 2e^{j\varphi})}{\bar{D}^2}\right\} + \frac{0.2 j\omega X_o^2 B^{2=} N1}{\bar{D}}\right] \tag{5-20}$$

By means of $\bar{E} = \bar{I}\bar{Z}$ we obtain finally:

$$\bar{Z} = 10^{-8}\pi N^2 1^2 j\omega\left[\frac{0.4}{1}\left\{X_o^2 - \frac{0.25\ 10^{-2} X_o^2 B^{2=} N^2 1^2(1 - 2e^{j\varphi})I^2}{\bar{D}^2}\right\} + \frac{0.2 X_o^2 B^{2=}}{\bar{D}}\right] \tag{5-21}$$

In equation (5-21) the first term in the square brackets represents the normal inductance of the coil. The second term is a non linear effect on the impedance due to the non-linearity of the system. The term I^2 will make this expression dependent on the current through the coil. We will concentrate on the third term, arising from the vibrations of the coil, but which is linear at constant $B^=$.

By using $v = \dfrac{\omega}{\omega_o} - \dfrac{\omega_o}{\omega}$

$$Q = \frac{1}{F_2} \left\{ \frac{M_2(K_1 K_2 + K_1 K_3 + K_2 K_3)}{K_1 + K_3} \right\}^{\frac{1}{2}}$$

and $\omega_o = \left\{ \dfrac{K_1 K_2 + K_1 K_3 + K_2 K_3}{M_2(K_1 + K_3)} \right\}^{\frac{1}{2}}$

we can write

$$\frac{1}{D} = \frac{1}{K_1 + K_3} + \frac{K_3^2}{j\omega(K_1 + K_3)^2 F_2} \left\{ \frac{1}{1 + v^2 Q^2} - \frac{j v Q}{1 + v^2 Q^2} \right\} \tag{5-22}$$

By substituting (5-22) into (5-21) and deleting the non-linear term, we find

$$Z = j\omega \, 10^{-8} \pi N^2 1^2 X_o^2 \left[\frac{0.4}{1} + \frac{0.2 \, B^2}{K_1 + K_3} + \frac{0.2 \, B^2 = K_3^2}{j\omega(K_1 + K_3)^2 F_2} \left\{ \frac{1}{1 + v^2 Q^2} - \frac{j v Q}{1 + v^2 Q^2} \right\} \right] \tag{5-23}$$

The last two terms in equation (5-23) are due to the electro-mechanical coupling, and show a resonant character. If plotted, the shape of the curve will be similar to the one indicated in fig. II-21. The curves of fig. II-21-b have actually been computed for a pure magnetical coupling of a resonator to the measuring system as indicated in fig. II-21-c. Equation (5-23) shows the resonance to be proportional to B^2, which is experimentally found.

In the cryostat of fig. II-20-b we only found a resonance of the glass tube on which the coil was wound. TIMOSHENKO[95] gives as the radial resonant frequency of a rod:

$$f = \frac{1}{2\pi} \sqrt{\frac{Eg}{\gamma \, r^2}}$$

Substitution of $E = 10^6$, $g = 1000$, $\gamma = 3$ and $r = 0.7$ gives $f = 120$ kHz. Experimentally we do find the resonance at 97 kHz.

LITERATURE

(Much of the work published in Dutch theses can also be found in articles in "Physica")

1. Waller I., Z. Phys. 79 (1932) 370
2. Gorter C.J., Physica 3 (1936) 503
3. De Haas W.J. and Du Pré F.K., Physica 5 (1938) 501
4. Gorter C.J., Paramagnetic relaxation (Elsevier, Amsterdam 1947)
5. Verstelle J.C., Thesis Leiden 1962
6. Bijl D., Thesis Leiden 1950
7. Van der Marel L.C., Thesis Leiden 1958
8. Van den Broek J., Thesis Leiden 1960
9. Bölger B., Thesis Leiden 1959
10. Gorter C.J., Fluctuation, Relaxation and Resonance in magnetic systems. D. ter Haar (Oliver and Boyd)
11. Dekker A.J., Solid State Physics, Prentice Hall, 1957
12. Lorentz H.A., Theory of Electrons, p. 138, 306. (Teubner, Leipzig 1909)
13. Onsager L., Journ. Am. Chem. Soc. 58 (1936) 1486
14. Van Vleck J.H., Journ. Chem. Phys. 5 (1937) 320
15. De Klerk D., Thesis Leiden 1949
16. Kittel C., Introduction to Solid State Physics (John Wiley (NY))
17. Casimir H.B.G. and Du Pré F.K., Physica 5 (1938) 507
18. Eisenstein J., Phys. Rev. 84 (1951) 548
19. Van den Broek J., Van der Marel L.C. and Gorter C.J., Comm. K.O. lab. 327
20. Fuoss R. and Kirkwood S.G., Journ. Am. Chem. Soc. 63 (1941) 385
21. Heitler W. and Teller E., Proc. Roy. Soc. A 155 (1936) 629
22. Fierz M., Physica 5 (1938) 433
23. Kronig R., Physica 6 (1939) 33
24. Van Vleck J.H., Phys. Rev. 57 (1940) 426
25. Orbach R., Proc. Phys. Soc. 77 (1961) 821
26. Orbach R., Proc. Phys. Soc. A 264 (1961) 458
27. Orbach R., Proc. Phys. Soc. A 264 (1961) 485

141

28. Finn C.B.P., Orbach R. and Wolf W.P., Proc. Phys. Soc. 77 (1961) 261

29. Kramers H.A., Proc. Kon. Ned. Akad. Wetenschappen 33 (1930) 959

30. Brons F., Thesis Groningen 1938

31. Orbach R. and Blume M., Phys. Rev. Letters 8 (1962) 478

32. Orbach R. and Blume M., Phys. Rev. 127 (1962) 1587

33. Leushin A.M., Soviet Phys. Solid State 5 (1963) 440

34. Leushin A.M., Soviet Phys. Solid State 5 (1963) 623

35. Ziman J.M., Proc. Roy. Soc. A 226 (1954) 436

36. Van Vleck J.H., Phys. Rev. 59 (1941) 724

37. Gorter C.J., Van der Marel L.C. and Bölger B., Physica 21 (1955) 103

38. Scott P.L. and Jeffries C.D., Phys. Rev. 127 (1962) 32

39. Van den Broek J. and Van der Marel L.C., Physica 30 (1964) 565

40. Van Vleck J.H., Quantum Electronics (1960) Townes

41. Kronig R. and Bouwkamp C.J., Physica 5 (1938) 521

42. Locher P.R., Thesis Leiden 1962

43. Caspers W.J., Physica 26 (1960) 778

44. Tjon J.A., Thesis Utrecht 1964

45. Bloembergen N., Shapiro S., Pershan P.S. and Artman J.A., Phys. Rev. 114 (1959) 445

46. Bloembergen N. and Pershan P.S., 2nd Conference Quantum Electronics (1961)

47. Grant W.J.C., Physical rev. 134 (1964) A 1554

48. Bloembergen N., Physica 15 (1949) 386 and 588

49. Hoffman W., Z. Kristallogr. 78 (1931) 279

50. Bleaney B. and Stevens K.W.H., Repts. Progress Physics 16 (1953) 107

51. Bowers K.D. and Owen J., Repts. Progress Physics 18 (1955) 304

52. Bleaney B. and Ingram D.J.E., Proc. Roy. Soc. A 205 (1951) 336

53. Abragam A. and Pryce M.H.L., Proc. Roy. Soc. A 206 (1951) 173

54. Tinkham M., Proc. Roy. Soc. A 68 (1955) 258

55. Tinkham M., Proc. Roy. Soc. A 236 (1956) 535

56. Griffiths J.H.E. and Owen J., Proc. Roy. Soc. A 213 (1952) 459

57. Broer L.J.F., Dijkstra L.J. and Gorter C.J., Physica 10 (1943) 324

58. Bogle G.S. and Symmons H.F., Proc. Phys. Soc. 79 (1962) 775

59. Van den Handel J., Thesis Leiden 1940

60. Cooke A.H., Edmond D.T., McKim F.R., Wolf W.P., Proc. Roy. Soc. London A 252 (1959) 246

61. Granberg G., Z. Physik 159 (1960) 125

62. Caruthers R.S., B.S.T.J. 18 (1939) 315

63. Darlington S., B.S.T.J. 29 (1950) 94

64. Van den Broek J., Thesis Leiden

65. Broer L.J.F., Thesis Amsterdam 1945

66. Treadwell F.P., Analytischer Chemie, Erster Band, (Wien, Franz Deuticke)

67. Z. Kristallograph A $\underline{101}$ (1939) 39
68. Metals Techn. $\underline{15}$ (1948)
69. Z. Kristallograph $\underline{84}$ (1933)
70. Benzie R.J. and Cooke A.H., Proc. Phys. Soc. A $\underline{63}$ (1950) 213
71. Benzie R.J., Cooke A.H., Whitley S., Proc. Roy. Soc. $\underline{232}$ (1955) 277
72. Du Pré F.K. and De Haas W.J., Physica $\underline{6}$ (1939) 705
73. Broer L.J.F. and Gorter C.J., Physica $\underline{10}$ (1943) 621
74. De Vrijer F.W., Volger J. and Gorter C.J., Physica $\underline{11}$ (1946) 412
75. Drewes G.W.J. and Gorter C.J., Proc. 8th Int. Conf. Low Temp. Physics London (1962) 291
76. Benzie R.J. and Cooke A.H., Proc. Phys. Soc. A $\underline{63}$ (1950) 201
77. Bijl D., Physica $\underline{8}$ (1941) 461
78. Van den Broek J., Van der Marel L., and Gorter C.J., Physica $\underline{24}$ (1958) 101
79. Volger J., Thesis Leiden 1946
80. Bleaney B., Penrose R.P. and Plumpton Betty I., Proc. Roy. Soc. $\underline{198}$ (1949) 406
81. Nash F.R., Phys. Rev. Letter $\underline{7}$ (1961) 59
82. De Vrijer F.W., Thesis Leiden 1951
83. Candela G.A., Journ. Chem. Phys. $\underline{42}$ (1965) 113
84. Bleaney B. and Ingram D.J.E., Proc. Roy. Soc. A $\underline{208}$ (1951) 143
85. Feher G., B.S.T.J. $\underline{26}$ (1957) 449
86. Pauling L., Nature of the Chemical bond (1945) Ithaca, p.346
87. Pershan P.S., Phys. Rev. $\underline{117}$ (1960) 109
88. Manenkov A.A. and Milyaev V.A., Soviet Physics J.E.T.P. $\underline{14}$ (1962) 76
89. Zverev G.M., Prokhorov A.M. and Shevchenko A.K., Sov. Phys. Solid State $\underline{4}$ (1963) 2297
90. Bloembergen N. and Persham P.S., Advances in Quantum Electronics p.373
91. Williams E.H., Phys. Rev. $\underline{46}$ (1934) 133
92. Hill and Smith, Proc. Phys. Soc. A $\underline{66}$ (1953) 228
93. Tjon J.A., Physica $\underline{30}$ (1964) 1 and 10
94. Caspers W.J., Physica $\underline{27}$ (1961) 1023
95. Timoshenko S., Vibration Problems in Engineering, Van Nostrand N.Y. p.406
96. Gorter C.J. and Kronig R., Physica $\underline{3}$ (1936) 1009
97. Bloembergen N., Physica $\underline{15}$ (1949) 386
98. Bleaney B., Scovil H.E.D. and Trenan R.S., Proc. Roy. Soc. A $\underline{223}$ (1954) 15
99. Buchmaster H.A., Canad. Journ. Physics $\underline{34}$ (1956) 341
100. Bleaney B., Elliott R.J., Scovil H.E.D. and Trenan R.S., Phil. Mag. $\underline{42}$ (1951) 1062

SUMMARY

In this thesis we introduced and discussed the design of a bridge and detector system to measure paramagnetic relaxations in the frequency range between 200 Hz and 1 MHz. The bridge is basically a simple ac Wheatstone bridge, each arm having a coil as its most important element (shown in fig. II-16 and II-17). The sample is moved from one coil to another and the difference in unbalance in the two positions is measured. The detection system employs synchronous detection and enables us to separate the output signal of the bridge into two components. One component gives information about the dispersion χ'/χ_o of the paramagnetic sample, the other about the absorption χ''/χ_o. The use of synchronous detection is also quite advantageous to improve the signal to noise ratio of the detected signal. To facilitate the design, the actual separation of the components is done at one fixed frequency of 1.5 MHz, different from the measuring frequency. The complete block diagram is shown in fig. II-11. The signals containing the information about the dispersion and the absorption are in the form of slowly varying dc voltages, making recording with an X-Y writer feasible, such that the dispersion (or absorption) is plotted directly against the magnetic field. With this bridge we are able to measure these quantities in the frequency range from 200 Hz to 1 MHz at any magnetic field between 0 and 4300 Oe with a conventional, water-cooled solenoid, while by means of a liquid nitrogen cooled magnet (fig. II-31) we have been able to measure the dispersion and absorption of some salts up to 14 kOe. Auxiliary equipment for this magnet is being completed, the maximum field strength obtained yet is 22 kOe. A liquid nitrogen cooled magnet may be used because of the high speed of the measuring equipment.

The measurements can be done in a semi-automatic way, reducing errors. Relaxation times between 100 msec. and several minutes can be studied introducing a fast variation of the magnetic field. Unfortunately the applicability of this method is limited, depending on the magnetic strength of the sample, to magnetic fields of a few times $(b/C)^{\frac{1}{2}}$ (see formula 1-29).

With this bridge we have done a series of measurements on some para-

magnetic salts. We extensively examined manganese tutton salt. We measured at helium, hydrogen and nitrogen temperatures and were able to obtain, with an estimated accuracy of $\pm 10\%$, relaxation times in the intermediate temperature ranges by slowly warming up of the cryostat.

Relaxation times over a range of more than 7 decades have been obtained in the temperature interval of $1^{\circ}K - 300^{\circ}K$. Our main emphasis has been on the influence of impurities on the relaxation times and the results of measurements on approximately 25 samples have shown (fig. III-3 and fig. III-5) that in one (or possibly more) temperature regions $T_L < T < T_H$ the relaxation time is often determined by impurities. The temperature limits depend on the type and concentration of the impurities and also on the magnitude of the constant magnetic field. In manganese tutton salt we found for sample a (fig. III-3), in which no impurities were intentionally added, $T_H \approx 50^{\circ}K$ at 750 Oe and T_L below $1^{\circ}K$, if a lower limit can be established at all. Addition of 1% Co^{2+} to the same salt affects relaxation times in an estimated range of $10^{\circ}K < T < 200^{\circ}K$. As a general rule we found that an influence of the relaxation time by the impurity can be expected if the impurity has a considerably shorter relaxation time (if definable) compared to the host material. Just below T_H one must expect the temperature variation of the relaxation time to become relatively weak. It may even be that this leads to a temperature region in which it hardly varies.

The fact that small concentrations ($< 0.1\%$, figs. III-3 and III-5) often influence the relaxation time of the complete specimen indicates that spin-spin processes, as well as cross relaxation and spin diffusion, apparently play a role. These latter processes in general slow down at higher magnetic fields and it is expected and observed that the influence of impurities reduces at higher magnetic fields.

By means of a thermodynamic model (a thermal block diagram) shown in fig. IV-1 we have been able formally to describe much of the experimental data in a satisfactory way (fig. IV-4).

Magnetic impurities are often effective; in the case of some manganese and copper tutton salts, K^+ ions have also been shown to be an important impurity. The mechanism of this influence is at present uncertain, the possibility of "exchange centers", acting as relaxation centers as mentioned as early as 1941 by Van Vleck, can be considered.

A few measurements were performed on gadolinium sulphate octahydrate (fig. III-10) and we have good reason to believe that an anomaly in the ρ-T curve, similar to the case of manganese tutton salt and earlier reported by Gorter and Broer, is mainly due to the same mechanism. The "pure" salt exhibited a temperature region in which the relaxation time was nearly constant, adding 1% Dy shifted this range considerably.

We have determined spin lattice relaxation times in copper cesium and

ammonium tutton salts. Again the relaxation times have been determined in a range of over 7 decades. The relaxation times at hydrogen and higher temperatures follow theoretical predictions in a reasonable way, at helium temperatures the temperature dependence resembles that of a direct process, but the dependency of the relaxation time on the field is not as predicted by the theory of Van Vleck (table I-3). In these two salts we have also been able to measure spin-spin relaxation phenomena (figs. III-16 and III-20). In our frequency range these absorptions occur at relatively high fields and have thus a small amplitude. The measuring methods, by which the absorptions are plotted as a continuous function of the magnetic field, enabled us to detect them without difficulties and we could determine the maxima with a good accuracy. The results obtained are compared in section 4.5 with the theoretical predictions of Caspers and Tjon. The theory of Tjon is found to describe the phenomena fairly well but the differences between the prediction and the results are still sizable for the copper cesium tutton salt.

We have done some investigations on several specimens of cobalt tutton salts (sections 3.7 and 4.4). In agreement with Van den Broek's results, sharp decreases in relaxation times are observed at a number of well defined magnetic field values, but the inconsistency of some of the data suggests that impurities may play an important role again. At present no good explanation is available for these phenomena. In all the cobalt tutton specimens we have been able to detect spin-spin absorptions. No attempt is made to compare the results with the theory of Caspers or Tjon, the salts deviating too much from the assumptions made in the theory.

Spin-spin relaxation phenomena mainly occur at frequencies between the radio and microwave range. We have observed in a few cases in agreement with Kronig and Bouwkamp's predictions (formula 1-37), that the spin-spin relaxation time can become long in high magnetic fields. When it reaches the value of the spin-lattice relaxation time the spin-spin absorption is found to disappear.

A few measurements have been done on hydrated copper sulphate and copper potassium chloride (sections 3.5 and 3.6). In the first salt we were able to show definitely the existence of a spin-lattice relaxation, in the second salt large deviations from Casimir-Du Pré relaxation curves at hydrogen temperatures are probably caused by poor heat conduction, as has been reported by Van den Broek in the helium range.

For most salts we have been able to determine the b/C value. In some of the earlier investigations the influence of deviations from Curie's law have been underestimated. We believe that in some cases our measurements have reduced the existing uncertainties in this quantity.

146

SAMENVATTING

In dit proefschrift beschrijven wij het ontwerp van een meet-brug voor het waarnemen en onderzoeken van paramagnetische relaxatie-verschijnselen. Relaxatietijden van 1 μsec. - enige minuten kunnen worden bepaald, een decade nabij 20 msec uitgezonderd. Een magnetisch veld kan, evenwijdig met het meet-veld, als een onafhankelijke parameter worden gevarieerd. Metingen kunnen worden gedaan in de gebruikelijke temperatuurgebieden van vloeibaar He, H_2 en N_2, de snelle werking van de brug maakt het mogelijk een redelijke schatting te verkrijgen van relaxatietijden in het gehele interval van $1^{\circ}K$ tot $300^{\circ}K$, indien de relaxatietijden in het meetgebied van de brug vallen. Uitvoerige onderzoekingen zijn verricht aan mangaan-tuttonzout. De oorzaak is gevonden waarom resultaten van vroegere onderzoekers niet reproduceerbaar waren. Ook zijn wij er in geslaagd experimenteel de verklaring te vinden voor een anomalie in dit zout, die vroeger reeds gevonden was in gadolinium-sulfaat; in beide zouten is de relaxatietijd in een vrij groot temperatuurgebied vrijwel constant. In de beschreven gevallen is het gebleken dat onzuiverheden daarvan de oorzaak zijn. Experimenteel hebben we aangetoond dat niet alleen paramagnetische onzuiverheden, maar ook bepaalde diamagnetische ionen (K^+) de relaxatietijd op een nog vooralsnog niet verklaarde manier kunnen beinvloeden. De meetresultaten kunnen formeel met een redelijke nauwkeurigheid met een eenvoudig blok-model worden beschreven. Metingen van de spin-roosterrelaxatietijden aan een serie koper- en cobaltzouten worden besproken. De markante resonanties in de relaxatietijden van sommige cobalt-zouten blijven raadselachtig.

In verschillende zouten waren we in staat spin-spinrelaxatietijden in grote constante velden te bepalen. Wanneer deze langer dreigen te worden dan de spin-roosterrelaxatietijden verdwijnt het spin-spin relaxatieverschijnsel.

Op verzoek van de Faculteit der Wiskunde en Natuurwetenschappen volgen hier enige persoonlijke gegevens.

In 1944 werd het eindexamen HBS-B te Delft afgelegd. Vanaf 1945 studeerde ik aan de Technische Hogeschool te Delft en behaalde in 1951 het diploma van electro-technisch ingenieur. Het werk voor het ingenieurs examen verrichtte ik bij Prof. Dr Ir W. Th. Bähler, bij wie ik tevens een jaar assistent was. Van 1951 tot 1954 werkte ik bij "Philips Telecommunicatie Industrie" te Hilversum, voornamelijk aan de ontwikkeling van draaggolf-systemen. Van 1954 tot 1962 was ik werkzaam bij "Zenith Radio Corporation" te Chicago, USA. Mijn werkzaamheden hebben voornamelijk bestaan uit onderzoek en ontwikkeling van codeer-systemen voor geluid en beeld voor de "subscription television". Verder heb ik een werkzaam aandeel gehad in de ontwikkeling van het in Amerika en nu ook in Europa gebruikte systeem voor overdracht van stereophonische muziek met een frequentie gemoduleerde zender.

De Zenith Radio Corporation verleende mij een studieverlof. In 1962 begon ik in het Kamerlingh Onnes Laboratorium aan het in mijn proefschrift beschreven onderwerp te werken in overleg met mijn promotor, Prof. Dr. C.J. Gorter. In Februari 1963 werd ik benoemd tot Wetenschappelijk ambtenaar 1^e klas voor halve werktijd.

Gedurende de gehele periode heeft de Heer J. W. M. Livius mij actief geholpen bij de bouw van de apparatuur en met de meeste metingen, in dit proefschrift beschreven. In een later stadium heeft ook de Heer A. J. van Duyneveldt medegewerkt aan verschillende experimenten. Gedurende kortere perioden hebben verder Drs. D. Z. Toet en de Heer D. Brom hun medewerking verleend. De metingen aan cobaltzouten zijn grotendeels uitgevoerd door Dr. D. A. Curtis. De adviezen van Dr. J. C. Verstelle op het gebied der paramagnetische relaxatie zijn voor mij steeds van waarde geweest en de discussies met hem en met Dr. D. A. Curtis hebben veel bijgedragen tot het uiteindelijke resultaat. De bouw en het gebruiken van deze nieuwe opstelling zou onmogelijk geweest zijn zonder de krachtige steun van de technische staf. Het mechanisch constructiewerk is voornamelijk verricht in de werkplaats van de Heer L. W. Muller, het glastechnische gedeelte door de Heer A. R. B. Gerritse en de speciale sterkstroomvoorzieningen voor de magneet door de Heer J. van Dunsbergen. De Heer D. de Jong was verantwoordelijk voor het gehele cryogene gedeelte van de opstelling. De tekeningen in dit proefschrift zijn grotendeels gemaakt door de Heer W. F. Tegelaar. Alle preparaten zijn vervaardigd door Mej. J. C. Bronkhorst.

STELLINGEN

I

De waargenomen spin-roosterrelaxatietijden van geconcentreerde paramagnetische zouten bij lage temperaturen worden in vele gevallen bepaald door een relatief kleine concentratie van verontreinigingen.

Dit proefschrift hoofdstuk 4.

II

De conclusie van Candela dat de door hem gevonden paramagnetische spin-roosterrelaxatietijd in kopersulfaat-pentahydraat onafhankelijk is van de grootte van de kristallen is onvoldoende gemotiveerd door zijn waarnemingen.

George Candela, Journ. Chem. Phys. 42 (1965) 113.

III

Onderzoek met behulp van electronenresonantie aan met Zn verdund mangaan-ammoniumtuttonzout en koperammoniumtuttonzout, beide met kaliumverontreinigingen zou kunnen leiden tot een beter begrip van de anomale relaxatieverschijnselen, die in de niet verdunde zouten zijn waargenomen.

Dit proefschrift pag. 125.

IV

Bij bepaalde onderzoekingen verdient een met vloeibare stikstof gekoelde magneetspoel uit financiële overwegingen de voorkeur boven een bij kamertemperatuur bedreven spoel.

Dit proefschrift pag. 73.

V

De moeilijkheden die Weber ondervond om met de stapmethode relaxatietijden bij hoge velden te meten waren te wijten aan de daling der gevoeligheid van deze methode bij hoge velden.

Gunther Weber, Zeitschrift für Physik 171 (1963) 341.

VI

De afwijkingen tussen de z.g. b/C-waarden die door verschillende onderzoekers voor enkele sterke paramagnetische zouten zijn gevonden zijn wellicht te wijten aan verschillen tussen de ontmagnetiserende invloeden.

Dit proefschrift pag. 132.

VII

De variatie van de door Senftleben opgegeven soortelijke warmte bij constante druk van argongas in het temperatuursinterval van $25^{\circ}C - 200^{\circ}C$ is waarschijnlijk niet juist.

H. Senftleben, Zeitschrift für angewandte Physik 17 (1964) 86-87.

VIII

Bij de huidige grootte van het beeldscherm van televisiebuizen zou combinatie van televisie met stereofonische geluidsweergave onnatuurlijk aandoen.

R.F.A. Mugie, Het PTT-bedrijf XIII, 1964, 9.

IX

Het is niet nodig ter bepaling van de vrije weglengte van electronen in dunne polykristallijne metaalmonsters naast metingen van de uitsterftijd van wervelstromen nog een gelijkstroommeting uit te voeren.

P. Cotti, Phys. Kondens. Materie 3 (1964) 40-74.

X

Hoewel de suggestie van Bloembergen om bij de opleiding van electrotechnische ingenieurs sterk nadruk te leggen op wiskundige vorming en studie der fundamentele natuurkundige verschijnselen waardevol is, zou het niet juist zijn de zuiver technologische eisen die aan een ingenieur moeten worden gesteld te verwaarlozen.

N. Bloembergen, Proc IEEE June 1965, 563.

XI

Voor het bereiken en langdurig handhaven van sterke kernpolarisaties bij lage temperaturen bieden magnetisch verdunde kristallen voordelen boven niet verdunde kristallen.

M.J. Steenland en H.A. Tolhoek, Progress in low temperature Physics II (C.J. Gorter).

XII

Het verdient aanbeveling binnen afzienbare tijd kabelnetwerken met een grote beschikbare bandbreedte te construeren, die particuliere woningen met centrale punten verbinden ten behoeve van het vervullen van allerlei diensten.

XIII

Bij de interpretatie van de drukafhankelijkheid van de kritische snelheid ván Helium II door een superlek is door Allen en Watmough onvoldoende aandacht besteed aan de mogelijkheid van het optreden van een temperatuurgradient.

J.F. Allen en D. Watmough, Symposium on liquid Helium St.Andrews, August 1965.

XIV

Het is wenselijk dat aan academici, die in het bedrijfsleven werkzaam zijn, op ruime schaal de gelegenheid wordt geboden om periodiek enige tijd aan een Universiteit of Hogeschool te werken.

A.J. de Vries   6 oktober 1965